ROTATING SHALLOW WATER - BEYOND THE TEXTBOOK

by

Alana McKenzie
B.Sc., University of British Columbia, 2004

A THESIS SUBMITTED IN PARTIAL FULFILLMENT
OF THE REQUIREMENTS FOR THE DEGREE OF
MASTER OF SCIENCE
in the Department
of
Mathematics

SIMON FRASER UNIVERSITY
Spring 2007

APPROVAL

Name: Alana McKenzie

Degree: Master of Science

Title of thesis: Rotating Shallow Water - Beyond the Textbook

Examining Committee: Dr. Rustum Choksi
Chair

Dr. David Muraki
Senior Supervisor

Dr. J.F. Williams
Supervisor

Dr. Mary Catherine Kropinski
Supervisor

Dr. John Stockie
Internal/External Examiner

Date Approved: February 15, 2007

Abstract

Rotating shallow water is traditionally the first model encountered in the study of geophysical fluid dynamics. Its simplicity and applicability at large scales make it a favourable starting point for understanding midlatitude atmospheric behaviour. The linearized model reveals two principal dynamical features - fast time-scale wave disturbances, and slow time-scale balanced flow. Textbook analysis typically includes linear wave properties, and the leading order balanced dynamics of quasigeostrophy. We seek to further understand the successes and limitations of rotating shallow water in modelling geophysical fluid dynamics. In this study, nonlinear wave dynamics are restricted to uniform potential vorticity. This reduced set of equations enables the computational analysis of nonlinear waves, devoid of balanced dynamics. Additionally, balanced dynamics are investigated beyond quasigeostrophy to include small Rossby number corrections. As anticipated, an asymmetry between cyclone and anticyclone vortices emerges; the biases are consistent with similar models, and contradict atmospheric behaviour.

To Keegan, for seeking beauty in simplicity; to Joey, for finding simplicity in everything.

Acknowledgments

First and foremost, I would like to extend my sincere gratitude to my supervisor, David Muraki, for sharing his enthusiasm and insight, entertaining my numerous questions and tangents, and subsequently bringing me back to reality.

Much appreciation is extended to J.F. Williams, for his invaluable advice, involvement and interest throughout this research.

Special thanks to Colin Macdonald and Youngsuk Lee, for the enlightening discussions and helpful explanations of the underlying mathematical and numerical methods needed for this project.

I am most grateful for the unconditional support and encouragement from my friends and family, who are always there to share good company, good food and good music.

Contents

List of Tables

List of Figures

Chapter 1

Introduction

Numerical weather prediction has come a long way from its early days in 1922 when Lewis Fry Richardson recorded the first six hour weather forecast... after six weeks of computation [13]. Modern weather prediction models include the ECMWF medium range forecast model, which boasts 76,757,590 grid points in the upper air (3,737,960 in the surface layer), tracks six variables, and produces four analysis reports daily [3]. What hasn't changed is the underlying primitive equations - the Navier-Stokes equations, the first law of thermodynamics and an equation of state relating temperature and pressure.

An understanding of the full primitive equations begins with a study of a simplified set of equations that supports particular solution classes. At synoptic and mesoscales, with horizontal features spanning 100 km to 1000 km and at altitudes where surface effects are negligible, the atmosphere is considered predominantly hydrostatic, geostrophic, Boussinesq and horizontal (see Section 2.2), as well as adiabatic[1] [2], [10]. Simplifying further to a two dimensional solution subclass unveils the Rotating Shallow Water (rSW) equations, which are, arguably, the simplest form of the large scale primitive equations that retains some degree of consistency in describing the atmosphere.

1.1 Rotating Shallow Water in a Nutshell

In addition to its simplicity, rSW provides a first glance of atmospheric behaviour. A significant measure in the rSW equations is the Rossby number, $\mathcal{R}$, a ratio of velocity

[1] In an adiabatic atmosphere there is no heat exchange between fluid parcels and the atmosphere itself.

advection to Coriolis effects[2]. $\mathcal{R}$ is small for atmospheric flows, and provides the distinction of leading order $\mathcal{R} = 0$ and first correction, $\mathcal{R} \ll 1$ analysis.

The leading order equations include three types of solutions - linear gravity and Rossby waves, and a zero frequency balance solution. Gravity waves predate the rSW equations [4], and their presence is widespread, from ripples on a pond to similar effects in the atmosphere over a larger scale. Rossby waves can be observed as strictly westerly propagating long waves in the upper atmosphere, and were discovered when Rossby introduced the β-plane to compensate for the change in Coriolis parameter with latitude [11]. Leading order balanced flow is reduced to the quasigeostrophic (QG) model, first proposed by Charney in 1948 [1], with the property of area-averaged symmetry in the primitive variables (see Section 3.2.4). Vorticity symmetry is retained in numerical solutions, with the symmetric emergence of coherent vortex structures, in both the cyclonic and anticylonic directions, from turbulent initial conditions [7]. Numerical evolution of the full rSW equations exhibits a breakdown of the vorticity symmetry between cyclones and anticylones, in a manner opposite to the atmosphere [12].

In this study we address two complications that arise in analysing rSW beyond leading order. The first is the increased order of negligible terms, from both the additional two-dimensional restrictions, and further simplification of the curved Earth with Cartesian coordinates. Both are dealt with carefully in the derivation in Chapter 2. The former, by carrying all negligible scales beyond the traditional synoptic and mesoscale assumptions through the derivation, and ultimately determining their required order. The latter exploits the reference independent nature of the rSW variables, and an oblique coordinate system is defined to minimize residual terms in the flat earth approximation.

The second is the interrelation between flow types, where even small gravity wave contributions could invalidate a balanced model [15]. Similarly, an expansion of the linear wave theory could include unwanted balanced solutions. In this study, we consider two models where flow behaviour remains distinct. A balanced model devoid of gravity wave behaviour is obtained in applying the general QG formulation of [9] to rSW. A gravity wave model devoid of balanced flow arises in the case of uniform potential vorticity [8]. Full definitions of each model are given in Chapter 3.

[2]Coriolis effects are the result of measuring velocities on a rotating planet.

1.2 Thesis Overview

Chapter 2 covers a derivation of the Rotating Shallow Water equations from the primitive Navier-Stokes equations. The derivation is unique in that the equations are described using oblique spherical coordinates, where the plane of origin is a tilted equator, as opposed to standard coordinates where the plane of origin is the equator. This increases the order of accuracy in the flat earth approximation, Section 2.3.3, and minimizes the effect of absolute position on the remaining spherical variables, Section 2.2. The negligible scales defining the two-dimensional rSW solution set are carefully carried through the derivation in Section 2.3, and their maximum scale size is determined relative to a variable system order of accuracy.

In Chapter 3 we consider the remaining scales as related to the Rossby number, $\mathcal{R}$. The full rSW equations are given, and area integral conservation properties are described. This provides the structure for the textbook leading order and deeper first correction analysis. At leading order, linear gravity and Rossby waves and nonlinear quasigeostrophy are recovered. At first corrections, gravity waves are considered for the proposed uniform potential vorticity formulation, and travelling wave solutions are discussed. The first correction QG model is specified, and the area integral conservation properties are revisited.

Chapter 4 outlines the numerical implementation of the balanced and wave models proposed in the previous chapter. Details in the application of spectral methods, integrating factor methods and third order Adams-Bashforth and Runge-Kutta methods are given. Numerical stability and spectral resolution are ensured in choosing an appropriate time step and artificial diffusion parameter. Convergence is verified with exact solutions where possible.

Chapter 5 provides details and results from the rSW QG numerical experiments. Qualitative analysis shows increased potential vorticity anticyclone intensity with $\mathcal{R}$, similar to the findings for vorticity in [12]. Further quantitative analysis reveals a linear trend between the median potential vorticity and $\mathcal{R}$.

Chapter 6 provides a summary of the outcomes of this project, and suggests areas for future work.

Chapter 2

From Navier-Stokes to Rotating Shallow Water

This chapter is devoted to a systematic derivation of the rSW equations from the primitive equations of atmospheric motion. The general approach taken, similar to that in Cushman-Roisin [2] and Pedlosky [10], begins from the scaling assumptions on the primitive variables, and systematically reduces the equations to include only the relevant terms. An analysis of the effects of each scaling parameter follows the more complete analysis in [6]. The constant density regime of rSW satisfies both the thermodynamic energy equation and the equation of state, and leaves the Navier-Stokes equations as the starting point.

2.1 Navier-Stokes Equations

Motion of a particle with velocity $\vec{u}$ in a fluid of density ρ and subject to pressure gradient force ∇p, potential force, $\nabla\Psi$, and frictional fluid force, $\vec{\mathrm{F}}$, is described by the Navier-Stokes equations of motion:

$$\rho\frac{\mathrm{D}\vec{u}}{\mathrm{D}t} = -\nabla p + \rho\nabla\Psi + \vec{\mathrm{F}}, \tag{2.1}$$

$$\frac{\mathrm{D}\rho}{\mathrm{D}t} + \rho\nabla\cdot\vec{u} = 0, \tag{2.2}$$

where

$$\frac{\mathrm{D}}{\mathrm{D}t} = \frac{\partial}{\partial t} + \vec{u}\cdot\nabla. \tag{2.3}$$

2.1.1 Rotating Reference Frame

The above form of the Navier-Stokes equations describes motion in an inertial (non-rotating) reference frame, while measurements taken on Earth are subject to the effects of the rotating planet. Velocity measured with respect to a reference frame rotating with angular velocity $\vec{\Omega}$ is related to velocity measured within an inertial frame by adding the velocity of the reference frame itself [10]:

$$\vec{u}\Big|_{\text{inertial}} = \vec{u} + \vec{\Omega} \times \vec{r}\Big|_{\text{rotating}}, \tag{2.4}$$

where $\vec{r}$ is the particle position measured within the rotating frame. The advective derivative (2.3) of velocity reveals three additional pseudo-forces in the rotating frame - Coriolis and centrifugal effects, and the effect of variations in $\vec{\Omega}$ [10]:

$$\frac{\mathrm{D}\vec{u}}{\mathrm{D}t}\Big|_{\text{inertial}} \Rightarrow \frac{\mathrm{D}\vec{u}}{\mathrm{D}t} + 2\vec{\Omega} \times \vec{u} + \vec{\Omega} \times \vec{\Omega} \times \vec{r} + \frac{\mathrm{D}\vec{\Omega}}{\mathrm{D}t} \times \vec{r}\Big|_{\text{rotating}}. \tag{2.5}$$

The centrifugal effect, $\vec{\Omega} \times \vec{\Omega} \times \vec{r}$, is considered as a potential function, and is incorporated into the total potential force, $\nabla\Psi$ [10]:

$$\vec{\Omega} \times \vec{\Omega} \times \vec{r} = \nabla\left(\frac{1}{2}|\vec{\Omega} \times \vec{r}|^2\right). \tag{2.6}$$

2.1.2 Preliminary Assumptions

The following general assumptions are considered valid for most atmospheric and oceanic flows [10].

1. Earth's rotation velocity is constant, which eliminates effects of the pseudo force associated with the varying reference frame angular velocity,

$$\frac{\mathrm{D}\vec{\Omega}}{\mathrm{D}t} \times \vec{r} = 0. \tag{2.7}$$

2. The potential force, $\nabla\Psi$, is the locally observed gravity, which includes both the gravitational force and centrifugal effects:

$$\nabla\Psi = \vec{g} = -g\frac{\vec{r}}{|\vec{r}|}. \tag{2.8}$$

3. The magnitude of the locally observed gravity, g, is constant.[1]

4. Fluids in the atmosphere and ocean behave as Newtonian fluids, with friction force

$$\vec{\mathrm{F}} = \mu\nabla^2\vec{u} + \frac{1}{3}\mu\nabla\left(\nabla\cdot\vec{u}\right) \tag{2.9}$$

where μ is the molecular viscosity.

2.1.3 Oblique Spherical Coordinates

While the vector form of the Navier-Stokes equations is independent of orientation and coordinate system, measurements of the primitive variables are taken with respect to an oriented coordinate system.
The motivation behind the choice of coordinate orientation is summarized by the following observation:

> To minimize coordinate system curvature near Vancouver, place Vancouver on the coordinate equator.

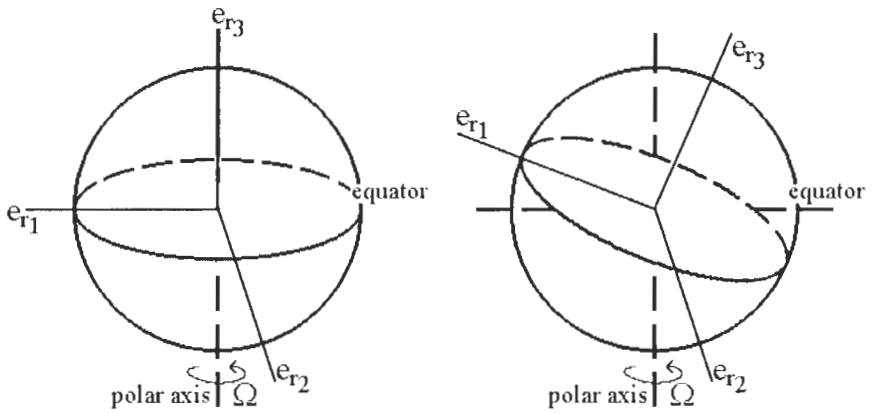

(a) Standard coordinates (b) Oblique coordinates

Figure 2.1: Coordinate systems on the Earth. (a) Standard coordinates, with the $e_{r_1}e_{r_2}$ plane through the equator. (b) Oblique coordinates, with the $e_{r_1}e_{r_2}$ plane through an arbitrary great circle.

[1] Assumptions 2 and 3 are equivalent to assuming a spherical earth. Implications of this assumption are discussed in Chapter 4 of [4].

Standard coordinate orientations consist of the $e_{r_1}e_{r_2}$ plane through the equator and the $e_{r_1}e_{r_3}$ plane though the polar axis, as shown in Figure 2.1a. This orientation is useful as it preserves east and north in the coordinate directions tangent to Earth's surface. By contrast, the class of oblique coordinate orientations has the $e_{r_1}e_{r_2}$ and $e_{r_1}e_{r_3}$ planes passing through any pair of perpendicular great circles[2]. The principal difference between coordinate orientations in our application is the effects of Earth's curvature, which increase with distance from the $e_{r_1}e_{r_2}$ plane. In order to recover the simplicity of the textbook rSW equations, we ultimately impose a flat earth approximation by assuming all curvature terms are negligible (see Section 2.3.3). These curvature terms are minimized for a particular region of interest when the $e_{r_1}e_{r_2}$ plane passes through a characteristic longitude, latitude point (Φ_0, Λ_0) of the region.

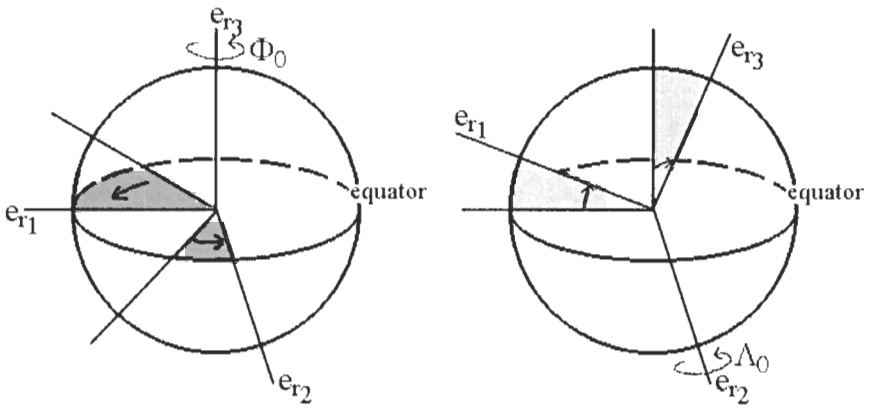

(a) First rotation (b) Second rotation

Figure 2.2: Transformation to the oblique coordinate system. (a) First rotation - Φ_0 degrees counterclockwise about e_{r_3}. (b) Second rotation - Λ_0 degrees clockwise about e_{r_2}.

Such an oblique coordinate system is obtained by rotating the standard coordinate system, first Φ_0 degrees counterclockwise about e_{r_3}, and then Λ_0 degrees clockwise about e_{r_2}, as shown in Figures 2.2a and 2.2b,

$$\begin{bmatrix} \cos\Phi_0\cos\Lambda_0 & \sin\Phi_0\cos\Lambda_0 & \sin\Lambda_0 \\ -\sin\Phi_0 & \cos\Phi_0 & 0 \\ -\cos\Phi_0\sin\Lambda_0 & -\sin\Phi_0\sin\Lambda_0 & \cos\Lambda_0 \end{bmatrix} \begin{bmatrix} e_{r_1} \\ e_{r_2} \\ e_{r_3} \end{bmatrix}_{\text{standard}} \Rightarrow \begin{bmatrix} e_{r_1} \\ e_{r_2} \\ e_{r_3} \end{bmatrix}_{\text{oblique}} \tag{2.10}$$

[2]A great circle is a curve on Earth's surface with radius equal to Earth's radius.

That is, rotate the coordinate system so the region of interest (Vancouver, for example) is located at the intersection of the $e_{r_1}e_{r_2}$ plane (coordinate equator) and the e_{r_1} axis.

Earth's angular velocity, $\vec{\Omega}$, has absolute direction about the polar axis, and is the only variable dependent on the oblique coordinate orientation:

$$\Omega e_{r_3}\Big|_{\text{standard}} \quad \Rightarrow \quad \Omega \sin\Lambda_0 e_{r_1} + \Omega\cos\Lambda_0 e_{r_3}\Big|_{\text{oblique}}. \tag{2.11}$$

Since measurements are taken relative to Earth's curved surface, spherical coordinates is a natural choice of coordinate system. The oblique spherical coordinate system is obtained by defining the zonal e_ϕ, meridional e_λ, and vertical e_r unit vectors,

$$\begin{bmatrix} \cos\phi\cos\lambda & \sin\phi\cos\lambda & \sin\lambda \\ -\sin\phi & \cos\phi & 0 \\ -\cos\phi\sin\lambda & -\sin\phi\sin\lambda & \cos\lambda \end{bmatrix} \begin{bmatrix} e_{r_1} \\ e_{r_2} \\ e_{r_3} \end{bmatrix}_{\text{oblique}} = \begin{bmatrix} e_r \\ e_\phi \\ e_\lambda \end{bmatrix}_{\text{oblique spherical}} \tag{2.12}$$

where ϕ is the oblique longitude, λ is the oblique latitude and r is the radius measured from Earth's centre, as shown in Figure 2.3.

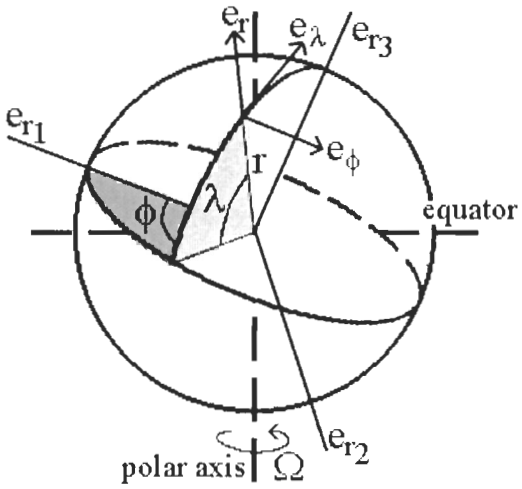

Figure 2.3: Spherical coordinates, measured from the oblique coordinate system, where ϕ, spanning the dark grey region, is the oblique longitude, λ, spanning the light grey region, is the oblique latitude and r is the radius.

Local gravity acts towards Earth's centre, and has the same representation in oblique and standard spherical coordiantes

$$\vec{g} \;=\; -ge_r. \tag{2.13}$$

The orientation-dependent angular velocity is written in oblique spherical coordinates by multiplying (2.11) by the spherical coordinate transformation matrix (2.12),

$$\vec{\Omega} = \Omega_\phi e_\phi + \Omega_\lambda e_\lambda + \Omega_r e_r, \tag{2.14}$$

where

$$\Omega_\phi = -\Omega \sin \Lambda_0 \sin \phi, \tag{2.15}$$

$$\Omega_\lambda = \Omega \cos \Lambda_0 \cos \lambda - \Omega \sin \Lambda_0 \cos \phi \sin \lambda, \tag{2.16}$$

$$\Omega_r = \Omega \cos \Lambda_0 \sin \lambda + \Omega \sin \Lambda_0 \cos \lambda \cos \phi. \tag{2.17}$$

Velocity has tangential components in the zonal, e_ϕ, and meridional, e_ϕ, directions, and a normal component in the vertical, e_r, direction

$$\vec{u} = u e_\phi + v e_\lambda + w e_r, \tag{2.18}$$

where

$$u = r \cos \lambda \frac{\mathrm{d}\phi}{\mathrm{d}t}, \qquad v = r \frac{\mathrm{d}\lambda}{\mathrm{d}t}, \qquad w = \frac{\mathrm{d}r}{\mathrm{d}t}. \tag{2.19}$$

While velocity equations are the same in standard and oblique coordinates, the longitude, ϕ, and latitude, λ, variables vary with orientation.

Friction, $\vec{\mathrm{F}}$, defined as a function of $\vec{u}$ in (2.9), although for simplicity, $\vec{\mathrm{F}}$ is written in terms of oblique spherical components, which are defined in Appendix B,

$$\vec{\mathrm{F}} = \mu \mathrm{F}_\phi + \mu \mathrm{F}_\lambda + \mu \mathrm{F}_r. \tag{2.20}$$

The spherical divergence, $\nabla \cdot$, gradient, ∇, and Laplacian ∇^2 operators are considered in Appendix A. Since the spherical coordinate unit vectors (e_ϕ, e_λ, e_r) are dependent on ϕ and λ, the gradient and Laplacian operators are applied to both the magnitude and direction components of $\vec{u}$. A discussion of the curvature terms resulting from the change in direction is left to Appendix A.

The Navier-Stokes equations, (2.1) and (2.2), in a rotating reference frame (2.5), with preliminary assumptions from Section 2.1.2 and measured in oblique spherical coordinates,

(2.10) and (2.12), are:

$$\rho\frac{\mathrm{D}u}{\mathrm{D}t}+\rho\frac{wu}{r}-\rho\frac{uv\tan\lambda}{r}+2\rho w\Omega_\lambda-2\rho v\Omega_r = \frac{-1}{r\cos\lambda}\frac{\partial p}{\partial\phi}+\mu\mathrm{F}_\phi, \quad (2.21)$$

$$\rho\frac{\mathrm{D}v}{\mathrm{D}t}+\rho\frac{wv}{r}+\rho\frac{u^2\tan\lambda}{r}+2\rho u\Omega_r-2\rho w\Omega_\phi = \frac{-1}{r}\frac{\partial p}{\partial\lambda}+\mu\mathrm{F}_\lambda, \quad (2.22)$$

$$\rho\frac{\mathrm{D}w}{\mathrm{D}t}-\rho\frac{u^2+v^2}{r}+2\rho v\Omega_\phi-2\rho u\Omega_\lambda = -\frac{\partial p}{\partial r}-\rho g+\mu\mathrm{F}_r, \quad (2.23)$$

$$\frac{\mathrm{D}\rho}{\mathrm{D}t}+\rho\frac{1}{r\cos\lambda}\frac{\partial u}{\partial\phi}+\rho\frac{1}{r}\frac{\partial v}{\partial\lambda}-\rho\frac{1}{r}v\tan\lambda+\rho\frac{\partial w}{\partial r}+\rho\frac{2}{r}w = 0, \quad (2.24)$$

where

$$\frac{\mathrm{D}}{\mathrm{D}t} = \frac{\partial}{\partial t}+u\frac{1}{r\cos\lambda}\frac{\partial}{\partial\phi}+v\frac{1}{r}\frac{\partial}{\partial\lambda}+w\frac{\partial}{\partial r}. \quad (2.25)$$

The only difference between the above oblique equations introduced here and standard equations in [10] and [4] is the definition of Ω_ϕ, Ω_λ and Ω_r in (2.15) - (2.17). The definition of the zonal and meridional directions (e_ϕ and e_λ) and the oblique longitude and latitude variables (ϕ and λ), however, depend on the orientation of the oblique coordinate system.

2.2 Scales in the Atmosphere

We now consider the assumptions necessary to apply the full Navier-Stokes equations to synoptic scale flow. In order to quantify the relative contribution of each term, each variable is separated into a constant characteristic scale and a dimensionless variable.[3] Different scales are given to the horizontal and vertical dependencies of the primitive variables, in anticipation that the two dimensional rSW solution class will impose further restrictions on the vertical components. Dimensionless parameters relating the characteristic scales are then defined.

$$r_0\phi\rightarrow L\phi_l, \quad r_0\lambda\rightarrow L\lambda_l, \quad r\rightarrow r_0+Hz, \quad t\rightarrow Tt, \quad (2.26)$$

where L is a characteristic length, H is the average height from Earth's surface, r_0, and T is a characteristic time scale. The subscript l is used to distinguish between angles ϕ and λ, and surface arc-lengths ϕ_l and λ_l.

$$\rho \rightarrow \rho_0+\Delta\rho\rho'(\phi_l,\lambda_l,z,t), \quad (2.27)$$

[3] Characteristic scales are selected so the dimensionless variable is $\mathcal{O}(1)$. This also implies that each variable remains $\mathcal{O}(1)$ in time.

where ρ_0 is the average density, and $\Delta\rho$ is the characteristic density variation.

$$p \rightarrow \mathcal{P}_0 p_0(z) + \mathcal{P}p(\phi_l, \lambda_l, t) + \Delta\mathcal{P}p'(\phi_l, \lambda_l, z, t), \tag{2.28}$$

where $\mathcal{P}_0$ is the characteristic pressure in the absence of motion, $\mathcal{P}$ is the characteristic pressure variation in the horizontal and $\Delta\mathcal{P}$ is the characteristic total pressure variation.

$$\begin{aligned} u &\rightarrow Uu(\phi_l, \lambda_l, t) + \Delta U u'(\phi_l, \lambda_l, z, t), \\ v &\rightarrow Uv(\phi_l, \lambda_l, t) + \Delta U v'(\phi_l, \lambda_l, z, t), \\ w &\rightarrow Ww(\phi_l, \lambda_l, z, t), \end{aligned} \tag{2.29}$$

where U and W are the characteristic horizontal and vertical velocities, ΔU is the characteristic horizontal velocity variation in the vertical.

The effects of Earth's curvature are measured by ξ and by the Coriolis parameter, f,

$$\xi = \frac{L}{r_0}, \qquad f = 2\Omega \sin \Lambda_0 \tag{2.30}$$

The Rossby number, $\mathcal{R}$, is the ratio of advection to Coriolis effects; the Froude number, $\mathcal{F}$, is the ratio of the intertial to gravitational force; the Ekman number, $\mathcal{E}k$, is the ratio of viscous forces to Coriolis effects, and the planetary number, β, is the of ratio of variations of the Coriolis effect with latitude to the Coriolis parameter

$$\mathcal{R} = \frac{U}{fL}, \qquad \mathcal{F} = \frac{U}{\sqrt{gH}}, \qquad \mathcal{E}k = \frac{\mu}{\rho_0 f H^2}, \qquad \beta = \xi \cot \Lambda_0. \tag{2.31}$$

All time derivatives are in the form of the advective derivative, so it is convenient to specify a relative time scale, $\mathcal{C}$, as a ratio of advective to actual time scale

$$\mathcal{C} = \frac{L/U}{T}. \tag{2.32}$$

Synoptic scale flows are typically found at length scales much larger than height scales, and their relative scales are quantified by the ε parameters,

$$\varepsilon_L = \frac{H}{L}, \qquad \varepsilon_u = \frac{W}{U}. \tag{2.33}$$

We anticipate the rSW solution class will impose strict restrictions on vertical variations, and introduce dimensonless γ parameters to denote the relative sizes of these variations within the primitive variables

$$\gamma_u = \frac{\Delta U}{U}, \qquad \gamma_\rho = \frac{\Delta\rho}{\rho_0}, \qquad \gamma_p = \frac{\Delta\mathcal{P}}{\mathcal{P}}.$$

2.2.1 Scaling Assumptions for Synoptic and Mesoscale Flow

The following scale assumptions distinguish synoptic and upper mesoscale flow from other classes of fluid flow [2], [10].

1. Synoptic to upper mesoscale length scale: the characteristic length scale is smaller than Earth's radius.

2. Boussinesq: the density variations are significantly smaller than the mean density.

3. Horizontal: the characteristic vertical scales are significantly smaller than horizontal scales.

$$\xi \ < \ 1, \qquad \gamma_\rho \ \ll \ 1, \qquad \varepsilon_L \ \ll \ 1, \qquad \varepsilon_u \ \ll \ 1. \tag{2.34}$$

4. Hydrostatic: the vertical pressure gradient balances the gravitational force.

5. Geostrophic: the horizontal pressure gradient balances the Coriolis effect due to horizontal velocities.

$$\mathcal{P}_0 \ \sim \ \rho_0 g H, \qquad \mathcal{P}, \Delta\mathcal{P} \ \sim \ \rho_0 f U L, \tag{2.35}$$

   where $\mathcal{F}^2 \lesssim \mathcal{R}$ ensures that the hydrostatic balance occurs at the largest scale in the vertical momentum equation, and $\mathcal{R} \lesssim 1$, $\mathcal{C} \lesssim 1$, and $\beta \ll 1$ ensures that the geostrophic balance occurs at the largest scale in the horizontal momentum equations.

6. Inviscid: all friction terms can be assumed negligible. A detailed account of the scaling of the friction variables is given in Appendix B.

$$\begin{aligned} \mu \mathrm{F}_\phi, \mu \mathrm{F}_\lambda \ &\sim \ \mu \frac{\Delta U}{H^2} + \mu \frac{U}{L^2} + \mu \frac{W}{H} \\ \mu \mathrm{F}_r \ &\sim \ \mu \frac{W}{H^2} + \mu \frac{U + \Delta U}{r_0 L} + \mu \frac{L}{r_0} \frac{\Delta U}{r_0 H}. \end{aligned} \tag{2.36}$$

2.3 Rotating Shallow Water

In addition to the synoptic and mesoscale assumptions, the rSW solution class is two-dimensional and homogeneous. We first consider the reduction to two-dimensional flow by imposing a vertical boundary condition, and then specify the scaling assumptions for the vertical components of all parameters.

The first reduction from three to two dimensional flow is made by introducing variations from mean surface height, $h = h(\phi_l, \lambda_l, t)$, as a function of horizontal parameters, and imposing the kinematic boundary condition at the vertical boundaries,

$$w(z_{\text{bottom}}) = 0, \qquad w(z_{\text{top}}) = \sigma \frac{\mathrm{D}h(\phi_l, \lambda_l, t)}{\mathrm{D}t}, \tag{2.37}$$

where $\sigma = \frac{\Delta H}{H}$ is the ratio of height variation to mean surface height, and we assume flat bottom, $z_{\text{bottom}} = 0$, and free surface, $z_{\text{top}} = 1 + \sigma h(\phi_l, \lambda_l, t)$, boundaries.

In addition, the two-dimensional homogeneous class of solutions arises when all terms containing ε and γ parameters, defined in (2.33) and (2.34), are negligible, so the system is devoid of any vertical structure.

The synoptic and mesoscale atmospheric and oceanic characteristic values support the scaling assumptions in Section 2.2.1 [2]. However, the same is not necessarily true of the additional rSW scale assumptions, where relatively small vertical variations are considered negligible. By carrying through the ultimately negligible ε and γ parameters, the relative scaling of each term and its maximum size in a system accurate to an $\mathcal{O}(\alpha)$ will be determined. While specific values of α are considered in Chapter 3, α remains arbitrary through the derivation.

The first benefit of the oblique coordinate system is now apparent. Where ε and γ terms multiply trigonometric functions, the order of cos, sin and tan affects the overall order of the negligible term. The order of the trigonometric functions in oblique coordinates is obtained by expanding in a Taylor series about $\lambda_0 = 0$ or $\phi_0 = 0$, in equation (C.13). This differs from the equations in standard coordinates, where the trigonometric functions are expanded about $\lambda_0 = \Lambda_0$.

We now substitute the scaled, dimensionless variables from Section 2.2, with the synoptic and mesoscale assumptions from Section 2.2.1, into the Navier-Stokes equations, (2.21) - (2.24). The following section provides highlights from the thorough derivation in Appendix C, which is unique to the oblique spherical coordinate system.

2.3.1 Continuity and Momentum Equations

The dimensionless continuity equation, (C.33), is

$$\frac{1}{\cos\xi\lambda_l}\frac{\partial u}{\partial\phi_l} + \frac{\partial v}{\partial\lambda_l} - \xi v\tan\lambda + \frac{\varepsilon_u}{\varepsilon_L}\frac{\partial w}{\partial z} \;=\; \mathcal{O}\left(\gamma_u, \gamma_\rho\left[1, \mathcal{C}_r\frac{\varepsilon_u}{\varepsilon_L}\right], \xi[\varepsilon_u, \varepsilon_L]\right), \tag{2.38}$$

which implies that the vertical to horizontal velocity ratio is bounded by the vertical to horizontal spatial ratio, $\varepsilon_u \lesssim \varepsilon_L$.

Since $u = u(\phi_l, \lambda_l, t)$ and $v = v(\phi_l, \lambda_l, t)$, defined in (2.29), are independent of z, integrating (2.38) from $z = 0$ to $z = 1 + \sigma h$, with the kinematic boundary condition (2.37), yields the *rSW Vertically Integrated Continuity Equation*:

$$(1+\sigma h)\left(\frac{1}{\cos\xi\lambda}\frac{\partial u}{\partial \phi_l} + \frac{\partial v}{\partial \lambda_l} - \xi v \tan\xi\lambda_l\right) + \sigma\frac{\mathrm{D}h}{\mathrm{D}t} = \mathcal{O}\left(\gamma_u, \gamma_\rho\left[1, \mathcal{C}\right], \xi\varepsilon_L\right) \tag{2.39}$$

The dimensionless vertical momentum equation, (C.43), where $\varepsilon_u \lesssim \varepsilon_L$, is

$$-\frac{\partial p_0}{\partial z} - 1 = \mathcal{O}\left(\gamma_\rho, \frac{\mathcal{F}^2}{\mathcal{R}}\gamma_\rho, \frac{\mathcal{F}^2}{\mathcal{R}}\varepsilon_L\left[\xi, \frac{\beta}{\xi}, \varepsilon_L\mathcal{E}k\right], \mathcal{F}^2\left[\varepsilon_L^2[1, \mathcal{C}]\right]\right) \tag{2.40}$$

Integrating in the vertical direction from z to $1+\sigma h(\phi_l, \lambda_l, t)$ gives an equation for pressure,

$$\begin{aligned} p_0(1+\sigma h) - p_0(z) &= -\left(1 + \sigma h(\phi_l, \lambda_l, t)\right) + z \\ &\quad + \mathcal{O}\left(\gamma_\rho, \frac{\mathcal{F}^2}{\mathcal{R}}\gamma_\rho, \frac{\mathcal{F}^2}{\mathcal{R}}\varepsilon_L\left[\xi, \frac{\beta}{\xi}, \varepsilon_L\mathcal{E}k\right], \mathcal{F}^2\left[\varepsilon_L^2[1, \mathcal{C}]\right]\right), \end{aligned} \tag{2.41}$$

where $p_0(1+\sigma h)$ is determined by evaluating (2.28) at the surface $z = 1 + \sigma h$, where $p(\phi_l, \lambda_l, 1+\sigma h, t) = 0$, relative to the ambient pressure,

$$p_0(1+\sigma h) + \frac{\mathcal{P}}{\mathcal{P}_0}p\left(\phi_l, \lambda_l, t\right) + \gamma_p\frac{\mathcal{P}}{\mathcal{P}_0}p'\left(\phi_l, \lambda_l, 1+\sigma h, t\right) = 0. \tag{2.42}$$

Substituting into (2.41),

$$\begin{aligned} -\frac{\mathcal{P}}{\mathcal{P}_0}p\left(\phi_l, \lambda_l, t\right) - p_0(z) &= -\left(1 + \sigma h(\phi_l, \lambda_l, t)\right) + z + \mathcal{O}\left(\gamma_p\frac{\mathcal{P}}{\mathcal{P}_0}\right) \\ &\quad + \mathcal{O}\left(\gamma_\rho, \frac{\mathcal{F}^2}{\mathcal{R}}\gamma_\rho, \frac{\mathcal{F}^2}{\mathcal{R}}\varepsilon_L\left[\xi, \frac{\beta}{\xi}, \varepsilon_L\mathcal{E}k\right], \mathcal{F}^2\left[\varepsilon_L^2[1, \mathcal{C}]\right]\right). \end{aligned} \tag{2.43}$$

Vertical pressure, $p_0(z)$, is then proportional to the height, z,

$$p_0(z) = 1 - z, \tag{2.44}$$

and horizontal pressure variations, $\frac{\mathcal{P}}{\mathcal{P}_0}p(\phi_l, \lambda_l, t)$, are proportional to variations from mean height,

$$\begin{aligned} \frac{\mathcal{P}}{\mathcal{P}_0}p(\phi_l, \lambda_l, t) &= \sigma h(\phi_l, \lambda_l, t) \\ &\quad + \mathcal{O}\left(\gamma_\rho, \left[\frac{\mathcal{F}^2}{\mathcal{R}}, \frac{\mathcal{P}}{\mathcal{P}_0}\right]\gamma_p, \frac{\mathcal{F}^2}{\mathcal{R}}\varepsilon_L\left[\xi, \frac{\beta}{\xi}, \varepsilon_L\mathcal{E}k\right], \mathcal{F}^2\left[\varepsilon_L^2[1, \mathcal{C}]\right]\right), \end{aligned} \tag{2.45}$$

and scale as

$$\sigma \sim \frac{\mathcal{P}}{\mathcal{P}_0} \sim \frac{\mathcal{F}^2}{\mathcal{R}}. \tag{2.46}$$

Dividing the horizontal pressure equation by σ,

$$p(\phi_l, \lambda_l, t) = h(\phi_l, \lambda_l, t) + \mathcal{O}\left(\frac{\gamma_\rho}{\sigma}, \gamma_p, \varepsilon_L\left[\xi, \frac{\beta}{\xi}, \varepsilon_L \mathcal{E}k\right], \mathcal{R}\left[\varepsilon_L^2[1, \mathcal{C}]\right]\right). \tag{2.47}$$

The dimensionless zonal and meridional momentum equations, (C.54) and (C.60), are

$$\mathcal{R}\frac{\mathrm{D}u}{\mathrm{D}t} - \mathcal{R}\xi uv\tan\lambda - v\Gamma_r = \frac{-1}{\cos\xi\lambda_l}\frac{\partial p}{\partial \phi_l} + \mathcal{O}\left(\gamma_u, \gamma_\rho, \gamma_p, \varepsilon_L\left[\xi, \frac{\beta}{\xi}\right], \mathcal{E}k\left[\gamma_u, \varepsilon_L^2\right]\right) \tag{2.48}$$

$$\mathcal{R}\frac{\mathrm{D}v}{\mathrm{D}t} + \mathcal{R}\xi u^2\tan\lambda + u\Gamma_r = -\frac{\partial p}{\partial \lambda_l} + \mathcal{O}\left(\gamma_u, \gamma_\rho, \gamma_p, \varepsilon_L\xi, \mathcal{E}k\left[\gamma_u, \varepsilon_L^2\right]\right), \tag{2.49}$$

where the Coriolis coefficent is rewritten as

$$\Gamma_r = \cos\xi\phi_l\cos\xi\lambda_l + \frac{\beta}{\varepsilon}\sin\xi\lambda_l, \tag{2.50}$$

and the horizontal advective derivative is[4]

$$\frac{\mathrm{D}}{\mathrm{D}t} = \mathcal{C}\frac{\partial}{\partial t} + u\frac{1}{\cos\xi\lambda_l}\frac{\partial}{\partial\phi_l} + v\frac{\partial}{\partial\lambda_l}. \tag{2.51}$$

Substituting (2.47) for p yields the *rSW Momentum Equations*,

$$\mathcal{R}\frac{\mathrm{D}u}{\mathrm{D}t} - \mathcal{R}\xi uv\tan\lambda - v\Gamma_r = -\frac{1}{\cos\xi\lambda_l}\frac{\partial h}{\partial\phi_l} + \mathcal{O}\left(\gamma_u, \frac{\gamma_\rho}{\sigma}, \gamma_p, \varepsilon_L\left[\xi, \frac{\beta}{\xi}\right], \mathcal{E}k\left[\gamma_u, \varepsilon_L^2\right], \mathcal{R}\left[\varepsilon_L^2[1, \mathcal{C}]\right]\right) \tag{2.52}$$

$$\mathcal{R}\frac{\mathrm{D}v}{\mathrm{D}t} + \mathcal{R}\xi u^2\tan\lambda + u\Gamma_r = -\frac{\partial h}{\partial\lambda_l} + \mathcal{O}\left(\gamma_u, \frac{\gamma_\rho}{\sigma}, \gamma_p, \varepsilon_L\xi, \mathcal{E}k\left[\gamma_u, \varepsilon_L^2\right], \mathcal{R}\left[\varepsilon_L^2[1, \mathcal{C}]\right]\right) \tag{2.53}$$

2.3.2 Divergence, Vorticity and Potential Vorticity

A complete set of rSW equations is contained within the *rSW Momentum Equations* and the *rSW Integrated Continuity Equation*, where pressure is defined by (2.47), and vertical velocity is defined on the boundaries. Further analysis includes taking combinations of these equations to obtain additional relations, which can either be used to obtain equivalent rSW

[4]We have dropped the l subscript from the notation in Appendix C.

equation sets, or supplementary properties. We consider the former here, where a potential vorticity equation will be used with the momentum equations in the set of rSW equations. A discussion of supplementary properties is continued in Chapter 3.

Horizontal divergence, δ, and vertical vorticity, ζ, are defined as

$$\delta = \nabla \cdot (u e_\phi + v e_\lambda) = \frac{1}{\cos \xi\lambda_l} \frac{\partial u}{\partial \phi_l} + \frac{\partial v}{\partial \lambda_l} - \xi v \tan \xi\lambda_l, \tag{2.54}$$

$$\zeta = (\nabla \times \vec{u}) \cdot e_r = \frac{1}{\cos \lambda_l} \frac{\partial v}{\partial \phi_l} - \frac{\partial u}{\partial \lambda_l} + \xi u \tan \xi\lambda_l. \tag{2.55}$$

Substituting δ into the *rSW Vertically Integrated Continuity Equation* (2.39) yields the *rSW Height-Divergence Equation*,

$$\delta = -\frac{\sigma}{(1+\sigma h)} \frac{\mathrm{D}h}{\mathrm{D}t} + \mathcal{O}\left(\gamma_u, \gamma_\rho\left[1, \mathcal{C}\right], \varepsilon_L\left[\xi, \frac{\beta}{\xi}\right]\right) \tag{2.56}$$

Combining the *rSW Horizontal Momentum Equations*, (2.52) and (2.53), in the following manner

$$\frac{1}{\cos \xi\lambda} \frac{\partial}{\partial \phi_l}(2.53) - \frac{\partial}{\partial \lambda_l}(2.52) + \xi \tan \xi\lambda_l (2.52) \tag{2.57}$$

yields the *rSW Vorticity-Divergence Equation*,

$$\mathcal{R}\frac{\mathrm{D}\zeta}{\mathrm{D}t} + \frac{\mathrm{D}\Gamma_r}{\mathrm{D}t} + \delta\left(\mathcal{R}\zeta + \Gamma_1\right) = \mathcal{O}\left(\gamma_u, \frac{\gamma_\rho}{\sigma}, \gamma_p, \varepsilon_L\left[\xi, \frac{\beta}{\xi}\right], \mathcal{E}k\left[\gamma_u, \varepsilon_L^2\right], \mathcal{R}\left[\varepsilon_L^2[1, \mathcal{C}]\right]\right) \tag{2.58}$$

Replacing δ with the *rSW Height-Divergence Equation*, the above equation is reduced to the advection of a single variable,

$$\frac{\mathrm{D}Q}{\mathrm{D}t} = \mathcal{O}\left(\gamma_u, \gamma_\rho\left[\frac{1}{\sigma}, \mathcal{C}\right], \gamma_p, \varepsilon_L\left[\xi, \frac{\beta}{\xi}\right], \mathcal{E}k\left[\gamma_u, \varepsilon_L^2\right], \mathcal{R}\left[\varepsilon_L^2[1, \mathcal{C}]\right]\right), \tag{2.59}$$

where Q is the Ertel potential vorticity, defined as

$$Q = \frac{\mathcal{R}\zeta + \Gamma_r}{1 + \sigma h}. \tag{2.60}$$

Since $\xi < 1$, the Coriolis parameter, Γ_r, can be written as a Taylor expansion about $\phi_l = 0 = \lambda_1$, where β is defined in (2.31),

$$\begin{aligned} \Gamma_r &= \cos \xi\lambda_l \cos \xi\phi_l + \frac{\beta}{\xi} \sin \xi\lambda_l \\ &= 1 + \beta\lambda_l - \frac{1}{2}\xi^2\left(\lambda_l^2 + \phi_l^2\right) + \ldots. \end{aligned} \tag{2.61}$$

The scale of Q, denoted by $\varphi_q \sim Q$, is defined as $\varphi_q = \max(\mathcal{R}, \sigma, \beta, \xi^2)$, and we define q as the dynamically active component of the potential vorticity, where $Q = 1+\varphi_q q$. Substituting into equations (2.59) and (2.60) results in an additional factor of φ_q multiplying each term, and dividing the equations by φ_q is effectively reducing the order of accuracy of the system. The *rSW Potential Vorticity Equation* becomes:

$$\frac{\mathrm{D}q}{\mathrm{D}t} = \mathcal{O}\left(\frac{1}{\varphi_q}\left(\gamma_u, \gamma_\rho\left[\frac{1}{\sigma}, \mathcal{C}\right], \gamma_p, \varepsilon_L\left[\xi, \frac{\beta}{\xi}\right], \mathcal{E}k\left[\gamma_u, \varepsilon_L^2\right], \mathcal{R}\left[\varepsilon_L^2[1, \mathcal{C}]\right]\right)\right) \tag{2.62}$$

where

$$(1+\sigma h)q = \frac{1}{\varphi_q}\left(-\sigma h + \mathcal{R}\zeta + \beta\lambda_l - \frac{1}{2}\xi^2\left(\phi_l^2 + \lambda_l^2\right) + \ldots\right). \tag{2.63}$$

Including the *rSW Potential Vorticity Equation* in the system of rSW equations means rescaling the order of accuracy of the entire system by an $\mathcal{O}(\varphi_q)$. That is, for a system accurate to $\mathcal{O}(\alpha)$, the additional specifications for this rSW solution class are:

$$\gamma_p, \gamma_u \lesssim \varphi_q\alpha, \qquad \gamma_\rho \lesssim \varphi_q\alpha \min\left(\sigma, \frac{1}{\mathcal{C}}\right), \qquad \mathcal{E}k \lesssim \varphi_q\alpha \min\left(\frac{1}{\varepsilon_L^2}, \frac{1}{\gamma_u}\right), \tag{2.64}$$

$$\varepsilon_L \lesssim \varphi_q\alpha \min\left[\frac{1}{\xi}, \frac{\xi}{\beta}\right], \qquad \varepsilon_L^2 \lesssim \varphi_q\alpha\frac{1}{\mathcal{R}} \min\left[1, \frac{1}{\mathcal{C}}\right]. \tag{2.65}$$

The oblique spherical rSW equations are comprised of the *rSW Momentum Equations* (2.52) and (2.53) and the *rSW Potential Vorticity Equation*, where with the above scale restriction the system is accurate to $\mathcal{O}(\alpha)$:

$$\mathcal{R}\frac{\mathrm{D}u}{\mathrm{D}t} - \mathcal{R}\xi uv\tan\lambda - v\Gamma_r = -\frac{1}{\cos\xi\lambda_l}\frac{\partial h}{\partial\phi_l} \tag{2.66}$$

$$\mathcal{R}\frac{\mathrm{D}v}{\mathrm{D}t} + \mathcal{R}\xi u^2\tan\lambda + u\Gamma_r = -\frac{\partial h}{\partial\lambda_l} \tag{2.67}$$

$$\frac{\mathrm{D}q}{\mathrm{D}t} = 0 \tag{2.68}$$

where

$$q = \frac{1}{\varphi_q}\left(-\sigma h + \mathcal{R}\zeta + \beta\lambda_l - \frac{1}{2}\xi^2\left(\phi_l^2 + \lambda_l^2\right) + \ldots\right), \tag{2.69}$$

$$\Gamma_r = \cos\xi\lambda_l\cos\xi\phi_l + \frac{\beta}{\xi}\sin\xi\lambda_l, \tag{2.70}$$

$$\zeta = \frac{1}{\cos\xi\lambda_l}\frac{\partial v}{\partial\phi_l} - \frac{\partial u}{\partial\lambda_l} + \xi u\tan\xi\lambda_l \tag{2.71}$$

and the horizontal advective derivative is

$$\frac{\mathrm{D}}{\mathrm{D}t} = \mathcal{C}\frac{\partial}{\partial t} + \frac{u}{\cos\xi\lambda_l}\frac{\partial}{\partial\phi_l} + v\frac{\partial}{\partial\lambda_l}. \tag{2.72}$$

2.3.3 Cartesian Coordinates

The transition from spherical coordinates to the Cartesian approximation has been simplified by the initial scaling of the angles, ϕ and λ, as arclengths, ϕ_l and λ_l. Following Cartesian notation, we let

$$\phi_l \;=\; x \qquad \lambda_l \;=\; y. \tag{2.73}$$

The Coriolis parameter is defined as in equation (2.61), and since traditionally higher order Coriolis terms are allowed, the expansion will be truncated later for consistency with the system order:

$$\Gamma_r \;=\; 1 + \beta y - \frac{1}{2}\xi^2\left(x^2 + y^2\right) + \ldots. \tag{2.74}$$

The remaining trigonometric functions are expanded in a Taylor series about $x_0 = 0 = y_0$, where only the ξ independent terms are permitted in the Cartesian equations:

$$\frac{1}{\cos\xi y} \;=\; 1 + \mathcal{O}\left(\xi^2\right) \qquad \tan\xi y \;=\; \mathcal{O}\left(\xi\right). \tag{2.75}$$

The second advantage of the tilted coordinates is now apparent. In standard coordinates $x_0 \neq 0$ and $y_0 \neq 0$, resulting in extra terms in the above trigonometric expansions. Specifically, cos would be truncated to $\mathcal{O}\left(\xi\right)$, and tan would be truncated to $\mathcal{O}\left(1\right)$, whereas the tilted coordinates allow for an extra ξ order of accuracy.

In the *rSW Momentum Equations*, (2.66) and (2.67), direct substitution reveals the largest ξ terms appear at $\mathcal{O}\left(\xi^2\right)$.

Scaling the *rSW Potential Vorticity Equation*, (2.66), requires a few steps. First, vorticity, ζ from (2.71), becomes

$$\zeta \;=\; \frac{1}{\cos\xi\lambda_l}\frac{\partial v}{\partial\phi_l} - \frac{\partial u}{\partial\lambda_l} + \xi u\tan\xi\lambda_l \;\rightarrow\; \frac{\partial v}{\partial x} - \frac{\partial u}{\partial y} + \mathcal{O}\left(\xi^2\right) \tag{2.76}$$

and the advective derivative, from (2.72), is rewritten as

$$\frac{\mathrm{D}}{\mathrm{D}t} \;\rightarrow\; \mathcal{C}\frac{\partial}{\partial t} + u\frac{\partial}{\partial x} + v\frac{\partial}{\partial y} + \mathcal{O}\left(\xi^2\right). \tag{2.77}$$

Substituting into the *rSW Potential Vorticity Equation*, (2.68) reveals curvature (ξ) terms of $\mathcal{O}\left(\frac{\xi^2}{\varphi_q}\left[\mathcal{R}\left[\mathcal{C},1\right],\sigma,\beta,\xi^2\right]\right)$.

Since the ξ terms are negligible, we let $\varphi_q = \max(\mathcal{R}, \sigma, \beta)$, and for a system accurate to $\mathcal{O}(\alpha)$, ξ is limited to

$$\xi^2 \lesssim \alpha \min\left(1, \frac{\varphi_q}{\mathcal{R}}\left[1, \frac{1}{\mathcal{C}}\right]\right). \tag{2.78}$$

With the above scaling assumption, the oblique Cartesian rSW equations to order α are obtained from (2.66) - (2.68),

$$\mathcal{R}\frac{\mathrm{D}u}{\mathrm{D}t} - v(1+\beta y) = -\frac{\partial h}{\partial x}, \tag{2.79}$$

$$\mathcal{R}\frac{\mathrm{D}v}{\mathrm{D}t} + u(1+\beta y) = -\frac{\partial h}{\partial y}, \tag{2.80}$$

$$\frac{\mathrm{D}q}{\mathrm{D}t} = 0, \tag{2.81}$$

where potential vorticity q is defined as

$$(1+\sigma h)q = \frac{1}{\varphi_q}\left(-\sigma h + \mathcal{R}\left(\frac{\partial v}{\partial x} - \frac{\partial u}{\partial y}\right) + \left(\beta y - \frac{1}{2}\xi^2\left(x^2+y^2\right) + \ldots\right)\right), \tag{2.82}$$

and the horizontal advective derivative is

$$\mathcal{C}\frac{\partial}{\partial t} + u\frac{\partial}{\partial x} + v\frac{\partial}{\partial y}. \tag{2.83}$$

The dimensionless parameters are

$$\mathcal{R} \sim \frac{U}{fL} \quad \xi \sim \frac{L}{r_0} \quad \beta \sim \xi\cot\Lambda_0 \quad \sigma \sim \frac{\Delta H}{H} \quad \varphi_q \sim \max(\mathcal{R}, \sigma, \beta, \xi^2). \tag{2.84}$$

From (2.78), the Cartesian representation holds for

$$\xi^2 \lesssim \alpha \min\left(1, \frac{\varphi_q}{\mathcal{R}}\left[1, \frac{1}{\mathcal{C}}\right]\right), \tag{2.85}$$

and from (2.64) and (2.65) the rSW solution regime is defined when

$$\gamma_p, \gamma_u \lesssim \varphi_q\alpha, \qquad \gamma_\rho \lesssim \varphi_q\alpha\min\left(\sigma, \frac{1}{\mathcal{C}}\right), \qquad \mathcal{E}k \lesssim \varphi_q\alpha\min\left(\frac{1}{\varepsilon_L^2}, \frac{1}{\gamma_u}\right), \tag{2.86}$$

$$\varepsilon_L \lesssim \varphi_q\alpha\min\left[\frac{1}{\xi}, \frac{\xi}{\beta}\right], \qquad \varepsilon_L^2 \lesssim \varphi_q\alpha\frac{1}{\mathcal{R}}\min\left[1, \frac{1}{\mathcal{C}}\right]. \tag{2.87}$$

where the ε and γ terms are defined in (2.33) and (2.34).

The additional *rSW Height-Divergence* equation, from (2.56), is

$$\delta = -\frac{\sigma}{1+\sigma h}\frac{\mathrm{D}h}{\mathrm{D}t}, \tag{2.88}$$

with horizonal divergence, δ,

$$\delta = \frac{\partial u}{\partial x} + \frac{\partial v}{\partial y}. \tag{2.89}$$

Chapter 3

Rotating Shallow Water - Textbook and Beyond

Now that the origins of the full rSW equations from the Navier-Stokes equations have been explained, we seek to further analyse particular solution classes. We begin by specifying parameter range where the Rossby number, $\mathcal{R}$, is the sole free parameter. The full rSW equations are considered, and following a standard textbook analysis, area integral properties of the rSW equations are discussed. Linear wave equations and quasigeostrophic theory are recovered as leading order $\mathcal{R}$ equations, and give a simplified interpretation of atmospheric behaviour discussed in most introductory geophysical fluid textbooks [2], [10]. The textbook discussion is provided as a starting point for parallel analysis with the first correction rSW equations, which includes the largest $\mathcal{R}$ terms, and are the first point of interest beyond the textbook level [12] .

3.1 Parameter Regimes

We now leave the generality maintained in the previous chapter and concentrate on particular solution regimes where the remaining parameters - σ, $\mathcal{C}$, α, β and ξ - are defined in terms of the geostrophically significant Rossby number, $\mathcal{R}$. The values are chosen so distinct solution types appear, although the solution types are not restricted to these particular choices of scales. A summary of the scale regimes, and solutions that arise from each, is provided in Table 3.1.

Height variation, σ. We scale the height variation as the Rossby number, $\sigma \sim \mathcal{R}$, as in [9]. Studies where this assumption is relaxed specify the Burger number, $\mathcal{B} = \frac{\sigma}{\mathcal{R}}$, and so comparison to these studies are made only for the case with $\mathcal{B} = 1$.

Advective time scale, $\mathcal{C}$. In the geostrophic assumption, the relative time scale was bounded above by $\mathcal{C} \sim \mathcal{R}^{-1}$. This is the time scale used in recovering gravity waves. Quasigeostrophic theory is recovered at the minimum time scale of $1 \sim \mathcal{C}$, and in addition to both endpoints, we consider Rossby waves at an intermediate time scale, $\mathcal{C} \sim \mathcal{R}^{-\frac{1}{2}}$.

System order of accuracy, α. In the textbook discussion, Section 3.2, linear gravity waves and quasigeostrophy are recovered when the order of accuracy of the system, $\alpha \sim \mathcal{R}$, while linear Rossby waves have larger corrections of $\alpha \sim \mathcal{R}^{\frac{1}{2}}$. Both the first correction gravity wave and quasigeostrophic equations, Section 3.3, include the $\mathcal{O}(\mathcal{R})$ terms, and are accurate to $\alpha \sim \mathcal{R}^2$.

Planetary number, β. In most cases, we restrict the planetary number to $\beta \lesssim \mathcal{R}$. The exception are Rossby waves, Section 3.2.2, where $\beta \sim \mathcal{R}^{\frac{1}{2}}$. Further restrictions result from horizontal periodicity in (3.9).

Potential vorticity scale, φ_q. The dynamically active component of the potential vorticity, q, defined in (2.62), scales as φ_q, where $\varphi_q \sim \max(\mathcal{R}, \sigma, \beta, \xi^2)$. From the discussion in Section 2.3.3 and the above $\sigma \sim \mathcal{R}$ specification, φ_q reduces to $\varphi_q \sim \max(\mathcal{R}, \beta)$. Only in specifying Rossby waves is $\varphi_q \sim \mathcal{R}^{\frac{1}{2}}$. In all other cases, $\varphi_q \sim \mathcal{R}$.

Relative length scales, ξ. The ratio of characteristic length to Earth's radius is limited by the Cartesian coordinate assumption, from (2.85),

$$\xi^2 \lesssim \alpha \min\left(1, \frac{\varphi_q}{\mathcal{R}}\left[1, \frac{1}{\mathcal{C}}\right]\right). \tag{3.1}$$

For synoptic and mesoscales flows, we will further restrict $\xi \gtrsim \mathcal{R}$, except where a more flexible scaling is required, where $\xi \gtrsim \mathcal{R}^{\frac{3}{2}}$. Further restrictions on ξ arise from horizontal periodicity in (3.9).

Characteristic latitude, Λ_0. In defining $\beta = \xi \cot \Lambda_0$, and specifying ξ and β, we determine the characteristic latitude,

$$\cot \Lambda_0 \sim \frac{\beta}{\xi}. \tag{3.2}$$

Table 3.1: A summary of the periodic rSW scale regimes and exact solutions, where $\mathcal{C}$ is the advective time scale, α is the order of accuracy of the system, ξ is the ratio of length scale to Earth's radius, β is the planetary number and $\varphi_q = \max(\mathcal{R}, \beta)$.

	Dimensionless Parameters					Exact Solution
	$\mathcal{C}$	α	ξ	β	φ_q	
Section 3.2.1 Linear gravity waves	$\mathcal{R}^{-1}$	$\mathcal{R}$	$\mathcal{R}$	$\lesssim \mathcal{R}^2$	$\mathcal{R}$	Fourier solution $\omega = \pm\sqrt{1+k^2+l^2}$
Section 3.2.2 Linear Rossby waves	$\mathcal{R}^{-\frac{1}{2}}$	$\mathcal{R}^{\frac{1}{2}}$	$\lesssim \mathcal{R}^{\frac{1}{2}}$	$\mathcal{R}^{\frac{1}{2}}$	$\mathcal{R}^{\frac{1}{2}}$	Fourier solution $\omega = \frac{-k}{1+k^2+l^2}$
Section 3.2.3 Leading order quasigeostrophy	1	$\mathcal{R}$	$\mathcal{R}$	with $\beta \sim \mathcal{R}$ w/o $\beta \lesssim \mathcal{R}^2$	$\mathcal{R}$	Travelling dipole Solution
Section 3.3.1 Nonlinear gravity waves	$\mathcal{R}^{-1}$	$\mathcal{R}^2$	$\mathcal{R}^{\frac{3}{2}}$	$\lesssim \mathcal{R}^3$	$\mathcal{R}$	Travelling wave solution
Section 3.3.3 First correction quasigeostrophy	1	$\mathcal{R}^2$	$\mathcal{R}^{\frac{3}{2}}$	1st corr. $\beta \sim \mathcal{R}^2$ w/o $\beta \lesssim \mathcal{R}^3$	$\mathcal{R}$	–

3.1.1 Horizontally Periodic Boundary Conditions

Since the experimental component of this study focuses on solutions which are horizontally periodic over the domain $D = [-D_x, D_x] \times [-D_y, D_y]$, this case will be considered in the following analysis. A particular limitation of the periodic case is the restriction of position-dependent Coriolis terms. The following change of variables allows for small β corrections, while retaining a periodic formulation in the *rSW Potential Vorticity Equation*:

$$q\Big|_{\text{aperiodic}} \Rightarrow q\Big|_{\text{periodic}} + \frac{\beta}{\varphi_q} y \tag{3.3}$$

and

$$\frac{\mathrm{D}q}{\mathrm{D}t}\Big|_{\text{aperiodic}} \Rightarrow \frac{\mathrm{D}q}{\mathrm{D}t}\Big|_{\text{periodic}} + \frac{\beta}{\varphi_q} v. \tag{3.4}$$

where $\varphi_q = \max(\mathcal{R}, \beta)$.

Substituting the above parameter restrictions and change of variable in q into the *rSW Momentum Equations*, (2.79) and (2.80), and the *rSW Potential Vorticity Equation*, (2.81),

$$\mathcal{R}\frac{\mathrm{D}u}{\mathrm{D}t} - v\,(1+\beta y) = -\frac{\partial h}{\partial x}, \tag{3.5}$$

$$\mathcal{R}\frac{\mathrm{D}v}{\mathrm{D}t} + u\,(1+\beta y) = -\frac{\partial h}{\partial y}, \tag{3.6}$$

$$\frac{\mathrm{D}q}{\mathrm{D}t} + \frac{\beta}{\varphi_q}v = 0, \tag{3.7}$$

where

$$(1+\mathcal{R}h)q = \frac{\mathcal{R}}{\varphi_q}\left(-h + \left(\frac{\partial v}{\partial x} - \frac{\partial u}{\partial y}\right)\right) - \frac{1}{\varphi_q}\left(\mathcal{R}\beta y h + \frac{1}{2}\xi^2\left(x^2+y^2\right)\right). \tag{3.8}$$

The class of periodic solutions is obtained when all ξ and β terms are negligible, except the β term in (3.7). This arises with the additional restrictions:

$$\beta \lesssim \alpha\frac{\varphi_q}{\mathcal{R}}\min\left(1, \frac{1}{\mathcal{C}}\right) \qquad \xi^2 \lesssim \alpha\varphi_q. \tag{3.9}$$

A summary of the scale regimes is provided in Table 3.1.

3.1.2 Integral Constraints - Full rSW

An interesting consequence of the above equations is the area integral conservation of four parameters - divergence, vorticity, height and energy [10]. The area integral is the mean value, and its conservation implies a zero mean. In this section we give an outline of the proofs for each conserved parameter, which will be followed in Sections 3.2.4 and 3.3.4 when we consider the whether conservation holds for the asymptotic models.

Restricting solutions to the periodic u, v, h and q simplifies the discussion since spatial derivatives of periodic functions have identically zero area integrals, (D.1) and (D.2). Since divergence, δ, and vorticity, ζ, are defined as spatial derivatives of periodic u and v,

$$\int_D \delta = 0 \quad \text{and} \quad \int_D \zeta = 0. \tag{3.10}$$

where

$$\delta = \frac{\partial u}{\partial x} + \frac{\partial v}{\partial y} \quad \text{and} \quad \zeta = \frac{\partial v}{\partial y} - \frac{\partial u}{\partial x} \tag{3.11}$$

Conservation of the remaining two parameters, height, h, and energy, E, is dependent upon the *rSW Height-Divergence Equation*, (2.88), which follows from the above *rSW Momentum Equations* (see Section 2.3.2)

$$\delta = -\frac{\mathcal{R}}{1+\mathcal{R}h}\frac{\mathrm{D}h}{\mathrm{D}t}. \tag{3.12}$$

By rewriting the above *rSW Height-Divergence Equation* as

$$\delta = -\mathcal{R}\left(\mathcal{C}\frac{\partial h}{\partial t} + \frac{\partial}{\partial x}(uh) + \frac{\partial}{\partial y}(vh)\right), \tag{3.13}$$

it becomes apparent that

$$\mathcal{R}\mathcal{C}\frac{\partial}{\partial t}\int_D h = -\int_D \delta = 0. \tag{3.14}$$

The conservation of energy E, as defined below, is derived from adding the *rSW Momentum Equations*, multiplied by $u(1+\mathcal{R}h)$ and $v(1+\mathcal{R}h)$ respectively, and substituting the *rSW Height-Divergence Equation*, as explained in [10]:

$$\frac{\partial}{\partial t}\int_D E = 0 \tag{3.15}$$

where

$$E = (1+\mathcal{R}h)\left(u^2+v^2\right) + h^2 \tag{3.16}$$

3.2 Leading Order Equations - Strictly Textbook

This textbook analysis follows an introductory discussion of rSW, as in [2] and [10]. Focusing on solutions at specific time scales reveals two types of linear wave solutions[1] - gravity and Rossby waves - and a zero frequency balanced solution. The scale assumptions for each case are summarized in Table 3.1.

3.2.1 Linear Gravity Waves

Linear gravity waves are recovered at the following scales, from Section 3.1:

$$\mathcal{C} \sim \mathcal{R}^{-1}, \quad \alpha \sim \mathcal{R}, \quad \beta \lesssim \mathcal{R}, \quad \varphi_q \sim \mathcal{R}. \quad \text{and} \quad \xi \sim \mathcal{R}.$$

[1] Additional wave solutions are supported at leading order, such as the Kelvin wave in the presence of a lateral boundary and topographic waves caused by a varying lower boundary [2].

The additional periodic restrictions, (3.9), limit $\beta \lesssim \mathcal{R}^2$. The characteristic latitude restriction, (3.2), is $\cot \Lambda_0 \lesssim \mathcal{R}$, spanning upper latitudes to polar regions.

The leading order equations are linear in u, v and h, which implies solutions of wave form. That is, u, v and h are constant multiples of the wave function $e^{i(kx+ly-\omega t)}$, where k and l are spatial wavenumbers, and ω is a temporal wave frequency. Substituting the wave solution into (3.5) - (3.8) [2],

$$-i\omega u - v = -ikh \tag{3.17}$$

$$-i\omega v + u = -ilh, \tag{3.18}$$

$$\omega \mathcal{R}^{-1} q = 0, \tag{3.19}$$

where

$$q = kv - lu + ih. \tag{3.20}$$

Non-trivial solutions exist when the dispersion relation is satisfied,

$$\mathcal{R}^{-1}\omega\left(-\omega^2 + 1 + k^2 + l^2\right) = 0. \tag{3.21}$$

The first case, where $\omega = \pm\sqrt{1 + k^2 + l^2}$, is the known form of rotating gravity waves [2]. The second case, where $\omega = 0$, yields the balanced solution, which remains constant at this time scale. Further analysis of these balanced dynamics is revealed in the quasigeostrophic solution class.

3.2.2 Linear Rossby Waves

Linear Rossby waves are recovered when (3.7) balances linear advection and the β effect, or $\mathcal{C}\mathcal{R} \sim \frac{\beta}{\varphi_q}$. One choice of scales is given below, from Section 3.1:

$$\mathcal{C} \sim \mathcal{R}^{-\frac{1}{2}}, \quad \alpha \sim \mathcal{R}^{\frac{1}{2}}, \quad \beta \sim \mathcal{R}^{\frac{1}{2}}, \quad \varphi_q \sim \mathcal{R} \quad \text{and} \quad \mathcal{R} \lesssim \xi \lesssim \mathcal{R}^{\frac{1}{4}}.$$

The adddditional periodic restrictions, (3.9), limit $\xi \lesssim \mathcal{R}^{\frac{1}{2}}$. Since β is fixed , while ξ can vary, the characteristic latitude restriction, (3.2), is $1 \lesssim \cot \Lambda_0 \lesssim \mathcal{R}^{-\frac{1}{2}}$, spanning subequatorial to midlatitudes. This is the case of equatorial Rossby waves.

The leading order terms yield a linear set of equations, and wave solutions are sought [2]:

$$-v = -ikh, \tag{3.22}$$

$$u = -ilh, \tag{3.23}$$

$$\mathcal{R}^{-\frac{1}{2}}\omega q + v = 0, \tag{3.24}$$

where

$$q = \mathcal{R}^{\frac{1}{2}}\left(kv - lu + ih\right). \tag{3.25}$$

Replacing q with the above definition and u and v with the geostrophic velocities, the dispersion relation is

$$\left(1 + k^2 + l^2\right)\omega + k = 0. \tag{3.26}$$

In this case only negative zonal phase velocity is permitted (westward in standard coordinates), and is the known Rossby wave [2].

3.2.3 Quasigeostrophy

The zero wave frequency solution arising in the short time scale solution (Section 3.2.1) is included in a general class of solutions where, from Section 3.1:

$$\mathcal{C} \sim \mathcal{R}^{-1}, \quad \alpha \sim \mathcal{R}, \quad \beta \lesssim \mathcal{R}, \quad \varphi_q \sim \mathcal{R}, \quad \text{and} \quad \xi \lesssim \mathcal{R}^{\frac{1}{2}}.$$

The additional periodic restrictions, (3.9), limit $\xi \lesssim \mathcal{R}$. Solutions include β effects in (3.7) when $\beta \sim \mathcal{R}$, and do not include β effects when $\beta \lesssim \mathcal{R}^2$. The characteristic latitude restriction, (3.2), is then $\cot\Lambda_0 \lesssim 1$ (with β effects, spanning midlatitudes to polar regions), or $\cot\Lambda_0 \lesssim \mathcal{R}$ (without β effects, spanning upper latitudes to polar regions).

At leading order, the *rSW Momentum Equations* (3.5), (3.6) become

$$-v = -\frac{\partial h}{\partial x}, \tag{3.27}$$

$$u = -\frac{\partial h}{\partial y}. \tag{3.28}$$

Substituting for u and v in the *rSW Potential Vorticity Equation*, (3.7), reduces the system to one equation [2]:

$$\frac{\partial q}{\partial t} + J\left(h, q\right) + \frac{\beta}{\mathcal{R}}\frac{\partial h}{\partial x} = 0, \tag{3.29}$$

where (3.8) becomes

$$q = \left(\nabla^2 - 1\right)h, \tag{3.30}$$

and the Jacobian of two functions is defined as

$$J(f, g) = \frac{\partial f}{\partial x}\frac{\partial g}{\partial y} - \frac{\partial f}{\partial y}\frac{\partial g}{\partial x}. \tag{3.31}$$

Strictly balanced flow is recovered when $\beta \lesssim \mathcal{R}^2$, while $\beta \sim \mathcal{R}$ allows for the formation of Rossby waves. Only the first case, without β effects, will be considered in the following chapters, and for the travelling dipole solution in the next section, while $\beta \sim \mathcal{R}$ case will be investigated the integral constraints of Section 3.2.4.

Travelling Dipole Solution

In the absence of β effects, a travelling dipole solution, advecting at a constant velocity $c > 0$ (Figure 3.1) is obtained by letting $\frac{\partial}{\partial t} = -c\frac{\partial}{\partial x}$ [5]. Substituting into the above potential vorticity advection (3.29),

$$J((h + cy), q) = 0, \tag{3.32}$$

which has the exact solution for $\sigma \geq 0$

$$q = -\sigma(h + cy) \tag{3.33}$$

For a dipole of radius a, σ is defined as

$$\sigma = \begin{cases} \sigma & r < a \\ 0 & r > a \end{cases} \tag{3.34}$$

and potential vorticity, q, is defined as a piecewise solution

$$q = \begin{cases} -\sigma(h + cy) & r < a \\ 0 & r > a \end{cases} \tag{3.35}$$

The complete solution form is given in Appendix E, where h, q and $\frac{\partial h}{\partial r}$ are continuous across the boundary at $r = a$, while $\frac{\partial q}{\partial r}$ is discontinuous.

3.2.4 Integral Constraints - Leading Order

The area integrals considered in Section 3.1.2 for the full rSW equations are now revisited for the leading order equations. In addition to divergence, vorticity, height and energy, potential vorticity is conserved in the leading order equations. Conservation of divergence and vorticitiy follow in the same manner as the full rSW case (3.10), and conservation of potential vorticity, height and energy in the linear wave equations follows directly. We can now focus on potential vorticity, height and energy conservation in the above quasigeostrophic equations.

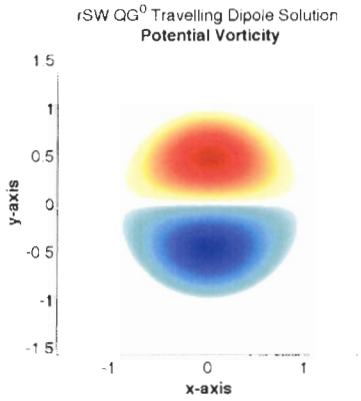

(a) Travelling dipole initial condition.

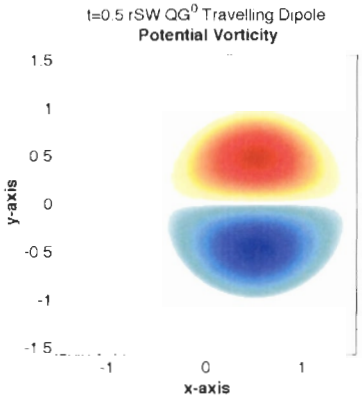

(b) Travelling dipole with speed c=1 at time t=0.5.

Figure 3.1: Travelling dipole solution to the leading order quasigeostrophic equations, with speed c=1.(a) Initial condition. (b) Time t = 0.5.

Conservation of potential vorticity is obtained by integrating (3.29), and noting that the area integral of a Jacobian is zero (where both functions are periodic, (D.2)).

$$\frac{\partial}{\partial t}\int_D q \;=\; -\int J(h,q)+\frac{\beta}{\mathcal{R}}v \;=\; 0. \tag{3.36}$$

Similarly, conservation of height is obtained by solving (3.30) for h.

$$\frac{\partial}{\partial t}\int_D h \;=\; \frac{\partial}{\partial t}\int_D \nabla^2 h - q \;=\; -\frac{\partial}{\partial t}\int_D q \;=\; 0. \tag{3.37}$$

This implies that an initially area-symmetric q ensures both h and q remain symmetric in time.

Conservation of the leading order quasigeostrophic energy,

$$E \;=\; \left(\frac{\partial h}{\partial y}\right)^2+\left(\frac{\partial h}{\partial x}\right)^2+h^2. \tag{3.38}$$

is shown by considering

$$\int_D \frac{\partial}{\partial t}(hq) \;=\; \int_D \boldsymbol{h}\frac{\partial q}{\partial t}+q\frac{\partial h}{\partial t} \tag{3.39}$$

which reduces by substituting (3.30) and (3.29), and using identities (D.3) and (D.6),

$$\frac{\partial}{\partial t}\int_D E \;=\; 0. \tag{3.40}$$

3.3 First Correction Equations - Beyond the Textbook

In the previous textbook analysis, we discussed the presence of both gravity and Rossby wave and balances solutions. These solution types are no longer distinct where the largest $\mathcal{R}$ correction terms are added. In venturing past the textbook analysis, we focus on methods for studying each type of flow independently.

3.3.1 Nonlinear Gravity Waves

Nonlinear gravity waves are recovered when, from Section 3.1:

$$\mathcal{C} \sim \mathcal{R}^{-1}, \quad \alpha \sim \mathcal{R}, \quad \beta \lesssim \mathcal{R}, \quad \varphi_q \sim \mathcal{R}, \quad \text{and} \quad \xi \sim \mathcal{R}^{\frac{3}{2}}.$$

The additional periodic restrictions (3.9) limit $\beta \lesssim \mathcal{R}^3$. The characteristic latitude restriction, (3.2), is $\cot \Lambda_0 \lesssim \mathcal{R}^2$, which spans polar regions only.

The leading order gravity wave equations, from Section 3.2.1, support three wave modes - two opposite travelling gravity wave solutions, and a balanced solution. In the first correction study, where $\mathcal{R}$ terms are included in the equations, we consider a solution regime where only gravity wave solutions are supported by following the method outlined in [8].

The main reduction is to the special case of uniform potential vorticity, or

$$(1 + \mathcal{R}h)\, q \;=\; \frac{\partial v}{\partial x} - \frac{\partial u}{\partial y} - h \;=\; 0. \tag{3.41}$$

Substituting for h in the *rSW Momentum Equations* yields the *rSW Wave* equations,

$$\frac{\partial u}{\partial t} + \mathcal{R}\left(u\frac{\partial u}{\partial x} + v\frac{\partial u}{\partial y}\right) - v \;=\; -\frac{\partial}{\partial x}\left(\frac{\partial v}{\partial x} - \frac{\partial u}{\partial y}\right), \tag{3.42}$$

$$\frac{\partial v}{\partial t} + \mathcal{R}\left(u\frac{\partial v}{\partial x} + v\frac{\partial v}{\partial y}\right) + u \;=\; -\frac{\partial}{\partial y}\left(\frac{\partial v}{\partial x} - \frac{\partial u}{\partial y}\right). \tag{3.43}$$

Travelling Wave Solution

One dimensional travelling wave solutions, considered here[2] in x, are formed by letting $\frac{\partial}{\partial t} = -c\frac{\partial}{\partial x}$ and $\frac{\partial}{\partial y} \equiv 0$. Details of the following are left to Appendix F.

Substituting the wave form into the momentum equations yields [8],

$$\frac{\partial u}{\partial x} \;=\; v\left(\frac{(c - \mathcal{R}u)^2}{c - (c - \mathcal{R}u)^3}\right) \tag{3.44}$$

$$\frac{\partial v}{\partial x} \;=\; \frac{u}{c - \mathcal{R}u}. \tag{3.45}$$

[2]The equations for the travelling wave in y are obtained by interchanging u and v and setting y to $-y$.

The equations are linearized about the fixed point $u = 0 = v$ by letting $c - \mathcal{R}u \approx c$, revealing an exact periodic solution,

$$u = iA\frac{c}{\sqrt{c^2-1}}e^{i\left(c^2-1\right)^{-\frac{1}{2}}x} - iB\frac{c}{\sqrt{c^2-1}}e^{-i\left(c^2-1\right)^{-\frac{1}{2}}x} \tag{3.46}$$

$$v = Ae^{i\left(c^2-1\right)^{-\frac{1}{2}}x} + Be^{-i\left(c^2-1\right)^{-\frac{1}{2}}x}. \tag{3.47}$$

for initial values A and B. Solutions are periodic for $|c| > 1$, with wavelength $\lambda = 2\pi\sqrt{c^2-1}$.

Returning to the nonlinear equations (3.44) and (3.45), since $\frac{\partial u}{\partial x}$ and $\frac{\partial v}{\partial x}$ are undefined for $\mathcal{R}u = c - c^{\frac{1}{3}}$ and $\mathcal{R}u = c$ respectively, for $c > 0$, $\mathcal{R}u \in \left(-\infty, c - c^{\frac{1}{3}}\right) \cup \left(c - c^{\frac{1}{3}}, c\right) \cup (c, \infty)$. Solutions sufficiently close to the fixed point $u = 0 = v$ such that $\mathcal{R}u < c - c^{\frac{1}{3}}$ will remain in that interval. Similarly, for $c < 0$ the limited range near the fixed point is $\mathcal{R}u > c - c^{\frac{1}{3}}$.

Sufficient manipulation of (3.44) and (3.45) reveals the first integral relation [8],

$$\left(1 - \frac{1}{(c-\mathcal{R}u)^2}\right)u^2 + v^2 = C, \tag{3.48}$$

for a constant C, and periodic solutions exist for $|c - \mathcal{R}u| > 1$. The phase portrait for $c = 2$ and $\mathcal{R} - 0.1$ is shown in Figure 3.2.

Combining the two restrictions on u, periodic solutions can occur for $c > 0$ when $\mathcal{R}u < c - c^{\frac{1}{3}} < c - 1$, or $c > 1$. A similar argument for $c < 0$ shows periodic solutions when $c < -1$, and $\mathcal{R}u > c - c^{\frac{1}{3}}$. This range of c is consistent with the linearized case, $|c| > 1$.

3.3.2 Rossby Waves

At the intermediate time scale, $\mathcal{C} \sim \mathcal{R}^{-\frac{1}{2}}$, the first correction equations include $\mathcal{R}^{\frac{1}{2}}$ terms. The emergence of Rossby waves relies on the planetary scaling $\beta \sim \mathcal{R}^{\frac{1}{2}}$; thus position dependent terms are inevitable, and periodic solutions cannot exist at first corrections. This implies that Rossby waves in other solution classes, notably the quasigeostrophic case, must remain leading order to support periodic solutions.

3.3.3 Quasigeostrophy

The quasigeostrophy scales, from Section 3.2.3, are expanded to first correction, from Section 3.1, by

$$\mathcal{C} \sim \mathcal{R}^{-1}, \quad \alpha \sim \mathcal{R}^2, \quad \beta \lesssim \mathcal{R}, \quad \varphi_q \sim \mathcal{R}, \quad \text{and} \quad \xi \sim \mathcal{R}.$$

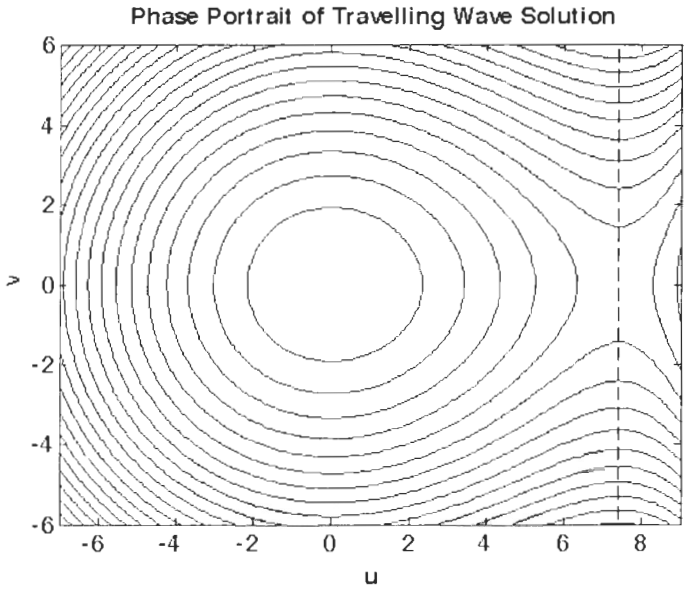

Figure 3.2: Phase portrait for the travelling wave solution to *rSW Wave* for $c = 2$ and $\mathcal{R} = 0.1$. Periodic solutions remain to the left of the dashed line at $\frac{1}{\mathcal{R}}\left(c - c^{\frac{1}{3}}\right) \approx 7.4$.

The additional periodic restrictions, (3.9), limit $\xi \sim \mathcal{R}^{\frac{3}{2}}$ and $\beta \sim \mathcal{R}^2$, (with first correction β effects), or $\beta \lesssim \mathcal{R}^3$ (without β effects). The characteristic latitude restriction, (3.2), is then $\cot \Lambda_0 \lesssim \mathcal{R}^{\frac{1}{3}}$ (with first correction β effects, spanning just above midlatitudes to polar regions), or $\cot \Lambda_0 \lesssim \mathcal{R}^2$ (without β effects, spanning polar regions only).

While only balanced flow, and Rossby waves when β effects are included, are supported at leading order, Section 3.2.3, the first correction quasigeostrophy equations contain three time derivatives, and enable the formation of gravity wave solutions. Thus, we reformulate following the method in [9] to obtain solutions devoid of gravity wave behaviour to $\mathcal{O}\left(\mathcal{R}^2\right)$. This method involves first rewriting the primitive variables in terms of potentials F, G and H:

$$u = -\frac{\partial H}{\partial y} - F, \tag{3.49}$$

$$v = \frac{\partial H}{\partial x} - G, \tag{3.50}$$

$$h = H + \frac{\partial F}{\partial y} - \frac{\partial G}{\partial x}, \tag{3.51}$$

and further expanding each potential in an asymptotic series for $\mathcal{R} < 1$

$$F = F_0 + \mathcal{R}F_1 + \mathcal{O}\left(\mathcal{R}^2\right), \tag{3.52}$$

$$G = G_0 + \mathcal{R}G_1 + \mathcal{O}\left(\mathcal{R}^2\right), \tag{3.53}$$

$$H = H_0 + \mathcal{R}H_1 + \mathcal{O}\left(\mathcal{R}^2\right). \tag{3.54}$$

Setting $\mathcal{R} = 0$, the equations must be consistent with the leading order equations (3.29) and (3.30), and the *rSW* QG^0 equations are

$$\frac{\partial q}{\partial t} + J(H_0, q) = 0 \tag{3.55}$$

where

$$\left(\nabla^2 - 1\right) H_0 = q \tag{3.56}$$

$$F_0 = 0 \tag{3.57}$$

$$G_0 = 0 \tag{3.58}$$

By defining q as a leading order variable, we retain the above definition of q to all orders of $\mathcal{R}$. Substituting the expanded potentials into the definition of q, (2.82), all $\mathcal{R}$ corrections add to zero:

$$\left(\nabla^2 - 1\right) H_1 - H_0 \left(\nabla^2 - 1\right) H_0 = 0. \tag{3.59}$$

The momentum equations are reformulated by adding spatial derivatives of the first $\mathcal{O}(\mathcal{R})$ correction of the *rSW Height-Divergence Equation*, (2.88):

$$\frac{\partial F_1}{\partial x} + \frac{\partial G_1}{\partial y} = \frac{\partial H_0}{\partial t} \tag{3.60}$$

which cancel out the time derivatives and leave the decoupled equations

$$\left(\nabla^2 - 1\right) F_1 = J\left(\frac{\partial H_0}{\partial x}, H_0\right) \tag{3.61}$$

$$\left(\nabla^2 - 1\right) G_1 = J\left(\frac{\partial H_0}{\partial y}, H_0\right). \tag{3.62}$$

All variables are thus defined in terms of H_0 and therefor q, which evolves in time according to the *rSW Potential Vorticity Equation* (2.81),

$$\frac{\partial q}{\partial t} = -J(H_0, q) + \mathcal{R}\left(-J(H_1, q) + F_1 \frac{\partial q}{\partial x} + G_1 \frac{\partial q}{\partial y}\right) - \frac{\beta}{\mathcal{R}} \frac{\partial H_0}{\partial x}. \tag{3.63}$$

The *rSW* QG^{+1} equations are comprised of (3.63), (3.59), (3.61) and (3.62), where q is defined in (3.56).

3.3.4 Integral Constraints - First Correction

We now revisit the area integral conservation properties from Sections 3.1.2 and 3.2.4 for full rSW and leading order equations. Recalling the discussion for the full rSW equations, the *rSW Height-Divergence Equation* (3.12) was necessary in deriving conservation of energy and height in the full rSW equations. While the *rSW Height-Divergence Equation* follows from the *rSW Wave* equations, it is not immediately apparent that the *rSW Height-Divergence Equation* (3.12) is retained in the *rSW* QG^{+1} model. So while energy, as defined in (3.15), height, h, and potential vorticity, q, remain conserved in the *rSW Wave* model (where by definition $q \equiv 0$), similar relations for the *rSW* QG^{+1} model are not immediately apparent. An outline of the results for the *rSW* QG^{+1} models are given here, with details left to Appendix D.

Area integrals of the potential functions F_1 and G_1, and thus velocities u and v (from (3.49) and (3.50)) , are obtained by integrating (3.61) and (3.62)

$$\int_D F_1 \;=\; \int_D \nabla^2 F_1 + J\left(\frac{\partial H_0}{\partial y}, H_0\right) \;=\; 0, \tag{3.64}$$

$$\int_D G_1 \;=\; \int_D \nabla^2 G_1 + J\left(\frac{\partial H_0}{\partial x}, H_0\right) \;=\; 0. \tag{3.65}$$

However, conservation of height, defined in (3.51), does not follow in the same manner, since by integrating (3.59),

$$\int_D H_1 \;=\; \int_D \nabla^2 H_0 - q \;= -\int_D H_0(\nabla^2 - 1)H_0 \;=\; -\int_D E_0 \tag{3.66}$$

where E_0 is the leading order quasigeostrophic energy,

$$E_0 \;=\; \left(\frac{\partial H_0}{\partial x}\right)^2 + \left(\frac{\partial H_0}{\partial y}\right)^2 + H_0^2, \tag{3.67}$$

and is not necessarily zero in the first correction equations. Conservation of E_0 is determined by considering

$$\int_D \frac{\partial}{\partial t}(H_0 q) \;=\; \int_D H_0 \frac{\partial q}{\partial t} + q\frac{\partial H_0}{\partial t}. \tag{3.68}$$

which reduces to (see Appendix D)

$$-\frac{1}{2}\int_D \frac{\partial}{\partial t} E_0 \;=\; \mathcal{R}\int_D H_0\left(-J(H_1, q) + F_1\frac{\partial q}{\partial x} + G_1\frac{\partial q}{\partial y}\right). \tag{3.69}$$

This is sufficient to show total height, (3.51), is conserved to $\mathcal{O}\left(\mathcal{R}^2\right)$.

Conservation of potential vorticity follows from integrating (3.63) (see Appendix D),

$$\int_D \frac{\partial q}{\partial t} = \int_D -J(H_0, q) + \mathcal{R}\left(-J(H_1, q) - F_1\frac{\partial q}{\partial x} - G_1\frac{\partial q}{\partial y}\right) - \frac{\beta}{\mathcal{R}}\frac{\partial H_0}{\partial x} = 0. \quad (3.70)$$

Chapter 4

Numerical Methods

This chapter goes through the numerical implementation of the balanced $rSW\ QG^0$ and $rSW\ QG^{+1}$ equations and the $rSW\ Wave$ equations formulated in the previous section. Numerical methods are outlined, from the general application of spectral methods to spatially periodic nonlinear equations, to scalar and vector integrating factor methods for each set of equations, and the selected numerical time integration methods. Freely decaying turbulent initial conditions are imposed to analyze the spectrum. Stability in the under-resolved short scales is ensured by introducing the hyperdiffusion variable, and selecting its value accordingly. Exact solutions to subsets of the equations are used to measure absolute convergence where such solutions exist, and relative convergence is measured in all other cases.

4.1 Spectral Methods

For a primitive variable $f(x, y, t)$, we apply the Fourier transform [14]:

$$f(x, y, t) = \int\int_{-\infty}^{\infty} \hat{f}(k, l, t) e^{i(kx+ly)} dk dl, \tag{4.1}$$

where

$$\hat{f}(k, l, t) = \frac{1}{4\pi^2} \int\int_{-\infty}^{\infty} f(x, y, t) e^{-i(kx+ly)} dx dy, \tag{4.2}$$

and where k, and l are wavenumbers, and x and y are spatial coordinates. Since the primitive variables are periodic in x and y, with period D_x and D_y respectively, we are able to discretise the Fourier transform [14]. The number of grid points, N_x and N_y are chosen

so that discrete wavenumbers k and l lie within:

$$k = \frac{2\pi}{D_x}\left[-\frac{N_x}{2}, \frac{N_x}{2}-1\right], \qquad l = \frac{2\pi}{D_x}\left[-\frac{N_y}{2}, \frac{N_y}{2}-1\right]. \tag{4.3}$$

Limiting the wavenumbers corresponds to the spatial discretization, $\Delta x = \frac{D_x}{N_x}$ and $\Delta y = \frac{D_y}{N_y}$ [14]. For simplicity, we let $N_x = N_y = N$ and $D_x = D_y = D$, and the discrete Fourier transform pair is:

$$f(x_m, y_n, t) = \sum_{s=-\frac{N}{2}}^{\frac{N}{2}-1} \sum_{t=-\frac{N}{2}}^{\frac{N}{2}-1} \hat{f}(k,l,t) e^{i(k_s x_m + l_t y_n)} \tag{4.4}$$

where s and t are the discrete wavenumber indices, and

$$\hat{f}(k,l,t) = \frac{1}{N^2} \sum_{m=-\frac{N}{2}}^{\frac{N}{2}-1} \sum_{n=-\frac{N}{2}}^{\frac{N}{2}-1} f(x_m, y_n, t) e^{-i(kx_m + l y_n)} \tag{4.5}$$

where n and m are the discrete spatial indices.

While linear terms, including derivatives, are easily calculated in Fourier space, nonlinear terms are not. For example, quadratic products in physical space correspond to a convolution in Fourier space,

$$\begin{aligned} \widehat{fg} &= \hat{f} \star \hat{g} \\ &= \frac{1}{N^2} \sum_{k_1, l_1} f(k_1, l_1, t) e^{-i(k_1 x + l_1 y)} dk_1 dl_1 \frac{1}{N^2} \sum_{k_2, l_2} g(k_2, l_2, t) e^{-i(k_2 x + l_2 y)} dk_2 dl_2. \end{aligned} \tag{4.6}$$

Two potential problems arise when such nonlinear terms are calculated on a discrete domain - cascading of high under-resolved wavenumbers into the fully resolved spectrum, and aliasing of wavenumbers beyond the discretized spectrum to wavenumbers within the spectrum. We define the fully resolved spectral domain as all wavenumbers where $\sqrt{k^2 + l^2} \lesssim \frac{D}{2\pi}(N-1)$, and any under-resolved modes are dampened by adding an artificial diffusion term to each time derivative:

$$\frac{\partial}{\partial t} \Rightarrow \frac{\partial}{\partial t} + \mu \left(\nabla^2\right)^4, \tag{4.7}$$

where μ is the artificial hyperdiffusion parameter, and will be selected qualitatively in Section 4.4. The fourth-order Laplacian is assumed to sufficiently diffuse the highest wavenumbers, while leaving the larger scales relatively unaffected [7].

Aliasing of higher wavenumbers is resolved by anticipating the extra $\frac{3}{2}N$ wavenumbers created by the quadratic convolution operator, (4.6) (zero-padding), and removing those extraneous wavenumbers after the multiplication (de-aliasing). This retains the consistency of the calculated solution to N modes [14].

4.1.1 Initial Conditions - Freely Decaying Turbulence

We now turn to understand the behaviour within the numerically resolved modes. With artificial diffusion acting on the highest wave modes, and zero padding ensuring a spectrally consistent solution, the numerically resolved spectrum remains. In order to understand the behaviour of an initially turbulent system within this spectrum, we the impose random turbulent initial conditions, as in [12], where the initial kinetic energy spectrum has random phase and amplitude given by

$$|E_K(k,l)| = \frac{|\vec{k}|^{\frac{m}{2}}}{\left(|\vec{k}| + |\vec{k}_0|\right)^m} \qquad |\vec{k}| = \sqrt{k^2 + l^2} \tag{4.8}$$

where the range of wavenumbers, k and l, is defined in (4.3), $|\vec{k}_0| = 1$ is the peak wavenumber and $m = 25$.

In the *rSW QG* models, $E_K(k,l)$ is the leading order kinetic energy,

$$|E_K(k,l)| = \frac{1}{2}|\vec{k}|^2|\hat{H}_0|^2. \tag{4.9}$$

where H_0 is defined in 3.59.

This differs from [12], where the total geostrophic kinetic energy is initialized[1], but is consistent with the asymptotic model in [9], where leading order and first correction are given identical initial values.

As opposed to the *rSW QG* models, where initial velocities are calculated with a single variable, the *rSW Wave* model requires both $\hat{u}$ and $\hat{v}$ to calculate the initial kinetic energy spectrum. A second condition comes from specifying initial velocities as a function of $\hat{\psi}$,

$$\hat{u} = \frac{\partial\hat{\psi}}{\partial x} \quad \text{and} \quad \hat{v} = -\frac{\partial\hat{\psi}}{\partial y}, \tag{4.10}$$

and the initial kinetic energy is given by

$$E_K(k,l) = \frac{1}{2}|\vec{k}|^2|\hat{\psi}|^2. \tag{4.11}$$

[1] In the *rSW QG* models, total geostrophic kinetic energy is $\frac{1}{2}|\vec{k}|^2|\hat{H}|^2$.

Spatial domain of $28\pi \times 28\pi$ and spatial resolution of 256×256 are also chosen for consistency with [12].

4.2 Integrating Factor Method

Since time advection of both q in the balance *rSW QG* models and u and v in the *rSW Wave* model consists of both linear and nonlinear operators, we use the known solution to the linear equations to simplify the total equation. The eighth order artificial diffusion terms in both models are linear, and by using the integrating factor method we can avoid any related high-order stability constraints. This is achieved by multiplying each set of equations by an integrating factor, which is chosen so as to group all linear terms under a single time derivative [14].

Consider first equation (3.63) of *rSW* QG^0 and *rSW* QG^{+1}, where for particular wave modes k and l,

$$\frac{\partial \hat{q}}{\partial t} + \mu |\vec{k}|^8 \hat{q} \;=\; \mathcal{N}_{\vec{k}}(\hat{q}), \tag{4.12}$$

with

$$\mathcal{N}_{\vec{k}}(\hat{q}) \;=\; -\widehat{u\frac{\partial q}{\partial x}} - \widehat{v\frac{\partial q}{\partial y}}. \tag{4.13}$$

Although u and v appear in the above equation, $\mathcal{N}_{\vec{k}} = \mathcal{N}_{\vec{k}}(\hat{q})$, since u and v are defined given $\hat{q}$ (see (3.27), (3.28) for *rSW* QG^0 and (3.61), (3.62) for *rSW* QG^{+1}).

The *rSW QG IF* equation is obtained in multiplying the above (4.12) equation by the integrating factor $e^{\mu(k^2+l^2)^4 t}$, and has the desired integrating factor form suggested above:

$$\frac{\partial}{\partial t}\left(e^{\mu|\vec{k}|^8 t}\hat{q}\right) \;=\; e^{\mu|\vec{k}|^8 t}\mathcal{N}_{\vec{k}}(\hat{q}), \tag{4.14}$$

Since *rSW Wave* is a system of two equations, we consider the matrix form for particular wave modes k and l:

$$\frac{\partial}{\partial t}\begin{bmatrix} \hat{u} \\ \hat{v} \end{bmatrix} + \vec{A}_{\vec{k}}\begin{bmatrix} \hat{u} \\ \hat{v} \end{bmatrix} \;=\; \vec{\mathcal{N}}_{\vec{k}}, \tag{4.15}$$

where

$$\vec{A}_{k,l} \;=\; \begin{bmatrix} kl + \mu\left(k^2+l^2\right)^4 & -\left(k^2+1\right) \\ 1-l^2 & -kl + \mu|\vec{k}|^8 \end{bmatrix} \quad \vec{\mathcal{N}}_{k,l} \;=\; -\begin{bmatrix} \widehat{u\frac{\partial u}{\partial x}} + \widehat{v\frac{\partial u}{\partial y}} \\ \widehat{u\frac{\partial v}{\partial x}} + \widehat{v\frac{\partial v}{\partial y}} \end{bmatrix} \tag{4.16}$$

We first simplify (4.15) by substituting the eigenvalue decomposition for $\vec{A}_{k,l}$, with eigenvectors and eigenvalues are

$$\vec{r}_1(k,l) = \begin{bmatrix} 1+k^2 \\ kl+i\omega \end{bmatrix}, \qquad \vec{r}_2(k,l) = \begin{bmatrix} 1+k^2 \\ kl-i\omega \end{bmatrix}, \tag{4.17}$$

$$\lambda_1 = \mu|\vec{k}|^8 - i\omega, \qquad \lambda_2 = \mu|\vec{k}|^8 + i\omega, \tag{4.18}$$

where $\omega = \sqrt{1+k^2+l^2}$.

Since $\begin{bmatrix} \vec{r}_1 \mid \vec{r}_2 \end{bmatrix}$ is non-singular for all $k, l \in \mathbb{R}$, given $\hat{u}(k,l,t)$ and $\hat{v}(k,l,t)$, there exist unique $\alpha(t)$ and $\beta(t)$ such that

$$\begin{bmatrix} \hat{u}(k,l,t) \\ \hat{v}(k,l,t) \end{bmatrix} = \begin{bmatrix} \vec{r}_1 \mid \vec{r}_2 \end{bmatrix} \begin{bmatrix} \alpha(t) \\ \beta(t) \end{bmatrix}. \tag{4.19}$$

Substituting (4.19) into (4.15) where $\vec{A}_{\vec{k}}$ is represented in terms of its eigenvalues and eigenvectors, and multiplying by $\begin{bmatrix} \vec{r}_1 \mid \vec{r}_2 \end{bmatrix}^{-1}$ yields,

$$\frac{\partial}{\partial t}\begin{bmatrix} \alpha(k,l,t) \\ \beta(k,l,t) \end{bmatrix} + \begin{bmatrix} \lambda_1 & 0 \\ 0 & \lambda_2 \end{bmatrix}\begin{bmatrix} \alpha(k,l,t) \\ \beta(k,l,t) \end{bmatrix} = -\begin{bmatrix} \vec{r}_1 \mid \vec{r}_2 \end{bmatrix}^{-1} \begin{bmatrix} \widehat{u\frac{\partial u}{\partial x}} + \widehat{v\frac{\partial u}{\partial y}} \\ \widehat{u\frac{\partial v}{\partial x}} + \widehat{v\frac{\partial v}{\partial y}} \end{bmatrix} \tag{4.20}$$

The *rSW Wave IF* equations are obtained in multiplying by the vector integrating factor $\begin{bmatrix} e^{\lambda_1 t} & 0 \\ 0 & e^{\lambda_2 t} \end{bmatrix}$ by the above (4.20), which has the same desired integrating factor form as equation (4.14):

$$\frac{\partial}{\partial t}\left(\begin{bmatrix} e^{\lambda_1 t} & 0 \\ 0 & e^{\lambda_2 t} \end{bmatrix}\begin{bmatrix} \alpha(k,l,t) \\ \beta(k,l,t) \end{bmatrix}\right) = \begin{bmatrix} e^{\lambda_1 t} & 0 \\ 0 & e^{\lambda_2 t} \end{bmatrix}\begin{bmatrix} \vec{r}_1 \mid \vec{r}_2 \end{bmatrix}^{-1} \vec{\mathcal{N}}_{\vec{k}}, \tag{4.21}$$

which has the same desired form as equation (4.14).

4.3 Numerical Time Integration Methods

The integrating factor equations, *rSW QG IF* (4.14), and *rSW Wave IF*, (4.21), are evolved in time by the third-order Adams-Bashforth method (AB3), where the first two steps are calculated using the third order Runge-Kutta method (RK3). Since the current equations have a time-dependent integrating factor, which would need to be recalculated at each time step, we now reformulate to remove this dependency in the overall numerical method. Given

here is the reformulation for *rSW QG IF*, while application to *rSW Wave IF* equations is sufficiently similar. Details for both the AB3 and RK3 formulations are given in Appendix G.

Third-order Adams-Bashforth, where n is the number of iterations and Δt is the uniform time step, is applied as:

$$\begin{aligned}\hat{q}_{n+1} &= e^{-\mu|\vec{k}|^8\Delta t}\hat{q}_n + \frac{\Delta t}{12}\Big(23e^{-\mu|\vec{k}|^8\Delta t}\mathcal{N}_{\vec{k}}\left(\hat{q}_n\right) \\ &\quad -16e^{-2\mu|\vec{k}|^8\Delta t}\mathcal{N}_{\vec{k}}\left(\hat{q}_{n-1}\right) + 5e^{-3\mu|\vec{k}|^8\Delta t}\mathcal{N}_{\vec{k}}\left(\hat{q}_{n-2}\right)\Big). \end{aligned} \tag{4.22}$$

Third-order Runge-Kutta is applied as:

$$\hat{q}_{n+1} = e^{-\mu|\vec{k}|^8\Delta t}\hat{q}_n + \frac{1}{6}\left(e^{-\mu|\vec{k}|^8\Delta t}s_1 + 4e^{-\frac{1}{2}\mu|\vec{k}|^8\Delta t}s_2 + s_3\right) \tag{4.23}$$

where

$$s_1 = \Delta t\mathcal{N}_{k,l}\left(\hat{q_n}\right) \tag{4.24}$$

$$s_2 = \Delta t\mathcal{N}_{k,l}\left(e^{-\frac{1}{2}\mu|\vec{k}|^8\Delta t}s_2 + \frac{1}{2}\left(\hat{q_n} + s_1\right)\right), \tag{4.25}$$

$$s_3 = \Delta t\mathcal{N}_{k,l}\left(e^{-\mu|\vec{k}|^8\Delta t}\left(\hat{q_n} - \frac{1}{2}s_1\right) + 2e^{-\frac{1}{2}\mu|\vec{k}|^8\Delta t}s_2\right).$$

The numerical integrating factor, $e^{-\mu|\vec{k}|^8\Delta t}$, is independent of accumulated time, and is expressed as a negative exponent, ensuring large wavenumbers do not cause numerical overflow.

4.4 Stability and Spectral Resolution

Instability in spectral methods can result when either the time step Δt or the artificial hyperdiffusion parameter μ are insufficiently small. The former is strongly apparent, and causes solution growth beyond measurable size. The latter, unlike in similar models, does not affect the stability of the rSW models considered here. Setting $\mu = 0$ yields numerically stable solutions, as shown in Figure 4.1 for the *rSW* QG^{+1} model. In order to ensure the appropriate spectral resolution, μ is selected qualitatively to ensure under-resolved wavenumbers do not cascade into the resolved spectrum.

An appropriate time step is estimated by the relation

$$\Delta t < \frac{\Delta x}{u_{\max}} \tag{4.26}$$

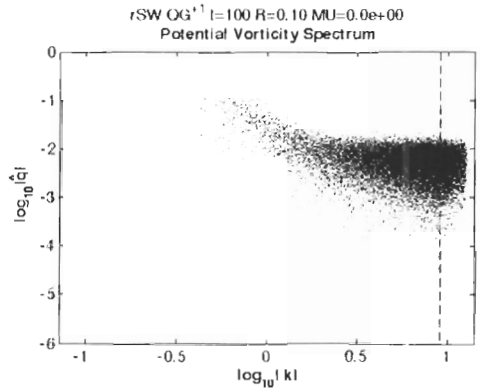

Figure 4.1: $\mu = 0$ *rSW* QG^{+1} potential vorticity spectrum at $t = 100$, for $N = 256$, $D = 28\pi$, and wavenumbers k and l defined in (4.3). The dashed line indicates the edge of the resolved spectrum at $|\vec{k}| \sim \frac{D}{2\pi}(N-1) \approx 0.8$. While the solution remains stable, the under-resolved spectrum can cascade into the resolved spectrum.

where $u_{\max}$ is the maximum velocity. In choosing scaling parameters in Section 2.2, velocities are assumed to be $\mathcal{O}(1)$ in time, and so the bound $|u| < 10$ should be a sufficient maximum. For $N = 256$ and $D = 28\pi$, the step is restricted to $\Delta t \lesssim 0.03$, and the step size of $\Delta t = 0.02$ is used.

As a result of the integrating factor, artificial diffusion is induced at each time step in the parameter $e^{-\mu|\vec{k}|^8\Delta t}$. The e-folding parameter, $ef(|\vec{k}|)$, then represents the number of time steps required to diffuse the coefficient at the l, k^{th} mode by a factor of e,

$$ef(|\vec{k}|) \;=\; \left(\mu|\vec{k}|\Delta t\right)^{-1}. \tag{4.27}$$

The first approximation of μ comes from restricting $10 \lesssim ef(|\vec{k}|) \lesssim 20$ at the highest resolved modes. Thus a first approximation is $\mu \approx 10^{-7}$.

For *rSW* QG^0 and *rSW* QG^{+1}, a larger value of $\mu = 10^{-6}$ produces a more qualitatively characteristic potential vorticity spectrum, shown in Figure 4.2a, while figures 4.2b and 4.2c show the features of an overdamped ($\mu = 10^{-5}$) and an underdamped ($\mu = 10^{-7}$) spectrum. For *rSW Wave*, the smaller $\mu = 2 \times 10^{-7}$ yields the desired velocity spectrum, as shown in 4.3. In all cases, the spectrum was considered once a limiting spectrum had been reached at $t = 100$.

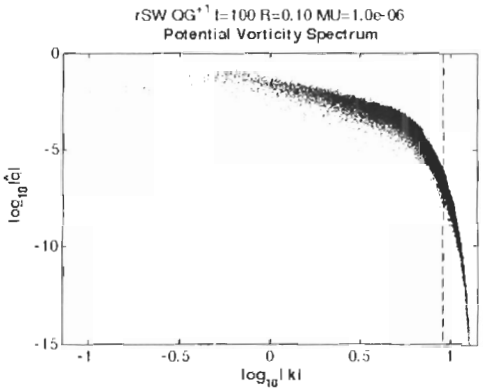

(a) Selectively damped spectrum, with $\mu = 10^{-6}$ at $t = 100$.

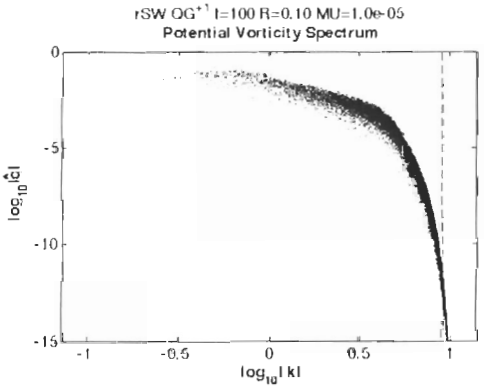

(b) Overdamped spectrum, with $\mu = 10^{-5}$ at $t = 100$.

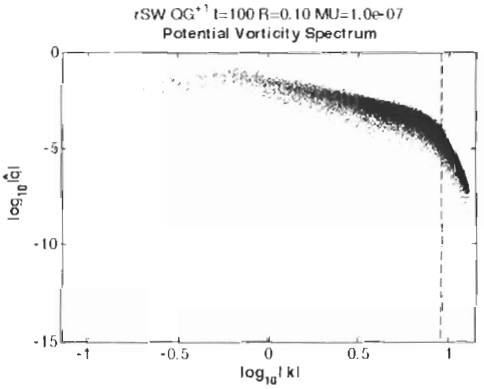

(c) Underdamped spectrum, with $\mu = 10^{-7}$ at $t = 100$.

Figure 4.2: Potential vorticity, q, spectra for various artificial diffusion parameters, μ, for $N = 256$, $D = 28\pi$, and wavenumbers k and l defined in (4.3). The dashed line indicates the edge of the resolved spectrum at $|\vec{k}| \sim \frac{D}{2\pi}(N-1) \approx 0.8$. (a) Selectively damped spectrum, $\mu = 10^{-6}$. (b) Overdamped spectrum, $\mu = 10^{-5}$. (c) Underdamped spectrum, $\mu = 10^{-7}$.

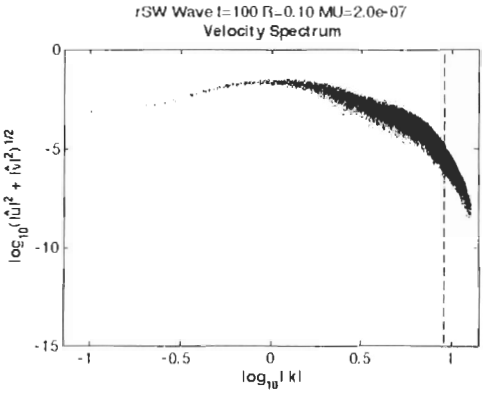

Figure 4.3: *rSW Wave* velocity ($\sqrt{u^2+v^2}$) spectrum with $\mu = 2 \times 10^{-7}$, $t = 100$, $N = 256$ and $D = 28\pi$. The dashed line indicates the edge of the resolved spectrum at $|\vec{k}| \sim \frac{D}{2\pi}(N-1) \approx 0.8$.

4.5 Convergence

Exact solution forms of both the balanced and wave equations provide benchmark tests for temporal convergence studies. For the wave code, the travelling wave solutions analyzed in Section 3.3.1 are calculated numerically, and used to determine absolute convergence. For the balanced code, the travelling dipole solution, considered in Section 3.2.3 and Appendix E, is used to determine relative convergence, since the solution is discontinuous in the first spatial derivative of q. Since there is no known solution to *rSW* QG^{+1}, relative convergence is tested with a sample turbulent initial condition, described in Section 4.1.1.

4.5.1 *rSW Wave* Convergence

The travelling wave solution in x to the *rSW Wave* equations, restated from (3.44) and (3.45), is

$$\frac{\partial u}{\partial x} = v\left(\frac{(c-\mathcal{R}u)^2}{c-(c-\mathcal{R}u)^3}\right) \tag{4.28}$$

$$\frac{\partial v}{\partial x} = \frac{u}{c-\mathcal{R}u}. \tag{4.29}$$

Although an analytic solution cannot be determined, the discussion from Section 3.3.1 and Appendix F shows the existence of periodic solutions for $c > 1$ and $u_0 < c - c^{\frac{1}{3}}$ or $c < 1$ and $u_0 > c - c^{\frac{1}{3}}$, which is sufficient for numerical computation. The method for solving the

travelling wave in x is given here, while a similar formulation is used to calculate solutions in y.

The linearized travelling wave solution, restated from (4.30) and (4.31), provides an initial approximation in determining the nonlinear solution, provided $u_0 << c$:

$$u = iA\frac{c}{\sqrt{c^2-1}}e^{i(c^2-1)^{-\frac{1}{2}}x} - iB\frac{c}{\sqrt{c^2-1}}e^{-i(c^2-1)^{-\frac{1}{2}}x} \tag{4.30}$$

$$v = Ae^{i(c^2-1)^{-\frac{1}{2}}x} + Be^{-i(c^2-1)^{-\frac{1}{2}}x}. \tag{4.31}$$

where A and B determine the initial values. Letting $A = \frac{1}{2}$ and $B = \frac{1}{2}$ provides a small amplitude initial condition consistent with $u_0 \ll c$. Given a wavelength λ, linear solutions are periodic when the wavespeed $c = \sqrt{\frac{\lambda^2}{4\pi^2}+1}$. This provides an initial wavespeed, c_0, for an iterative calculation of the nonlinear wavespeed required for solutions periodic in $x = \lambda$.

Given λ and c_n, $u(\lambda, c_n)$ and $v(\lambda, c_n)$ are obtained using fourth order Runge-Kutta with $128N$ steps (where $N = 256$). The Secant method is then used to determine the next iteration, c_{n+1}:

$$c_{n+1} = c_n - [u(\lambda, c_n) - u(0, c_n)]\frac{c_n - c_{n-1}}{u(\lambda, c_n) - u(\lambda, c_{n-1})}. \tag{4.32}$$

For $\lambda = 7\pi$, $u_0 = 0$ and $v_0 = 1$, $c \approx 3.6402371130 48$.

Convergence is tested for $\Delta t = \frac{\Delta x}{c}2^{-n}$, n = 1 to 5, which spans a range of $\Delta t = 4.7\times10^{-2}$ to 2.9×10^{-3}. Both the RK3 method, used to calculate initial steps, and the full RK3 + AB3 method were tested, and the RMS error of velocity was calculated,

$$\text{RMS}\left(|\vec{u}_{\text{actual}}| - |\vec{u}_{\text{approx}}|\right) = \sqrt{\sum\left(|\vec{u}_{\text{actual}}| - |\vec{u}_{\text{approx}}|\right)^2} \qquad |\vec{u}| = \sqrt{u^2+v^2}. \tag{4.33}$$

Travelling wave solutions in both x and y were found to have a similar convergence rates, and are shown in Figure 4.4 for waves travelling in x. For the RK3 method, the RMS error $\approx \Delta t^{3.0}$ and for the RK3 + AB3 method, the RMS error $\approx \Delta t^{2.9}$, where 8 RK3 steps are used in calculating each of the initial two iterations.

4.5.2 *rSW QG*^{0} and *rSW QG*$^{+1}$ Convergence

For the *rSW QG*^{0} code, the travelling dipole solution, considered in Section 3.2.3 and Appendix E, with radius a and advecting with constant speed c has the following piecewise form [5].

$$q = \begin{cases} -\sigma(H_0 + cy) & r < a \\ 0 & r > a \end{cases} \tag{4.34}$$

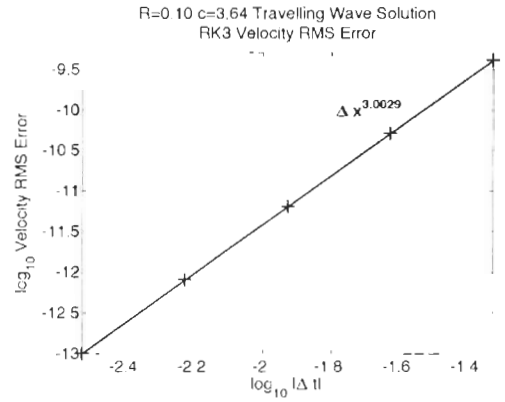

(a) RK3 convergence for travelling wave solution in x - RMS error $\approx \Delta t^{3.0}$

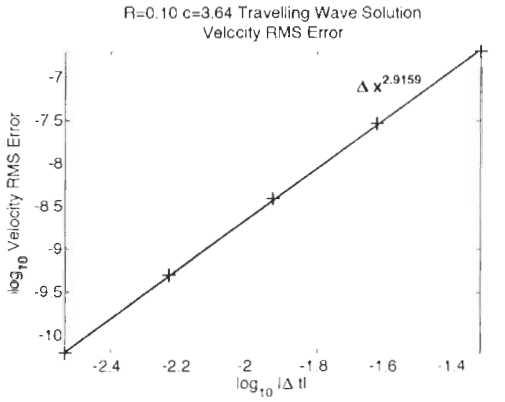

(b) RK3 + AB3 convergence for travelling wave solution in x - RMS error $\approx \Delta t^{2.9}$

Figure 4.4: Convergence plots for the travelling wave solution to the *rSW Wave* equations. (a) RK3 with $\Delta t^{3.0}$. (b) RK3 + AB3 with $\Delta t^{2.9}$.

where

$$H_0 = \begin{cases} \frac{ac}{\sigma-1}\left(\frac{J_1(r\sqrt{\sigma-1})}{J_1(a\sqrt{\sigma-1})} - \frac{r\sigma}{a}\right)\frac{y}{R} & r < a \\ -ac\frac{K_1(r)}{K_1(a)}\frac{y}{r} & r > a \end{cases}. \tag{4.35}$$

The above solution is continuous in q and H_0 across the boundary at $r = a$. Continuity in $\frac{\partial h}{\partial r}$ is retained when a and σ satisfy

$$(\sigma - 1)\frac{K_0(a)}{K_1(a)} + \frac{2\sigma}{a} = \sqrt{\sigma - 1}\frac{J_0(a\sqrt{\sigma - 1})}{J_1(a\sqrt{\sigma - 1})}. \tag{4.36}$$

Given $a = 1$, the smallest $\sigma \approx 16.3868925833852$.

The $\frac{\partial q}{\partial r}$ discontinuity at $r = a$ affects the stability and spatial convergence of the numerical solution. To ensure numerical stability, time steps are taken on the interval $\Delta t \in \left[7.67 \times 10^{-4}, 1.20 \times 10^{-5}\right]$ with $\Delta x = \pi/256$. Since the spectral spatial convergence accuracy is compromised, the spatial convergence is assumed algebraic. We therefore test convergence by assuming that the numerical solution q can be written as a sum of the actual solution q_{act} and algebraic error terms,

$$q(\Delta x, \Delta t) = q_{\text{act}} + C\Delta x^n + D\Delta t^m. \tag{4.37}$$

To approximate the order of the temporal convergence,

$$\frac{\text{RMS}\left(|q(\Delta x, \Delta t) - q(\Delta x, \Delta t/2)|\right)}{\text{RMS}\left(|q(\Delta x, \Delta t/2) - q(\Delta x, \Delta t/4)|\right)} = 2^m. \tag{4.38}$$

where the RMS error is defined in (4.33). The approximate convergence order is given in Table 4.5.2, and which tends towards 3 with decreasing Δt.

Table 4.1: Convergence rates for $rSW\ QG^0$ with travelling dipole initial condition.

Δt	$\mathrm{RMS}\left(\lvert q(\Delta t) - q(\Delta t/2)\rvert\right)$	$\frac{\mathrm{RMS}(\lvert q(\Delta t) - q(\Delta t/2)\rvert)}{\mathrm{RMS}(\lvert q(\Delta t/2) - q(\Delta t/4)\rvert)}$	m
7.67×10^{-4}	1.25×10^{-2}	7.33	2.87
3.83×10^{-4}	1.71×10^{-3}	7.69	2.94
1.92×10^{-4}	2.22×10^{-4}	7.86	2.97
9.59×10^{-5}	2.82×10^{-5}	7.93	2.99
4.79×10^{-5}	3.56×10^{-6}	7.97	2.99
2.39×10^{-5}	4.47×10^{-7}	-	-
1.20×10^{-5}	-	-	-

Since there is no known solution to the $rSW\ QG^{+1}$ equations, we use the above method (4.38) to approximate the rate of convergence for a solution with random initial conditions, as specified in 4.1.1. Results are given in Table 4.5.2, and tend towards third order with decreasing Δt.

Table 4.2: Convergence rates for $rSW\ QG^{+1}$ with turbulence initial condition.

Δt	$\mathrm{RMS}\left(\lvert q(\Delta t) - q(\Delta t/2)\rvert\right)$	$\frac{\mathrm{RMS}(\lvert q(\Delta t) - q(\Delta t/2)\rvert)}{\mathrm{RMS}(\lvert q(\Delta t/2) - q(\Delta t/4)\rvert)}$	m
2.00×10^{-2}	4.31×10^{-2}	5.43	2.44
1.00×10^{-2}	7.94×10^{-3}	5.97	2.58
5.00×10^{-3}	1.33×10^{-3}	6.44	2.69
2.50×10^{-3}	2.07×10^{-4}	6.90	2.79
1.25×10^{-3}	3.00×10^{-5}	7.31	2.87
3.13×10^{-4}	4.10×10^{-6}	7.60	2.93
6.25×10^{-4}	5.39×10^{-7}	7.60	2.96
1.56×10^{-4}	6.92×10^{-8}	7.79	–
7.81×10^{-5}	–	–	–

Chapter 5

Numerical Experiment and Results

In this chapter, we investigate the nature of the asymmetry between potential vorticity cyclones and anticyclones in the $rSW\ QG^{+1}$ model. In full rSW, Polvani et al [12] found that the bias towards more intense and more numerous vorticity anticyclones increases with Froude number, $\mathcal{F}$. With the assumption that $\mathcal{F} \sim \mathcal{R}$, an increase of anticyclonic intensity with $\mathcal{R}$ would be consistent with [12]. Due to the asymptotic nature of the $rSW\ QG^{+1}$ model, only $\mathcal{O}(\mathcal{R})$ dependencies can be measured as significant representations of the full rSW equations. To determine such a relation we proceed in the following manner. First, we consider a qualitative analysis of the potential vorticity evolution from turbulent initial conditions. We then turn to quantitative analysis by considering the potential vorticity distribution, and use the median and peak descriptive statistics in quantifying the asymmetry. A relation between the statistical estimators and $\mathcal{R}$ is then verified with ANOVA, and the desired linear relationship is determined.

5.1 Experiment Outline and Qualitative Analysis

The survey was comprised of 20 runs for each $\mathcal{R} = 0.05,\ 0.1,\ 0.15$ and 0.20 from the $rSW\ QG^{+1}$ model, and 20 runs from the $rSW\ QG^{0}$ model with $\mathcal{R} = 0$. Numerical code was implemented in MATLAB, and run on a 2.5 GHz PowerMac G5. The $rSW\ QG^{0}$ simulations ran for 10 hours to reach $t = 1500$, while the $rSW\ QG^{+1}$ simulations ran for 18 hours to reach $t = 1500$. Turbulent initial conditions were specified, as in Section 4.1.1, where each run had distinct random phase values, with a spatial domain of $28\pi \times 28\pi$ and spatial resolution of 256×256. Potential vorticity, q, was collected at $t = 1500$ dimensionless time

units.

As a first qualitative look, the potential vorticity field at $t = 1500$ for $\mathcal{R} = 0$, $\mathcal{R} = 0.1$ and $\mathcal{R} = 0.2$ is shown in Figure 5.1. In all three cases, coherent vorticies develop from the turbulent initial conditions, shown in Figure 5.1a, with the expected statistical symmetry between anticyclonic (negative, blue) and cyclonic (positive, red) vortices in the $\mathcal{R} = 0$ case, Figure 5.1b. However, as found in [12], the symmetry appears to break down with increasing $\mathcal{R}$, where for $\mathcal{R} = 0.1$, Figure 5.1c, the size and intensity of anticyclones appears greater than that of the cyclones. These trends are more prevailent for $\mathcal{R} = 0.2$, Figure 5.1d, which shows a dominance of anticyclonic vortices in a cyclonic flow.

5.2 Descriptive Statistics

While the mean potential vorticity remains zero, as shown analytically in Section 3.3.4, the bias in the potential vorticity field indicates a skewed distribution. As a quantitative approach, we consider the probability mass function (PMF), where potential vorticity is sorted into bins of width $N^2/32=256^2/32$, as shown in Figure 5.2. Most notable is the location of highest concentration, or peak, potential vorticity, which appears near zero when $\mathcal{R} = 0$, and is shifted towards cyclonic values with increasing $\mathcal{R}$, indicating a background cyclonic flow. The range of cyclonic values also appears to decrease with $\mathcal{R}$, characterizing the greater intensity of anticyclonic vortices.

This asymmetry is quantified by two estimators - peak and median potential vorticity. The peak, akin to the mode, is chosen as a clear qualitative distinction between the PMF for various $\mathcal{R}$ values. The peak is calculated as the maximum of the cubic best fit to the upper 36% of the potential vorticity PMF, as shown in Figure 5.3. The median is calculated as well, since it's a known unbiased estimator.

A trend between peak or median potential vorticity with $\mathcal{R}$ is indicated from Figure 5.4, showing notched box plots of peak and median potential vorticity for the five different values of $\mathcal{R}$. That the 95% confidence intervals, indicated by the notches, do not overlap indicates a relation between peak or median and $\mathcal{R}$. We assume that this relation has the same perturbation expansion as the variables in the $rSW\ QG^{+1}$ model, and is approximated by fitting the least-squares quadratic to the data,

$$P(\mathcal{R}) = -0.0040 + 3.4850\mathcal{R} - 4.6484\mathcal{R}^2, \qquad \text{Peak}, \tag{5.1}$$

$$M(\mathcal{R}) = 0.0014 + 3.0357\mathcal{R} - 3.9032\mathcal{R}^2. \qquad \text{Median}, \tag{5.2}$$

as shown in Figure 5.5. The accuracy of the approximations is verified, since the constant terms are approximately zero, and consistent with the leading order ($\mathcal{R} = 0$) symmetry. The approximations are asymptotically consistent so long as the last two terms remain asymptotically ordered, which occurs for $\mathcal{R} < 0.75$ in the peak q and $\mathcal{R} < 0.78$ in the median q approximation. This implies an approximately linear relationship between peak or median potential vorticity and $\mathcal{R}$ in the small $\mathcal{R}$ limit, which is within the range of applicability of the $rSW\ QG^{+1}$ perturbation model.

The results found here are consistent with those in [12], in that the cyclone/anticyclone asymmetry, developing from the turbulent initial conditions specified in Section 4.1.1, has a strong dependence on $\mathcal{F}(\sim \mathcal{R}$ in this study). One of the possible causes for this asymmetry, considered in [12], is the interaction between gravity waves and balanced vortices in the full rSW equations. That the asymmetry is retained in the balanced $rSW\ QG^{+1}$ model indicates that gravity waves interaction is not the sole cause.

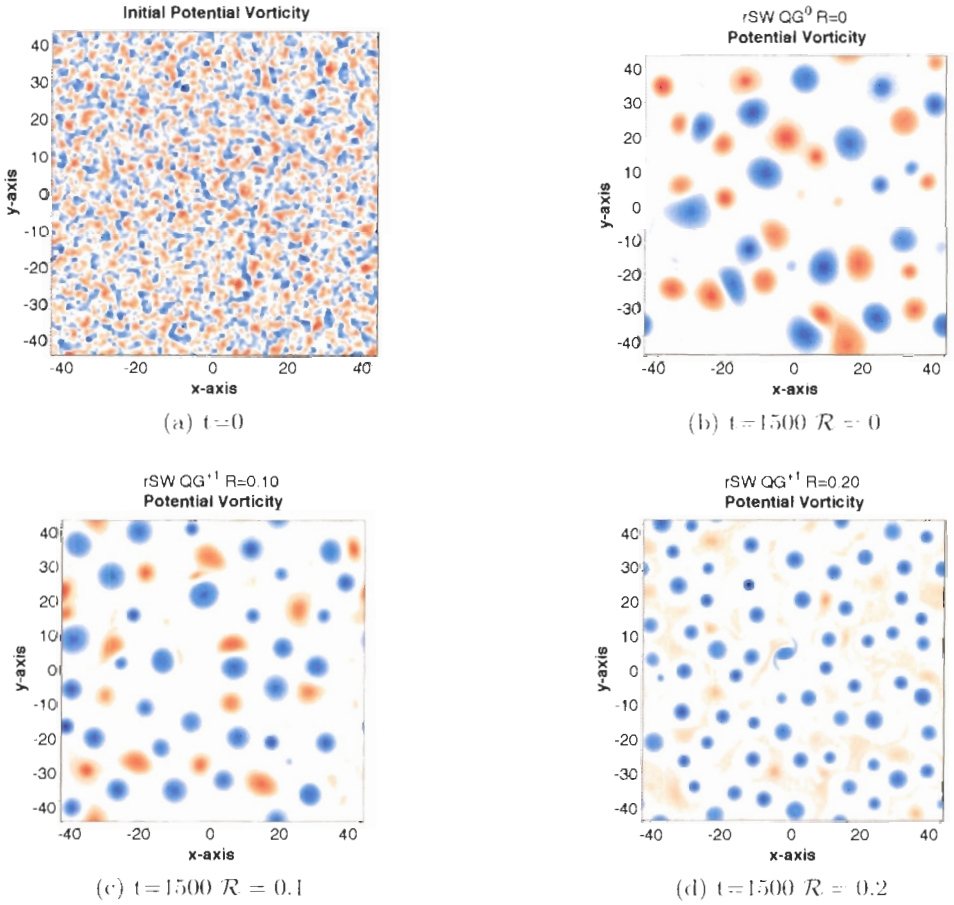

(a) t=0 (b) t=1500 $\mathcal{R} = 0$

(c) t=1500 $\mathcal{R} = 0.1$ (d) t=1500 $\mathcal{R} = 0.2$

Figure 5.1: Potential vorticity for three (statistically distinct) initially turbulent runs. (a) Sample turbulence initial condition. (b) At t=1500 for $\mathcal{R} = 0$, symmetric growth of cyclones (red) and anticyclones (blue). (c) At t=1500 for $\mathcal{R} = 0.1$, somewhat greater anticyclonic intensity and number, and weaker yet more prevalent cyclonic flow. (d) At t=1500 for $\mathcal{R} = 0.2$, the asymmetries are more pronounced - intense anticyclones immersed in a cyclonic flow.

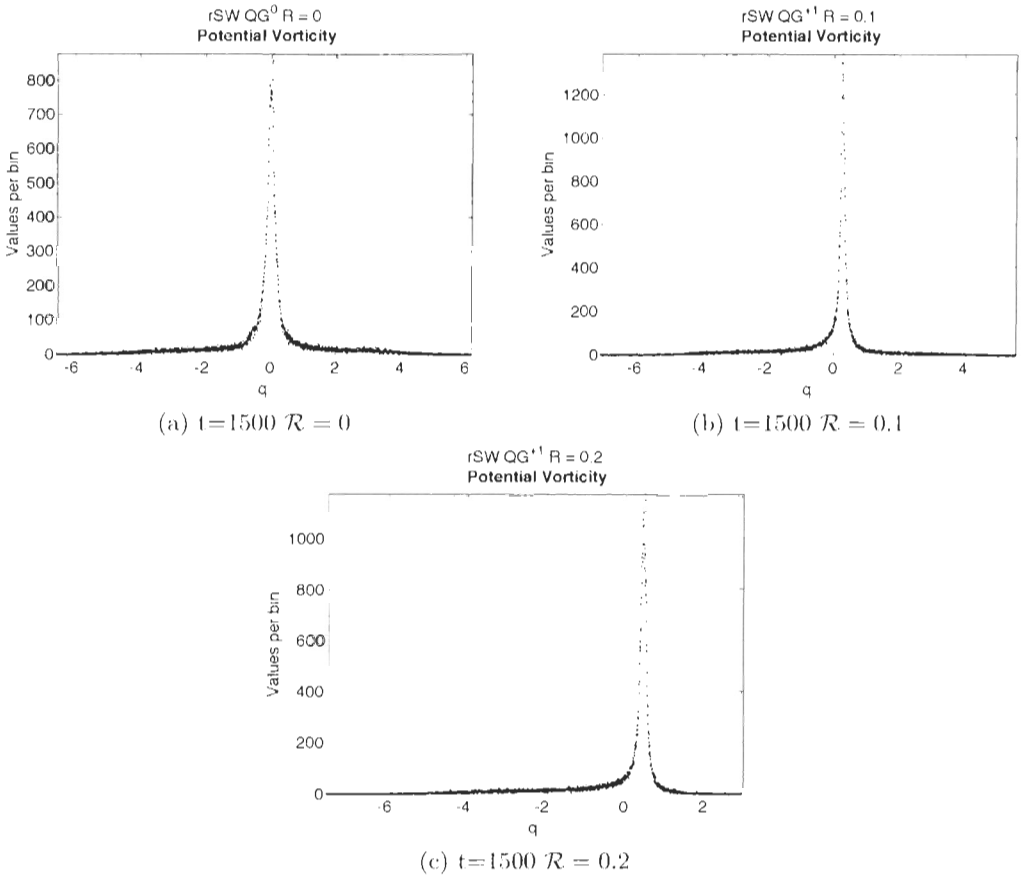

Figure 5.2: Potential vorticity probability mass functions (PMF) for three initially turbulent runs. (a) At t=1500 for $\mathcal{R} = 0$, the PMF peaks near at $q = 0$, and spans an equal range of negative and positive values. (b) At t=1500 for $\mathcal{R} = 0.1$, the PMF peak is shifted to the positive (cyclonic) side, indicating a weak background cyclonic flow. The range of positive q has decreased, indicating more intense anticyclonic formation. (c) At t=1500 for $\mathcal{R} = 0.2$, there is a larger PMF peak shift, indicating a stronger background cyclonic flow, and the range of positive q is smaller still.

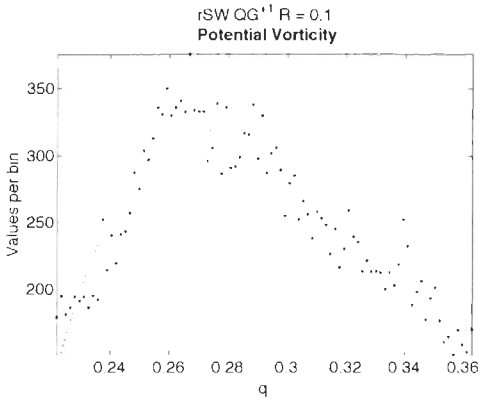

Figure 5.3: Calculating the peak potential vorticity from the PMF - bestfit cubic to the upper 36% of the PMF shown in Figure 5.2b at $t = 1500$ for $\mathcal{R} = 0.1$.

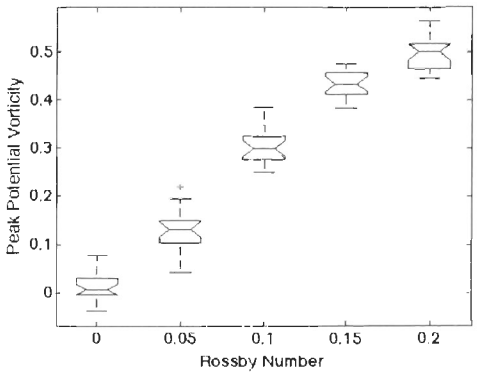

(a) Peak potential vorticity with $\mathcal{R}$

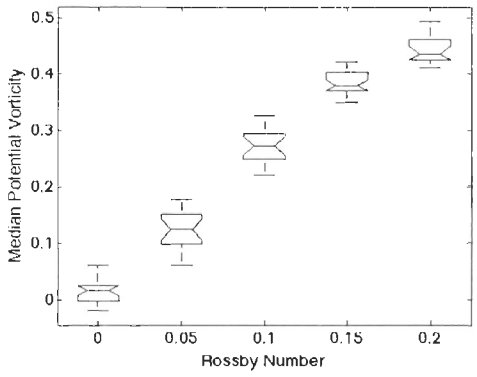

(b) Median potential vorticity with $\mathcal{R}$

Figure 5.4: Box plots, with horizontal lines indicating the lower quartile, median and upper quartile, notches indicating the 95% median confidence intervals, and whiskers indicating the data range, with outliers shown where necessary. (a) Peak potential vorticity at t=1500. (b) Median potential vorticity at t=1500.

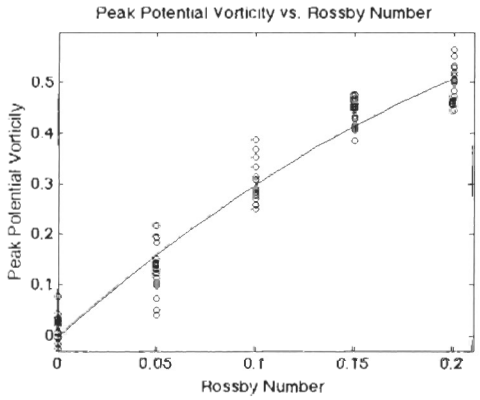

(a) Peak potential vorticity with $\mathcal{R}$

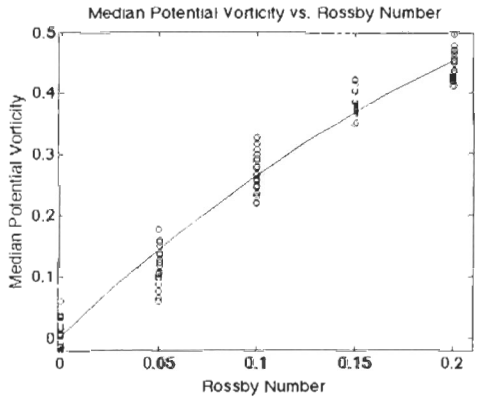

(b) Median potential vorticity with $\mathcal{R}$

Figure 5.5: Best fit quadratic functions to median and peak potential vorticity vs Rossby number. (a) Peak potential vorticity vs Rossby number at t=1500. (b) Median potential vorticity vs Rossby number at t=1500.

Chapter 6

Summary and Future Work

The initial aim of this project was to investigate two subclasses of solutions of the two-dimensional, homogeneous Rotating Shallow Water (rSW) equations. The first is the special case of uniform potential vorticity at fast time scales, which supports only gravity wave behaviour. The second is the first correction $\mathcal{R}$ perturbation expansion to quasigeostrophic theory, a solution class describing slower time scale balanced flow. The intent for the second case was to show that the breakdown of symmetry between cyclones and anticyclones in the full rSW model, as found in [12], did not occur, or occurred only weakly in the strictly balanced model. This was not the outcome, as discussed in Chapter 5. The breakdown of cyclone/anticyclone asymmetry depends strongly on $\mathcal{R}$, where from turbulent initial conditions, anticyclones develop to be more numerous and more intense, while anticyclones develop weaker and more dispersed. A linear dependency between median potential vorticity and $\mathcal{R}$ is obtained, which is within the range of the asymptotic model.

This led to what became a principal focus of this work - do the rSW equations accurately represent the atmosphere, and can quasigeostrophy be justified as a first correction theory?

In similar considerations of rSW, for example [10] and [2], only the leading order terms are retained, and any smaller terms are considered negligible. A thorough discussion of the required scalings in various classes of shallow water solutions is considered in [6], although the quasigeostrophic formulation is dismissed as an adequate leading order model, describing both β effects, considered in Section 3.2.3, and the effects of bottom topography, considered in [2].

The largest term dismissed in the leading order equations come as a result of using standard coordinates, where latitudes are measured from the equator, and curvature within

the coordinate system increases with distance from the equator. This is less of a problem if the equations are considered in spherical coordinates, but Cartesian models assume these curvature terms are negligible. The solution can be summarized as:

> To minimize coordinate system curvature near Vancouver, place Vancouver on the coordinate equator.

That is, change coordinate systems, from the standard equatorial coordinate system to an oblique coordinate system, with the equator passing through the latitude, longitude point of interest. Details and images of this transform are given in Section 2.1.3. Applied to the Navier-Stokes equations, the only artifact of the oblique coordinate system is the definition of Coriolis parameters, which are a result of the rotating reference frame (earth), in equation (2.11).

The remainder of Chapter 2 is devoted to a systematic scaling derivation of the rSW equations from the oblique Navier-Stokes equations. This derivation is unique in that terms scale independently of an initial longitude, latitude point[1]. The order of ultimately negligible terms is carried through the derivation, and the necessary scaling assumptions to obtain rSW to a variable order of accuracy is given in (2.64) and (2.65). A similar reduction from spherical to Cartesian coordinate representation is considered in Section 2.3.3. Cartesian coordinates are recovered when the coordinate curvature terms are negligible, which reduces to the scale assumption in (2.78).

In Chapter 3, particular solution regimes of rSW are considered, where gravity waves, Rossby waves and quasigeostrophic theory are recovered. The chosen scales for periodic solutions, and any exact solutions to the resulting equations, are summarized in Table 3.1. Future projects may include a similar study where the aperiodic Coriolis terms, unique to the oblique coordinate frame, are included in the equations.

One of the properties of the full rSW equations is the area conserved quantities of density, vorticity, height and energy (see Section 3.1.2), and is revisited in the leading order, Section 3.2.4, and first correction, Section 3.3.4, quasigeostrophic equations. In addition to the four listed quantities, potential vorticity is also conserved at leading order. In the first correction equations, density, vorticity and potential vorticity are conserved, while height is conserved

[1]The only exception is the $f = 2\sin\Lambda_0$ and $\beta = \xi\cot\Lambda_0$ terms, which scale the Coriolis effect. That these terms remain small is characteristic of geostrophic flow, considered in Section 2.2, and not a result of coordinate system.

to $\mathcal{O}\left(\mathcal{R}^2\right)$, which is consistent with the asymptotic model. It remains as future work to determine whether energy is conserved, or whether an equivalent energy variable can be found.

Chapter 4 outlines the numerical methods used in evolving the *rSW QG* models (from Section 3.2.3), and the *rSW Wave* model (from Section 3.2.1), which consist of spectral methods in space and third-order Adams-Bashforth in time, with initial third-order Runge-Kutta steps. Spectral resolution is ensured by introducing a hyperdiffusion variable, μ, which dampens the highest, underresolved wave numbers. As opposed to similar models, setting $\mu = 0$ yields stable solutions. Further work could include an analysis of the characteristic spectrum for area integral conserved variables.

The statistical experiment in Chapter 5 shows a breakdown in vortex symmetry, consistent with that found in [12]. Where the Polvani [12] analysis differs, and what could lead to futher work, is in the calculation of the asymmetry. Since mean potential vorticity is not conserved in the full rSW equations, vorticity was used in quantifying the asymmetry in [12], and instead of a mode or median statistic, which appears centered at zero, the kurtosis[2] provided a measure of skewness [12]. Also, wide range of $\mathcal{F}$ and $\mathcal{R}$ values were considered, and the dependency was found to be dependent on $\mathcal{F}$ alone.

While statistical experiment was run with the first correction balanced model, numerical solutions to the nonlinear wave model have yet to be analyzed, and are also a point of future work.

[2]Kurtosis $= \frac{\int_D \zeta^3}{\left(\int_D \zeta^2\right)^{\frac{3}{2}}}$ where ζ is the vorticity, and D is the horizontal domain.

Appendix A

Spherical Operators and Curvature Terms

This appendix fills in the remaining details in the transformation from the orientation and coordinate independent vector Navier-Stokes equations, (2.1) and (2.2), to the oblique spherical Navier-Stokes equations in (2.21) - (2.24). First, the spherical operators are defined, and then the curvature terms are determined, which result from the spherical operators acting on the ϕ and λ dependent spherical coordinate directions.

The divergence operator in spherical coordinates, acting on a vector $\vec{A} = A_\phi e_\phi + A_\lambda e_\lambda + A_r e_r$, is

$$\nabla \cdot \vec{A} = \frac{2}{r} A_r + \frac{\partial A_r}{\partial r} + \frac{1}{r \cos\lambda} \frac{\partial A_\phi}{\partial \phi} + \frac{1}{r} \frac{\partial A_\lambda}{\partial \lambda} - \frac{A_\lambda \tan\lambda}{r}. \tag{A.1}$$

The gradient and Laplacian operators in spherical coordinates, acting on a scalar a, are

$$\nabla a = \frac{\partial f}{\partial r} e_r + \frac{1}{r \cos\lambda} \frac{\partial f}{\partial \boldsymbol{\phi}} \boldsymbol{e_\phi} + \frac{1}{\boldsymbol{r}} \frac{\partial f}{\partial \boldsymbol{\lambda}} \boldsymbol{e_\lambda}, \tag{A.2}$$

$$\nabla^2 a = \frac{2}{r} \frac{\partial a}{\partial r} + \frac{\partial^2 \boldsymbol{a}}{\partial \boldsymbol{r^2}} + \frac{1}{r^2 \cos^2\lambda} \frac{\partial^2 a}{\partial \phi^2} - \frac{\tan\lambda}{r} \frac{\partial a}{\partial \lambda} + \frac{1}{r^2} \frac{\partial^2 a}{\partial \lambda^2} \tag{A.3}$$

The gradient operator appears in the advective derivative, as

$$\frac{\mathrm{D}}{\mathrm{D}t} = \frac{\partial}{\partial t} + \vec{u} \cdot \nabla \tag{A.4}$$

$$= \frac{\partial}{\partial t} + w \frac{\partial}{\partial r} + \frac{u}{r \cos\lambda} \frac{\partial}{\partial \phi} + \frac{v}{r} \frac{\partial}{\partial \lambda}. \tag{A.5}$$

The advective derivative acts on $\vec{u} = u e_\phi + v e_\lambda + w e_r$ as

$$\frac{\mathrm{D}\vec{u}}{\mathrm{D}t} = \frac{\mathrm{D}w}{\mathrm{D}t} e_r + w \frac{\mathrm{D}e_r}{\mathrm{D}t} + e_\phi \frac{\mathrm{D}u}{\mathrm{D}t} + u \frac{\mathrm{D}e_\phi}{\mathrm{D}t} + e_\lambda \frac{\mathrm{D}v}{\mathrm{D}t} + v \frac{\mathrm{D}e_\lambda}{\mathrm{D}t}, \tag{A.6}$$

where advective derivative curvature terms are

$$\begin{aligned} w\frac{\mathrm{D}e_r}{\mathrm{D}t} &= \frac{uw}{r\cos\lambda}\frac{\partial e_r}{\partial\phi} + \frac{vw}{r}\frac{\partial e_r}{\partial\lambda}, \\ u\frac{\mathrm{D}e_\phi}{\mathrm{D}t} &= \frac{u^2}{r\cos\lambda}\frac{\partial e_\phi}{\partial\phi} + \frac{vu}{r}\frac{\partial e_\phi}{\partial\lambda} \\ v\frac{\mathrm{D}e_\lambda}{\mathrm{D}t} &= \frac{uv}{r\cos\lambda}\frac{\partial e_\lambda}{\partial\phi} + \frac{v^2}{r}\frac{\partial e_\lambda}{\partial\lambda}. \end{aligned}$$

The product rule for the Laplacian operator is

$$\nabla^2(fg) = f\nabla^2 g + 2(\nabla f)\cdot(\nabla g) + g\nabla^2 f, \tag{A.7}$$

where

$$(\nabla f)\cdot(\nabla g) = \frac{\partial f}{\partial r}\frac{\partial g}{\partial r} + \frac{1}{r^2\cos^2\lambda}\frac{\partial f}{\partial\phi}\frac{\partial g}{\partial\phi} + \frac{1}{r^2}\frac{\partial f}{\partial\lambda}\frac{\partial g}{\partial\lambda}. \tag{A.8}$$

The Laplacian acts on $\vec{u}$ as

$$\begin{aligned} \nabla^2\vec{u} = {} & \left(\nabla^2 w\right)e_r + 2(\nabla w)\cdot(\nabla e_r) + w\left(\nabla^2 e_r\right) + e_\phi\left(\nabla^2 u\right) + 2(\nabla u)\cdot(\nabla e_\phi) \\ & + u\left(\nabla^2 e_\phi\right) + e_\lambda\left(\nabla^2 v\right) + 2(\nabla v)\cdot(\nabla e_\lambda) + v\left(\nabla^2 e_\lambda\right), \end{aligned} \tag{A.9}$$

where the Laplacian curvature terms are

$$2(\nabla w)\cdot(\nabla e_r) = \frac{2}{r^2\cos^2\lambda}\frac{\partial w}{\partial\phi}\frac{\partial e_r}{\partial\phi} + \frac{2}{r^2}\frac{\partial w}{\partial\lambda}\frac{\partial e_r}{\partial\lambda} \tag{A.10}$$

$$w\nabla^2 e_r = \frac{w}{r^2\cos^2\lambda}\frac{\partial^2 e_r}{\partial\phi^2} - \frac{w\tan\lambda}{r^2}\frac{\partial e_r}{\partial\lambda} + \frac{w}{r^2}\frac{\partial^2 e_r}{\partial\lambda^2} \tag{A.11}$$

$$2(\nabla u)\cdot(\nabla e_\phi) = \frac{2}{r^2\cos^2\lambda}\frac{\partial u}{\partial\phi}\frac{\partial e_\phi}{\partial\phi} + \frac{2}{r^2}\frac{\partial u}{\partial\lambda}\frac{\partial e_\phi}{\partial\lambda} \tag{A.12}$$

$$u\nabla^2 e_\phi = \frac{u}{r^2\cos^2\lambda}\frac{\partial^2 e_\phi}{\partial\phi^2} - \frac{u\tan\lambda}{r^2}\frac{\partial e_\phi}{\partial\lambda} + \frac{u}{r^2}\frac{\partial^2 e_\phi}{\partial\lambda^2} \tag{A.13}$$

$$2(\nabla v)\cdot(\nabla e_\lambda) = \frac{2}{r^2\cos^2\lambda}\frac{\partial v}{\partial\phi}\frac{\partial e_\lambda}{\partial\phi} + \frac{2}{r^2}\frac{\partial v}{\partial\lambda}\frac{\partial e_\lambda}{\partial\lambda} \tag{A.14}$$

$$v\nabla^2 e_\lambda = \frac{v}{r^2\cos^2\lambda}\frac{\partial^2 e_\lambda}{\partial\phi^2} - \frac{v\tan\lambda}{r^2}\frac{\partial e_\lambda}{\partial\lambda} + \frac{v}{r^2}\frac{\partial^2 e_\lambda}{\partial\lambda^2} \tag{A.15}$$

Derivatives of the spherical coordinate directions are obtained by differentiating the spherical

coordinate transformation matrix, (2.12),

$$\frac{\partial}{\partial\phi}\begin{bmatrix} e_r \\ e_\phi \\ e_\lambda \end{bmatrix} = \begin{bmatrix} 0 & \cos\lambda & 0 \\ -\cos\lambda & 0 & \sin\lambda \\ 0 & -\sin\lambda & 0 \end{bmatrix}\begin{bmatrix} e_r \\ e_\phi \\ e_\lambda \end{bmatrix}, \tag{A.16}$$

$$\frac{\partial}{\partial\lambda}\begin{bmatrix} e_r \\ e_\phi \\ e_\lambda \end{bmatrix} = \begin{bmatrix} 0 & 0 & 1 \\ 0 & 0 & 0 \\ -1 & 0 & 0 \end{bmatrix}\begin{bmatrix} e_r \\ e_\phi \\ e_\lambda \end{bmatrix}. \tag{A.17}$$

The advective derivative and Laplacian of $\vec{u}$ in oblique spherical coordinates are

$$\begin{aligned} \frac{\mathrm{D}\vec{u}}{\mathrm{D}t} &= \left(\frac{\mathrm{D}w}{\mathrm{D}t} - \frac{u^2+v^2}{r^2}\right)\boldsymbol{e_r} + \left(\frac{\mathrm{D}u}{\mathrm{D}t} - \frac{vu\tan\lambda}{r} + \frac{wu}{r}\right)e_\phi \\ &\quad + \left(\frac{\mathrm{D}v}{\mathrm{D}t} + \frac{u^2\tan\lambda}{r} + \frac{wv}{r}\right)e_\lambda, \end{aligned} \tag{A.18}$$

$$\begin{aligned} \nabla^2\vec{u} &= \left(\nabla^2 u + \frac{2}{r^2\cos^2\lambda}\left[-\frac{u}{2} + \cos\lambda\frac{\partial w}{\partial\phi} - \sin\lambda\frac{\partial v}{\partial\phi}\right]\right)e_\phi \\ &\quad + \left(\nabla^2 v + \frac{2}{r^2}\left[\frac{\partial w}{\partial\lambda} + \frac{\tan\lambda}{\cos\lambda}\frac{\partial u}{\partial\phi} - \frac{v}{2\cos^2\lambda}\right]\right)e_\lambda \\ &\quad + \left(\nabla^2 w - \frac{2}{r^2}\left[w - \frac{1}{\cos\lambda}\frac{\partial u}{\partial\phi} - \frac{\partial v}{\partial\lambda} + v\tan\lambda\right]\right)e_r. \end{aligned} \tag{A.19}$$

These equations are equivalent to the standard spherical coordinate equations found in [10] and [4]. The difference in the oblique coordinate representation is the zonal and meridional directions, e_ϕ and e_λ, and longitude and latitude variables, ϕ and λ, are dependent upon the oblique coordinate system.

Appendix B

Friction Force Defined and Scaled

B.1 Definition of Friction Force

From the preliminary assumptions in Section 2.1.2, the friction force, $\vec{\mathrm{F}}$, is the viscosity of a Newtonian fluid,

$$\vec{\mathrm{F}} = \mu\nabla^2\vec{u} + \frac{\mu}{3}\nabla\left(\nabla\cdot\vec{u}\right). \tag{B.1}$$

In terms of the oblique spherical coordinate directions,

$$\vec{\mathrm{F}} = \mu\mathrm{F}_\phi + \mu\mathrm{F}_\lambda + \mu\mathrm{F}_r \tag{B.2}$$

where

$$\mathrm{F}_\phi = \nabla^2 u + \widetilde{\nabla^2}_\phi + \frac{1}{r\cos\lambda}\frac{\partial}{\partial\phi}\left(\nabla\cdot\vec{u}\right) \tag{B.3}$$

$$\mathrm{F}_\lambda = \nabla^2 v + \widetilde{\nabla^2}_\lambda + \frac{1}{r}\frac{\partial}{\partial\lambda}\left(\nabla\cdot\vec{u}\right) \tag{B.4}$$

$$\mathrm{F}_r = \nabla^2 w + \widetilde{\nabla^2}_r + \frac{\partial}{\partial r}\left(\nabla\cdot\vec{u}\right) \tag{B.5}$$

with the Laplacian defined in A.3,

$$\nabla^2 = \frac{2}{r}\frac{\partial}{\partial r} + \frac{\partial^2}{\partial r^2} + \frac{1}{r^2\cos^2\lambda}\frac{\partial^2}{\partial\phi^2} - \frac{\tan\lambda}{r^2}\frac{\partial}{\partial\lambda} + \frac{1}{r^2}\frac{\partial^2}{\partial\lambda^2}, \tag{B.6}$$

the Laplacian curvature terms, from A.10,

$$\widetilde{\nabla^2}_\phi = \frac{2}{r^2\cos^2\lambda}\left[-\frac{u}{2}+\cos\lambda\frac{\partial w}{\partial\phi}-\sin\lambda\frac{\partial v}{\partial\phi}\right] \tag{B.7}$$

$$\widetilde{\nabla^2}_\lambda = \frac{2}{r^2}\left[\frac{\partial w}{\partial\lambda}+\frac{\tan\lambda}{\cos\lambda}\frac{\partial u}{\partial\phi}-\frac{v}{2\cos^2\lambda}\right]e_\lambda \tag{B.8}$$

$$\widetilde{\nabla^2}_r = -\frac{2}{r^2}\left[w-\frac{1}{\cos\lambda}\frac{\partial u}{\partial\phi}-\frac{\partial v}{\partial\lambda}+v\tan\lambda\right], \tag{B.9}$$

and velocity divergence from (A.1),

$$\nabla\cdot\vec{u} = \frac{1}{r\cos\lambda}\frac{\partial u}{\partial\phi}+\frac{1}{r}\frac{\partial v}{\partial\lambda}-\frac{v\tan\lambda}{r}+\frac{2}{r}w+\frac{\partial w}{\partial r}. \tag{B.10}$$

with derivatives

$$\frac{\partial}{\partial\phi}(\nabla\cdot\vec{u}) = \frac{1}{r\cos\lambda}\frac{\partial^2 u}{\partial\phi^2}+\frac{1}{r}\frac{\partial^2 v}{\partial\lambda\partial\phi}-\frac{\partial v}{\partial\phi}\frac{\tan\lambda}{r}+\frac{2}{r}\frac{\partial w}{\partial\phi}+\frac{\partial^2 w}{\partial r\partial\phi} \tag{B.11}$$

$$\begin{aligned}\frac{\partial}{\partial\lambda}(\nabla\cdot\vec{u}) &= \frac{\tan\lambda}{r\cos\lambda}\frac{\partial u}{\partial\phi}+\frac{1}{r\cos\lambda}\frac{\partial^2 u}{\partial\lambda\partial\phi}+\frac{1}{r}\frac{\partial^2 v}{\partial\lambda^2}\\ &\quad -\frac{v}{r\cos^2\lambda}-\frac{\partial v}{\partial\lambda}\frac{v}{r}+\frac{2}{r}\frac{\partial w}{\partial\lambda}+\frac{\partial^2 w}{\partial r\partial\lambda}\end{aligned} \tag{B.12}$$

$$\begin{aligned}\frac{\partial}{\partial r}(\nabla\cdot\vec{u}) &= -\frac{1}{r^2}\left(\frac{\partial u}{\partial\phi}+\frac{\partial v}{\partial\lambda}-v\tan\lambda+2w\right)\\ &\quad +\frac{1}{r\cos\lambda}\frac{\partial^2 u}{\partial\phi\partial r}+\frac{1}{r}\frac{\partial^2 v}{\partial\lambda\partial r}-\frac{\tan\lambda}{r}\frac{\partial v}{\partial r}+\frac{2}{r}\frac{\partial w}{\partial r}+\frac{\partial^2 w}{\partial r^2}\end{aligned} \tag{B.13}$$

B.2 Scaled Friction Force in Oblique Spherical Coordinates

The characteristic scales F_ϕ, F_λ and F_r are found by first replacing each variable with a characteristic scale and a dimensionless $\mathcal{O}(1)$ variable, as described in Section 2.2. The scaling of functions and operators are then found, and substituted into the equations for F_ϕ, F_λ and F_r. The largest terms are kept as the characteristic scales, where the synoptic and mesoscale scaling assumptions from Section 2.2.1 are used in determining the relative size of each term.

For the velocity and position variables the substitutions are, from Section 2.2.1,

$$r_0\phi \to L\phi_l \quad r_0\lambda \to L\lambda_l \quad r \to r_0+Hz \tag{B.14}$$

$$u \to Uu(\phi_l,\lambda_l,t)+\Delta Uu'(\phi_l,\lambda_l,z,t) \tag{B.15}$$

$$v \to Uv(\phi_l,\lambda_l,t)+\Delta Uv'(\phi_l,\lambda_l,z,t) \tag{B.16}$$

$$w \to Ww(\phi_l,\lambda_l,z,t) \tag{B.17}$$

From the synoptic and upper mesoscale scaling assumptions of Section 2.2.1, the horizontal length scale is less than Earth's radius, $H \ll L$, and the vertical height scale is significantly smaller than the horizontal length scale, $L \ll r_0$. This allows for the following variables to scale as the first term in their Taylor expansion.

$$\frac{1}{r} \rightarrow \frac{1}{r_0 + Hz} \sim \frac{1}{r_0} \tag{B.18}$$

$$\cos\lambda \rightarrow \cos\frac{L}{r_0}\lambda_l \sim 1 \tag{B.19}$$

$$\sin\frac{L}{r_0}\lambda \rightarrow \sin\frac{L}{r_0}\lambda_l \sim \frac{L}{r_0} \tag{B.20}$$

$$\tan\lambda \rightarrow \tan\frac{L}{r_0}\lambda_l \sim \frac{L}{r_0}. \tag{B.21}$$

This oblique scaling of the trigonometric functions, which are expanded about λ_0, differs from the standard scaling, where the Taylor expansions are taken about Λ_0. Thus, the scaling of the friction parameters in oblique coordinates is independent of the characteristic latitude Λ_0.

Since zonal and meridional velocities, u and v, have tangential and vertical variation components, the tangential and vertical position derivatives scaling accordingly. The u position derivatives are given below, while the v derivatives scale similarly,

$$\frac{\partial u}{\partial\phi}, \frac{\partial u}{\partial\lambda} \sim r_0\frac{U + \Delta U}{L} \qquad \frac{\partial u}{\partial r} \sim \frac{\Delta U}{H} \tag{B.22}$$

$$\frac{\partial^2 u}{\partial\phi^2}, \frac{\partial^2 u}{\partial\lambda^2}, \frac{\partial^2 u}{\partial\phi\partial\lambda} \sim r_0^2\frac{U + \Delta U}{L^2} \quad \frac{\partial^2 u}{\partial\lambda\partial r}, \frac{\partial^2 u}{\partial\phi\partial r} \sim r_0\frac{\Delta U}{LH} \quad \frac{\partial^2 u}{\partial r^2} \sim \frac{\Delta U}{H^2}. \tag{B.23}$$

Vertical velocity has one scale for both tangential and vertical variations, and its derivatives scale as

$$\frac{\partial u}{\partial\phi}, \frac{\partial u}{\partial\lambda} \sim r_0\frac{W}{L} \qquad \frac{\partial u}{\partial r} \sim \frac{W}{H} \tag{B.24}$$

$$\frac{\partial^2 w}{\partial\phi^2}, \frac{\partial^2 w}{\partial\lambda^2}, \frac{\partial^2 w}{\partial\phi\partial\lambda} \sim r_0^2\frac{W}{L^2} \quad \frac{\partial^2 w}{\partial\lambda\partial r}, \frac{\partial^2 w}{\partial\phi\partial r} \sim r_0\frac{W}{LH} \quad \frac{\partial^2 w}{\partial r^2} \sim \frac{W}{H^2} \tag{B.25}$$

We now substitute the characteristic function and operator scales into the definitions of F_ϕ, F_λ and F_r, where the relative size of each term is found by recalling the synoptic and mesoscale and horizontal assumptions from Section 2.2.1,

$$\frac{L}{r_0} < 1, \qquad \frac{H}{L} \ll 1, \qquad \frac{W}{U} \ll 1. \tag{B.26}$$

The Laplacian terms, (B.6), scale as

$$\begin{aligned} \nabla^2 u, \nabla^2 v &\sim \frac{\Delta U}{r_0 H} + \frac{\Delta U}{H^2} + \frac{U+\Delta U}{L^2} + \frac{U+\Delta U}{r_0^2} \\ &\sim \frac{\Delta U}{H^2} + \frac{U}{L^2} \end{aligned} \tag{B.27}$$

$$\begin{aligned} \nabla^2 w &\sim \frac{W}{r_0 H} + \frac{W}{H^2} + \frac{W}{L^2} + \frac{W}{r_0^2} \\ &\sim \frac{W}{H^2} \end{aligned} \tag{B.28}$$

The Laplacian curvature terms, (B.7)-(B.9), scale as

$$\widetilde{\nabla^2}_\phi, \widetilde{\nabla^2}_\lambda \sim \frac{U+\Delta U}{r_0^2} + \frac{W}{r_0 L}, \tag{B.29}$$

$$\begin{aligned} \widetilde{\nabla^2}_r &\sim \frac{W}{r_0^2} + \frac{U+\Delta U}{r_0 L} \\ &\sim \frac{U+\Delta U}{r_0 L} \end{aligned} \tag{B.30}$$

The velocity divergence derivative terms, (B.11)-(B.13), scale as

$$\begin{aligned} \frac{1}{r\cos\lambda}\frac{\partial}{\partial\phi}\left(\nabla\cdot\vec{u}\right), \frac{1}{r}\frac{\partial}{\partial\lambda}\left(\nabla\cdot\vec{u}\right) &\sim \frac{U+\Delta U}{L^2} + \frac{U+\Delta U}{r_0^2} + \frac{W}{r_0 L} + \frac{W}{LH} \\ &\sim \frac{U+\Delta U}{L^2} + \frac{W}{LH} \end{aligned} \tag{B.31}$$

$$\begin{aligned} \frac{\partial}{\partial r}\left(\nabla\cdot\vec{u}\right) &\sim \frac{U+\Delta U}{r_0 L} + \frac{L}{r_0}\frac{U+\Delta U}{r_0^2} + \frac{L}{r_0}\frac{\Delta U}{r_0 H} + \frac{W}{r_0 H} + \frac{W}{H^2} \\ &\sim \frac{U+\Delta U}{r_0 L} + \frac{L}{r_0}\frac{\Delta U}{r_0 H} + \frac{W}{H^2} \end{aligned} \tag{B.32}$$

Summing the tangential components, (B.27), (B.29) and (B.31), and reducing to the largest relative terms, yields the characteristic scales for the horizontal friction terms,

$$\begin{aligned} \mathrm{F}_\phi, \mathrm{F}_\lambda &\sim \frac{\Delta U}{H^2} + \frac{U}{L^2} + \cancel{\frac{U+\Delta U}{r_0^2}} + \cancel{\frac{W}{r_0 L}} + \cancel{\frac{U+\Delta U}{L^2}} + \frac{W}{LH} \\ &\sim \frac{\Delta U}{H^2} + \frac{U}{L^2} + \frac{W}{LH}. \end{aligned} \tag{B.33}$$

Summing the vertical components, (B.28), (B.30) and (B.32), yields the characteristic scales for the vertical friction terms,

$$\mathrm{F}_r \sim \frac{W}{H^2} + \frac{U+\Delta U}{r_0 L} + \frac{L}{r_0}\frac{\Delta U}{r_0 H}. \tag{B.34}$$

Appendix C

Scaled, Dimensionless rSW Equations

C.1 Scales, Dimensionless Parameters and Operators

We begin by recalling the discussion from Section 2.2, where variables are represented as a constant characteristic scale and a dimensionless $\mathcal{O}(1)$ variable. Here, we represent the characteristic scales in terms of the dimensionless constants also specified in Section 2.2.

$$\xi = \frac{L}{r_0}, \quad \mathcal{C} = \frac{L}{UT}, \quad \varepsilon_L = \frac{H}{L}, \quad \varepsilon_u = \frac{W}{U}, \quad \gamma_\rho = \frac{\Delta\rho}{\rho_0}, \tag{C.1}$$

where at synoptic and mesoscales, $\xi < 1$, $\varepsilon_L \ll 1$, $\varepsilon_u \ll 1$, at geostrophic time scales $\mathcal{C} < \mathcal{R}^{-1}$ and in the Boussinesq approximation, $\gamma_\rho \ll 1$ (see Section 2.2.1).

$$\gamma_u = \frac{\Delta U}{U}, \qquad \gamma_p = \frac{\Delta \mathcal{P}}{\mathcal{P}}, \tag{C.2}$$

where we assume $\gamma_u < 1$ and $\gamma_p < 1$.

The position and time variables, from (2.26), become

$$\phi \to \xi\phi_l \qquad \lambda \to \xi\lambda_l \qquad r \to r_0(1 + \varepsilon_L\xi) \qquad t \to \frac{\mathcal{C}U}{L}t \tag{C.3}$$

where trigonometric functions of ϕ and λ become

$$\cos\phi \to \cos\xi\phi_l \qquad \sin\phi \to \sin\xi\phi_l, \tag{C.4}$$

$$\cos\lambda \to \cos\xi\lambda_l \qquad \sin\lambda \to \sin\xi\lambda_l \qquad \tan\lambda \to \tan\xi\lambda_l. \tag{C.5}$$

Velocities, from (2.29), become

$$\begin{aligned} u &\rightarrow U\left[u(\phi_l,\lambda_l,t)+\gamma_u u(\phi_l,\lambda_l,z,t)\right] \\ v &\rightarrow U\left[v(\phi_l,\lambda_l,t)+\gamma_u v(\phi_l,\lambda_l,z,t)\right] \\ w &\rightarrow U\varepsilon_u\left[w(\phi_l,\lambda_l,z,t)\right] \end{aligned} \tag{C.6}$$

density, from (2.27), becomes

$$\rho \rightarrow \rho_0\left[1+\gamma_\rho\rho'(\phi_l,\lambda_l,z,t)\right] \tag{C.7}$$

and pressure, from (2.28), becomes

$$p \rightarrow \rho_0 g\left[p_0(z)\right]+\boldsymbol{\rho_0 fUL}\left[\boldsymbol{p(\phi_l,\lambda_l,t)}+\gamma_p p'(\phi_l,\lambda_l,z,t)\right] \tag{C.8}$$

where the hydrostatic, $\mathcal{P}_0 \sim \rho_0 gH$, and geostrophic, $\mathcal{P} \sim \rho_0 fUL$, approximations from (2.35) have been substituted.

By defining $f = 2\Omega\cos\Lambda_0$ and $\beta = \xi\cot\Lambda_0$, as in (2.30) and (2.31), the Coriolis parameters, (2.15) - (2.17), are rewritten as

$$\Omega_\phi = -\frac{f}{2}\sin\xi\phi_l, \tag{C.9}$$

$$\Omega_\lambda = \frac{f}{2}\left[-\cos\xi\phi_l\sin\xi\lambda_l+\frac{\beta}{\xi}\cos\xi\lambda_l\right], \tag{C.10}$$

$$\Omega_r = \frac{f}{2}\left[\cos\xi\phi_l\cos\xi\lambda_l+\frac{\beta}{\xi}\sin\xi\lambda_l\right]. \tag{C.11}$$

C.1.1 Taylor Expansion

The quotient $\frac{1}{r}$ arises frequently, and can be expressed as an $\mathcal{O}(\varepsilon_L\xi)$ deviation from Earth's radius, r_0, by considering the Taylor expansion in small $\varepsilon_L\xi z$.

$$\begin{aligned} \frac{1}{r} &\rightarrow \frac{1}{r_0\left(1+\varepsilon_L\xi z\right)} \\ &\rightarrow \frac{1}{r_0}\left[1-\varepsilon_L\xi z+\ldots\right] \\ &\rightarrow \frac{1}{r_0}\left[1+\mathcal{O}\left(\varepsilon_L\xi\right)\right] \end{aligned} \tag{C.12}$$

When multiplied by γ and ε terms, the order of the trig functions affects the overall scale size. In this case, we expand about $\lambda_0 = 0$ and $\phi_0 = 0$,

$$\begin{aligned} \cos\xi\phi_l, \cos\xi\lambda_l &= \mathcal{O}(1) \\ \sin\xi\phi_l, \sin\xi\lambda_l, \tan\xi\lambda_l &= \mathcal{O}(\xi) \end{aligned} \tag{C.13}$$

As a result of the oblique spherical coordinate system, the order of the trigonometric functions does not depend on Λ_0.

If we substitute the order of the above trigonometric functions into the Coriolis terms, we find that

$$\Omega_\phi \;=\; \frac{f}{2}\mathcal{O}\left(\xi\right), \qquad \Omega_\lambda \;=\; \frac{f}{2}\mathcal{O}\left(\xi, \frac{\beta}{\xi}\right), \qquad \Omega_r \;=\; \frac{f}{2}\mathcal{O}\left(1, \beta\right). \tag{C.14}$$

where $\frac{\beta}{\xi} = \cot\Lambda_0$ becomes very large near the equator ($\Lambda_0 = 0$), and is the only term in the oblique spherical equations to have such a latitude dependence.

C.1.2 Scaled Operators

The scaled operators are obtained in two steps:

1. Nondimensionalize and scale the position and time variables by substituting (C.3), and replace $\frac{1}{r}$ with its Taylor expansion, (C.12). Where necessary, substitute for the velocity variables (C.6).

2. Determine the order of any ε, γ terms, where trig functions multiplying ε, γ terms are replaced with (C.13).

First derivatives in ϕ_l and λ_l are obtained by applying steps 1 and 2,

$$\begin{aligned}
\frac{1}{r\cos\phi}\frac{\partial}{\partial\phi} \;&\rightarrow\; \frac{1+\mathcal{O}\left(\varepsilon_L\xi\right)}{r_0}\frac{1}{\cos\xi\lambda_l}\frac{1}{\xi}\frac{\partial}{\partial\phi_l} \\
&\rightarrow\; \frac{1}{L}\left[\frac{1}{\cos\xi\lambda_l}\frac{\partial}{\partial\phi_l} + \mathcal{O}\left(\varepsilon_L\xi\right)\right] \qquad \text{(C.15)} \\
\frac{1}{r}\frac{\partial}{\partial\lambda} \;&\rightarrow\; \frac{1+\mathcal{O}\left(\varepsilon_L\xi\right)}{r_0}\frac{1}{\xi}\frac{\partial}{\partial\phi_l} \\
&\rightarrow\; \frac{1}{L}\left[\frac{\partial}{\partial\lambda_l} + \mathcal{O}\left(\varepsilon_L\xi\right)\right] \qquad \text{(C.16)}
\end{aligned}$$

while first derivatives in z and t are obtained by differentiating (C.3),

$$\frac{\partial}{\partial r} \;\rightarrow\; \frac{1}{r_0\varepsilon_L\xi}\frac{\partial}{\partial z} \;\rightarrow\; \frac{1}{L\varepsilon_L}\frac{\partial}{\partial z} \tag{C.17}$$

$$\frac{\partial}{\partial t} \;\rightarrow\; \frac{\mathcal{C}U}{L}\frac{\partial}{\partial t} \tag{C.18}$$

The advective derivative,

$$\frac{\mathrm{D}}{\mathrm{D}t} \;=\; \frac{\partial}{\partial t} + \frac{u}{r\cos\lambda}\frac{\partial}{\partial\phi} + \frac{v}{r}\frac{\partial}{\partial\lambda} + \frac{\partial w}{\partial r}, \tag{C.19}$$

is scaled and nondimensionalized by applying steps 1 and 2, where the derivatives are replaced with the above scaled dimensionless forms,

$$\begin{aligned}\frac{\mathrm{D}}{\mathrm{D}t} \quad \rightarrow \quad & \frac{U\mathcal{C}}{L}\frac{\partial}{\partial t} + U(u+\gamma_u u')\frac{\left[1+\mathcal{O}\left(\varepsilon_L\xi\right)\right]}{r_0\cos\xi\lambda_l}\frac{1}{\xi}\frac{\partial}{\partial\phi_l} \\ & + U(v+\gamma_u v')\frac{\left[1+\mathcal{O}\left(\varepsilon_L\xi\right)\right]}{r_0}\frac{1}{\xi}\frac{\partial}{\partial\lambda_l} + \frac{U}{L}\frac{\varepsilon_u}{\varepsilon_L}\frac{\partial w}{\partial z} \\ \rightarrow \quad & \frac{U}{L}\left[\frac{\partial}{\partial t} + \frac{u}{\cos\xi\lambda_l}\frac{\partial}{\partial\phi_l} + v\frac{\partial}{\partial\lambda_l}\right. \\ & \left. + \frac{\varepsilon_u}{\varepsilon_L}w\frac{\partial}{\partial z} + \mathcal{O}\left(\gamma_u,\varepsilon_L\xi\right)\left(\frac{\partial}{\partial\phi_l}+\frac{\partial}{\partial\lambda_l}\right)\right] \end{aligned} \tag{C.20}$$

Since the advective derivative acts on velocities, (C.6), and density, (C.7), which are dependent on ϕ_l and λ_l, the horizontal derivatives are assumed $\mathcal{O}(1)$, and the scaled advective derivative is

$$\frac{\mathrm{D}}{\mathrm{D}t} \quad \rightarrow \quad \frac{U}{L}\left(\frac{\mathrm{D}_l}{\mathrm{D}t} + \frac{\varepsilon_u}{\varepsilon_L}w\frac{\partial}{\partial z} + \mathcal{O}\left(\gamma_u,\varepsilon_L\xi\right)\right), \tag{C.21}$$

where the dimensionless horizontal advective derivative is defined as

$$\frac{\mathrm{D}_l}{\mathrm{D}t} \quad = \quad \mathcal{C}\frac{\partial}{\partial t} + \frac{u(\phi_l,\lambda_l)}{\cos\xi\lambda_l}\frac{\partial}{\partial\phi_l} + v(\phi_l,\lambda_l)\frac{\partial}{\partial\lambda_l}. \tag{C.22}$$

C.2 Scaling and Nondimensionalizing the Navier-Stokes Equations

We now scale and nondimensionalize the oblique, spherical Navier-Stokes equations, (2.21) - (2.24), to obtain the rSW class of solutions, where all ε, γ terms can be assumed negligible. In this derivation, we are interested in determining the maximum size of the ε, γ terms, where the system is accurate to $\mathcal{O}(\alpha)$, for an arbitrary α. This is done in four steps:

1. For each term, nondimensionalize and scale the position and time variables by substituting (C.3), and replace $\frac{1}{r}$ with its Taylor expansion, (C.12). Scale velocities by substituting (C.6), density by substituting (C.7), pressure by substituting (C.8), and Coriolis parameters by substituting (C.9) - (C.11).

2. Determine the order of any ε, γ terms within each term, where any trigonometric functions multiplying ε, γ terms are replaced with (C.13).

3. Sum all terms, and nondimensionalize by dividing by the appropriate equation scaling, specified for each equation, and simplify to multiples of the dimensionless parameters, from (2.31),

$$\mathcal{R} \;=\; \frac{U}{fL}, \qquad \mathcal{F} \;=\; \frac{U}{\sqrt{gH}}, \qquad \mathcal{E}k \;=\; \frac{\mu}{\rho_0 f H^2} \tag{C.23}$$

4. Determine the order of the ε, γ terms, where the synoptic and mesoscale assumptions are used, from (2.34),

$$\xi \;<\; 1, \qquad \gamma_\rho \;\ll\; 1, \qquad \varepsilon \;\ll\; 1, \qquad \varepsilon_u \;\ll\; 1, \tag{C.24}$$

in addition to $\gamma_u < 1$ and $\gamma_\rho < 1$ as additional assumptions within the rSW solution regime.

C.2.1 Dimensionless Continuity Equation

The oblique spherical Navier-Stokes continuity equation, (2.24), is

$$\frac{\mathrm{D}\rho}{\mathrm{D}t} + \rho\frac{1}{r\cos\lambda}\frac{\partial u}{\partial\phi} + \rho\frac{1}{r}\frac{\partial v}{\partial\lambda} - \rho\frac{1}{r}v\tan\lambda + \rho\frac{\partial w}{\partial r} + \rho\frac{2}{r}w \;=\; 0 \tag{C.25}$$

Steps 1-2 from Section C.2 are applied to each term from the above continuity equation,

$$\begin{aligned}
\frac{\mathrm{D}\rho}{\mathrm{D}t} \;&\rightarrow\; \frac{U}{L}\left[\frac{\mathrm{D}_l}{\mathrm{D}t} + \frac{\varepsilon_u}{\varepsilon_L}w\frac{\partial}{\partial z} + \mathcal{O}\left(\gamma_u, \varepsilon_L\xi\right)\right]\rho_0\gamma_\rho \\
&\rightarrow\; \rho_0\mathcal{O}\left(\gamma_\rho\left[1, \mathcal{C}, \frac{\varepsilon_u}{\varepsilon_L}\right]\right) \qquad \text{(C.26)} \\
\rho\frac{1}{r\cos\lambda}\frac{\partial u}{\partial\phi} \;&\rightarrow\; \rho_0(1+\gamma_\rho\rho')\frac{\left[1+\mathcal{O}\left(\varepsilon_L\xi\right)\right]}{r_0\cos\xi\lambda_l}\frac{1}{\xi}\frac{\partial}{\partial\phi_l}U(u+\gamma_u u') \\
&\rightarrow\; \frac{\rho_0 U}{L}\left[\frac{1}{\cos\xi\lambda_l}\frac{\partial u}{\partial\phi_l} + \mathcal{O}\left(\gamma_u, \gamma_\rho, \varepsilon_L\xi\right)\right] \qquad \text{(C.27)} \\
\rho\frac{1}{r}\frac{\partial v}{\partial\lambda} \;&\rightarrow\; \rho_0(1+\gamma_\rho\rho')\frac{\left[1+\mathcal{O}\left(\varepsilon_L\xi\right)\right]}{r_0}\frac{1}{\xi}\frac{\partial}{\partial\lambda_l}U(v+\gamma_u v') \\
&\rightarrow\; \frac{\rho_0 U}{L}\left[\frac{\partial v}{\partial\lambda_l} + \mathcal{O}\left(\gamma_u, \gamma_\rho, \varepsilon_L\xi\right)\right] \qquad \text{(C.28)} \\
-\rho\frac{v}{r}\tan\lambda \;&\rightarrow\; -\rho_0(1+\gamma_\rho\rho')\frac{\left[1+\mathcal{O}\left(\varepsilon_L\xi\right)\right]}{r_0}U(v+\gamma_u v')\tan\xi\lambda_l \\
&\rightarrow\; -\frac{\rho_0 U}{L}\left[\xi v\tan\lambda + \mathcal{O}\left(\xi^2[\gamma_u, \gamma_\rho, \varepsilon_L\xi]\right)\right] \qquad \text{(C.29)}
\end{aligned}$$

$$\begin{aligned}
\rho\frac{\partial w}{\partial r} &\rightarrow \frac{\rho_0 U}{L}(1+\gamma_\rho\rho')\frac{\varepsilon_u}{\varepsilon_L}\frac{\partial w}{\partial z} \\
&\rightarrow \frac{\rho_0 U}{L}\left[\frac{\varepsilon_u}{\varepsilon_L}\frac{\partial w}{\partial z}+\mathcal{O}\left(\gamma_\rho\left[1,\frac{\varepsilon_u}{\varepsilon_L}\right]\right)\right] \qquad \text{(C.30)} \\
\rho\frac{2}{r}w &\rightarrow 2\rho_0(1+\gamma_\rho\rho')\frac{1+\mathcal{O}(\varepsilon_L\xi)}{r_0}U\varepsilon_u w \\
&\rightarrow \frac{\rho_0 U}{L}\mathcal{O}(\xi\varepsilon_u) \qquad \text{(C.31)}
\end{aligned}$$

Step 3 is applied by summing the above terms, and dividing by the characteristic scale $\rho_0 U/L$,

$$\begin{aligned}
&\mathcal{O}\left(\gamma_\rho\left[1,\mathcal{C},\frac{\varepsilon_u}{\varepsilon_L}\right]\right)+\left[\frac{1}{\cos\xi\lambda_l}\frac{\partial u}{\partial\phi_l}+\mathcal{O}(\gamma_u,\gamma_\rho,\varepsilon_L\xi)\right] \\
&+\left[\frac{\partial v}{\partial\lambda_l}+\mathcal{O}(\gamma_u,\gamma_\rho,\varepsilon_L\xi)\right]-\left[\xi v\tan\lambda+\mathcal{O}\left(\xi^2[\gamma_u,\gamma_\rho,\varepsilon_L\xi]\right)\right] \\
&+\left[\frac{\varepsilon_u}{\varepsilon_L}\frac{\partial w}{\partial z}+\mathcal{O}\left(\gamma_\rho\left[1,\frac{\varepsilon_u}{\varepsilon_L}\right]\right)\right]+\mathcal{O}(\xi\varepsilon_u) \;=\; 0 \qquad \text{(C.32)}
\end{aligned}$$

The dimensionless continuity equation is obtained by applying Step 4 and determining the order of negligible terms,

$$\frac{1}{\cos\xi\lambda_l}\frac{\partial u}{\partial\phi_l}+\frac{\partial v}{\partial\lambda_l}-\xi v\tan\lambda+\frac{\varepsilon_u}{\varepsilon_L}\frac{\partial w}{\partial z} \;=\; \mathcal{O}\left(\gamma_u,\gamma_\rho\left[1,\mathcal{C},\frac{\varepsilon_u}{\varepsilon_L}\right],\xi[\varepsilon_u,\varepsilon_L]\right). \qquad \text{(C.33)}$$

C.2.2 Dimensionless Vertical Momentum Equation

The oblique spherical Navier-Stokes vertical momentum equation, (2.23), is

$$\rho\frac{\mathrm{D}w}{\mathrm{D}t}-\rho\frac{u^2+v^2}{r}+2\rho v\Omega_\phi-2\rho u\Omega_\lambda \;=\; -\frac{\partial p}{\partial r}-\rho g+\mu\mathrm{F}_r. \qquad \text{(C.34)}$$

where from (2.36), the vertical friction force scales as $F_r \sim \frac{W}{H^2}+\frac{U+\Delta U}{L^2}+\frac{L}{r_0}\frac{\Delta U}{r_0 H}$.

Steps 1 and 2 from Section C.2 are applied to each term of the vertical momentum equation. In anticipation of the large equation scaling, some non-ε, γ terms are written as an order only.

$$\begin{aligned}
\rho\frac{\mathrm{D}w}{\mathrm{D}t} &\rightarrow \rho_0\left(1+\gamma_\rho\rho'\right)\frac{U}{L}\left[\frac{\mathrm{D}_l}{\mathrm{D}t}+\frac{\varepsilon_u}{\varepsilon_L}w\frac{\partial}{\partial z}+\mathcal{O}(\gamma_u,\varepsilon_L\xi)\right]U\varepsilon_u w \\
&\rightarrow \frac{\rho_0 U^2}{L}\mathcal{O}\left(\varepsilon_u\left[1,\mathcal{C},\frac{\varepsilon_u}{\varepsilon_L}\right]\right) \qquad \text{(C.35)}
\end{aligned}$$

$$
\begin{aligned}
-\rho\frac{u^2+v^2}{r} &\rightarrow -\rho_0\left(1+\gamma_\rho\rho'\right)U^2\left[(u+\gamma_u u')^2+(v+\gamma_u v')^2\right]\frac{1+\mathcal{O}\left(\varepsilon_L\xi\right)}{r_0} \\
&\rightarrow -\frac{\rho_0 U^2}{L}\mathcal{O}\left(\xi\right) && \text{(C.36)} \\
2\rho v\Omega_\phi &\rightarrow \rho_0\left(1+\gamma_\rho\rho'\right)U(v+\gamma_u v')(-f\sin\xi\phi_l) \\
&\rightarrow -\rho_0 U f\mathcal{O}\left(\xi\right) && \text{(C.37)} \\
-2\rho u\Omega_\lambda &\rightarrow -\rho_0\left(1+\gamma_\rho\rho'\right)U(u+\gamma_u u')\left(-\cos\xi\phi_l\sin\xi\lambda_l+\frac{\beta}{\xi}\cos\xi\lambda_l\right) \\
&\rightarrow \rho_0 fU\mathcal{O}\left(\xi,\frac{\beta}{\xi}\right) && \text{(C.38)} \\
-\frac{\partial p}{\partial r} &\rightarrow \frac{-1}{L\varepsilon_L}\frac{\partial}{\partial z}\left[\rho_0 gHp_0(z)+\rho_0 fUL\left(p(\phi_l,\lambda_l,t)+\gamma_p p'(\phi_l,\lambda_l,z,t)\right)\right] \\
&\rightarrow -\rho_0 g\frac{\partial p_0}{\partial z}-\frac{\rho_0 fU}{\varepsilon_L}\gamma_p\frac{\partial p'}{\partial z} && \text{(C.39)} \\
-\rho g &\rightarrow -\rho_0\left(1+\gamma_\rho\rho'\right)g \rightarrow -\rho_0 g\left(1+\mathcal{O}\left(\gamma_\rho\right)\right) && \text{(C.40)} \\
\mu\mathrm{F}_r &\sim \frac{W}{H^2}+\frac{U+\Delta U}{L^2}+\frac{L}{r_0}\frac{\Delta U}{r_0 H} \\
&\rightarrow \rho_0 fU\mathcal{O}\left(\mathcal{E}k\left[\varepsilon_u,\varepsilon_L^2,\gamma_u\varepsilon_L\xi\right]\right) && \text{(C.41)}
\end{aligned}
$$

Step 3 is applied by summing the above terms, and dividing by the characteristic scale $\rho_0 g$. Note that $\frac{\rho_0 U}{L}\frac{1}{\rho_0 g}=\mathcal{F}^2\varepsilon_L$ and $\rho_0 fU\frac{1}{\rho_0 g}=\frac{\mathcal{F}^2}{\mathcal{R}}\varepsilon_L$.

$$
\begin{aligned}
&\mathcal{F}^2\varepsilon_L\mathcal{O}\left(\varepsilon_u\left[1,\mathcal{C},\frac{\varepsilon_u}{\varepsilon_L}\right]\right)-\mathcal{F}^2\varepsilon_L\mathcal{O}\left(\xi\right) \\
&\quad -\frac{\mathcal{F}^2}{\mathcal{R}}\varepsilon_L\mathcal{O}\left(\xi\right)+\frac{\mathcal{F}^2}{\mathcal{R}}\varepsilon_L\mathcal{O}\left(\xi,\frac{\beta}{\xi}\right) = -\frac{\partial p_0}{\partial z}-\frac{\mathcal{F}^2}{\mathcal{R}}\gamma_p\frac{\partial p'}{\partial z}-1+\mathcal{O}\left(\gamma_\rho\right) \\
&\qquad\qquad +\frac{\mathcal{F}^2}{\mathcal{R}}\varepsilon_L\mathcal{O}\left(\mathcal{E}k\left[\varepsilon_u,\varepsilon_L^2,\gamma_u\varepsilon_L\xi\right]\right) \qquad \text{(C.42)}
\end{aligned}
$$

The dimensionless vertical momentum equation is obtained by applying Step 4 and determining the order of the negligible terms,

$$
\begin{aligned}
-\frac{\partial p_0}{\partial z}-1 &= \mathcal{O}\left(\gamma_\rho,\frac{\mathcal{F}^2}{\mathcal{R}}\gamma_p,\frac{\mathcal{F}^2}{\mathcal{R}}\varepsilon_L\left[\xi,\frac{\beta}{\xi},\mathcal{E}k\left[\varepsilon_u,\varepsilon_L^2,\varepsilon_L\xi\gamma_u\right]\right],\right. \\
&\qquad\left.\mathcal{F}^2\left[\varepsilon_u^2,\varepsilon_L\varepsilon_u[1,\mathcal{C}]\right]\right) \qquad \text{(C.43)}
\end{aligned}
$$

C.2.3 Dimensionless Zonal Momentum Equation

The oblique spherical Navier-Stokes zonal momentum equation, (2.21), is

$$
\rho\frac{\mathrm{D}u}{\mathrm{D}t}+\rho\frac{uw}{r}-\rho\frac{uv\tan\lambda}{r}+2\rho v\Omega_\lambda-2\rho v\Omega_r = \frac{-1}{r\cos\lambda}\frac{\partial p}{\partial\phi}+\mu\mathrm{F}_\phi \qquad \text{(C.44)}
$$

where from (2.36), the vertical friction force scales as $F_\phi \sim \frac{\Delta U}{H^2} + \frac{U}{L^2} + \frac{W}{HL}$.

Steps 1 and 2 from Section C.2 are applied to the zonal momentum equation,

$$\begin{aligned}
\rho\frac{\mathrm{D}u}{\mathrm{D}t} &\rightarrow \rho_0\left(1+\gamma_\rho\rho'\right)\frac{U}{L}\left[\frac{\mathrm{D}_l}{\mathrm{D}t}+\frac{\varepsilon_u}{\varepsilon_L}w\frac{\partial}{\partial z}+\mathcal{O}\left(\gamma_u,\varepsilon_L\xi\right)\right]U(u+\gamma_u u') \\
&\rightarrow \frac{\rho_0 U}{L}\left[\frac{\mathrm{D}_l u}{\mathrm{D}t}+\mathcal{O}\left([\gamma_u,\gamma_\rho]\left[1,\mathcal{C},\frac{\varepsilon_u}{\varepsilon_L}\right],\varepsilon_L\xi\right)\right] \qquad \text{(C.45)} \\
\rho\frac{wu}{r} &\rightarrow \rho_0\left(1+\gamma_\rho\rho'\right)U^2\varepsilon_u w(u+\gamma_u u')\frac{1+\mathcal{O}\left(\varepsilon_L\xi\right)}{r_0} \\
&\rightarrow \frac{\rho_0 U^2}{L}\mathcal{O}\left(\xi\varepsilon_u\right) \qquad \text{(C.46)} \\
-\rho\frac{uv\tan\lambda}{r} &\rightarrow \rho_0\left(1+\gamma_\rho\rho'\right)U^2(u+\gamma_u u')(v+\gamma_u v')\frac{1+\mathcal{O}\left(\varepsilon_L\xi\right)}{r_0}\tan\xi\lambda_l \\
&\rightarrow -\frac{\rho_0 U^2}{L}\left[\xi uv\tan\lambda+\mathcal{O}\left(\xi^2[\gamma_u,\gamma_\rho],\xi^3\varepsilon_L\right)\right] \qquad \text{(C.47)} \\
2\rho w\Omega_\lambda &\rightarrow \rho_0\left(1+\gamma_\rho\rho'\right)U\varepsilon_u w f\left(-\cos\xi\phi_l\sin\xi\lambda_l+\frac{\beta}{\xi}\cos\xi\lambda_l\right) \\
&\rightarrow \rho_0 fU\mathcal{O}\left(\varepsilon_u\left[\xi,\frac{\beta}{\xi},\gamma_\rho\right]\right) \qquad \text{(C.48)} \\
-2\rho v\Omega_r &\rightarrow -\rho_0\left(1+\gamma_\rho\rho'\right)U(v+\gamma_u v')f\left(\cos\xi\phi_l\cos\xi\lambda_l+\frac{\beta}{\xi}\sin\xi\lambda_l\right) \\
&\rightarrow -\rho_0 fU\left[v\left(\cos\xi\phi_l\cos\xi\lambda_l+\frac{\beta}{\varepsilon}\sin\xi\lambda_l\right)+\mathcal{O}\left(\gamma_u,\gamma_\rho\right)\right] \qquad \text{(C.49)} \\
\frac{-1}{r\cos\lambda}\frac{\partial p}{\partial\phi} &\rightarrow \frac{-1}{L}\left[\frac{1}{\cos\xi\lambda_l}\frac{\partial}{\partial\phi_l}+\mathcal{O}\left(\varepsilon_L\xi\right)\right]\rho_0 fUL\left(p\left(\phi_l,\lambda_l,t\right)+\gamma_p p'\left(\phi_l,\lambda_l,z,t\right)\right) \\
&\rightarrow \rho_0 fU\left[\frac{-1}{\cos\xi\lambda_l}\frac{\partial p}{\partial\phi_l}+\mathcal{O}\left(\gamma_p,\varepsilon_L\xi\right)\right] \qquad \text{(C.50)} \\
\mu\mathrm{F}_\phi &\sim \frac{\Delta U}{H^2}+\frac{U}{L^2}+\frac{W}{HL} \\
&\rightarrow \rho_0 fU\mathcal{O}\left(\mathcal{E}k\left[\gamma_u,\varepsilon_L^2,\varepsilon_L\varepsilon_u\right]\right) \qquad \text{(C.51)}
\end{aligned}$$

Step 3 is applied by summing the above terms, and dividing by the characteristic scale, $\rho_0 fU$. Note that $\frac{\rho_0 U^2}{L}\frac{1}{\rho_0 fU} = \mathcal{R}$.

$$\begin{aligned}
&\mathcal{R}\left[\frac{\mathrm{D}_l u}{\mathrm{D}t}+\mathcal{O}\left([\gamma_u,\gamma_\rho]\left[1,\mathcal{C},\frac{\varepsilon_u}{\varepsilon_L}\right],\varepsilon_L\xi\right)\right] \\
&+\mathcal{R}\mathcal{O}\left(\xi\varepsilon_u\right)-\mathcal{R}\left[\xi uv\tan\lambda+\mathcal{O}\left(\xi^2[\gamma_u,\gamma_\rho],\xi^3\varepsilon_L\right)\right] \\
&+\mathcal{O}\left(\varepsilon_u\left[\xi,\frac{\beta}{\xi},\gamma_\rho\right]\right)-\left[v\Gamma_r+\mathcal{O}\left(\gamma_u,\gamma_\rho\right)\right] \;=\; \frac{-1}{\cos\xi\lambda_l}\frac{\partial p}{\partial\phi_l}+\mathcal{O}\left(\gamma_p,\varepsilon_L\xi\right) \\
&\qquad\qquad +\mathcal{O}\left(\mathcal{E}k\left[\gamma_u,\varepsilon_L^2,\varepsilon_L\varepsilon_u\right]\right) \qquad \text{(C.52)}
\end{aligned}$$

where the scaled Coriolis parameter, Γ_r, is

$$\Gamma_r = \cos\xi\phi_l \cos\xi\lambda_l + \frac{\beta}{\xi}\sin\xi\lambda_l. \tag{C.53}$$

The dimensionless zonal momentum equation is obtained by applying Step 4 and determining the order of negligible terms,

$$\begin{aligned}\mathcal{R}\frac{\mathrm{D}_l u}{\mathrm{D}t} - \mathcal{R}\xi uv\tan\lambda - v\Gamma_r &= \frac{-1}{\cos\xi\lambda_l}\frac{\partial p}{\partial\phi_l} + \mathcal{O}\left(\left[\gamma_u,\gamma_\rho\right]\left[1,\frac{\varepsilon_u}{\varepsilon_L}\right],\gamma_p,\varepsilon_u\frac{\beta}{\xi},\xi\left[\varepsilon_u,\varepsilon_L\right]\right)\\ &\quad +\mathcal{O}\left(\mathcal{E}k\left[\gamma_u,\varepsilon_L^2,\varepsilon_L\varepsilon_u\right]\right)\end{aligned} \tag{C.54}$$

C.2.4 Dimensionless Meridional Momentum Equation

The oblique spherical Navier-Stokes meridional momentum equation, (2.22), is

$$\rho\frac{\mathrm{D}v}{\mathrm{D}t} + \rho\frac{uv}{r} + \rho\frac{u^2\tan\lambda}{r} + 2\rho u\Omega_r - 2\rho w\Omega_\phi = \frac{-1}{r}\frac{\partial p}{\partial\lambda} + \mu\mathrm{F}_\lambda \tag{C.55}$$

from (2.36), the vertical friction force scales as $F_\lambda \sim \frac{\Delta U}{H^2} + \frac{U}{L^2} + \frac{W}{HL}$. Since the horizontal momentum equations in both x and y scale in a similar manner, only the Coriolis terms are considered here, while the order of the remaining terms is implied from the above analysis of the zonal momentum equations.

$$\begin{aligned}2\rho u\Omega_r &\rightarrow \rho_0\left(1+\gamma_\rho\rho'\right)U(u+\gamma_u u')f\left(\cos\xi\phi_l\cos\xi\lambda_l + \frac{\beta}{\xi}\sin\xi\lambda_l\right)\\ &\rightarrow \rho_0 fU\left[u\left(\cos\xi\phi_l\cos\xi\lambda_l + \frac{\beta}{\xi}\sin\xi\lambda_l\right) + \mathcal{O}\left(\gamma_u,\gamma_\rho\right)\right] \qquad \text{(C.56)}\\ -2\rho w\Omega_\phi &\rightarrow \rho_0\left(1+\gamma_\rho\rho'\right)U\varepsilon_u w f(-\sin\xi\phi_l)\\ &\rightarrow \rho_0 fU\mathcal{O}\left(\xi\varepsilon_u\right) \qquad \text{(C.57)}\end{aligned}$$

Step 3 is applied by summing the above terms, and dividing by the characteristic scale, $\rho_0 fU$. Note that $\frac{\rho_0 U^2}{L}\frac{1}{\rho_0 fU} = \mathcal{R}$.

$$\begin{aligned}&\mathcal{R}\left[\frac{\mathrm{D}_l v}{\mathrm{D}t} + \mathcal{O}\left(\left[\gamma_u,\gamma_\rho\right]\left[1,\mathcal{C},\frac{\varepsilon_u}{\varepsilon_L}\right],\varepsilon_L\xi\right)\right]\\ &+\mathcal{R}\mathcal{O}\left(\xi\varepsilon_u\right) + \mathcal{R}\left[\xi u^2\tan\lambda + \mathcal{O}\left(\xi^2[\gamma_u,\gamma_\rho],\xi^3\varepsilon_L\right)\right]\\ &\qquad + \left[u\Gamma_r + \mathcal{O}\left(\gamma_u,\gamma_\rho\right)\right] + \mathcal{O}\left(\xi\varepsilon_u\right) = \left[-\frac{\partial p}{\partial\lambda_l} + \mathcal{O}\left(\gamma_p,\varepsilon_L\xi\right)\right]\\ &\qquad\qquad +\mathcal{O}\left(\mathcal{E}k\left[\gamma_u,\varepsilon_L^2,\varepsilon_L\varepsilon_u\right]\right)\end{aligned} \tag{C.58}$$

where the scaled Coriolis parameter, Γ_r, is

$$\Gamma_r = \cos\xi\phi_l \cos\xi\lambda_l + \frac{\beta}{\xi}\sin\xi\lambda_l. \tag{C.59}$$

The dimensionless meridional momentum equation is obtained by applying Step 4 and determining the order of negligible terms,

$$\begin{aligned}\mathcal{R}\frac{\mathrm{D}_l v}{\mathrm{D}t} + \mathcal{R}\xi u^2 \tan\lambda + u\Gamma_r &= -\frac{\partial p}{\partial \lambda_l} + \mathcal{O}\left(\left[\gamma_u, \gamma_\rho\right]\left[1, \frac{\varepsilon_u}{\varepsilon_L}\right], \gamma_p, \xi\left[\varepsilon_u, \varepsilon_L\right]\right) \\ &\quad + \mathcal{O}\left(\mathcal{E}k\left[\gamma_u, \varepsilon_L^2, \varepsilon_L\varepsilon_u\right]\right)\end{aligned} \tag{C.60}$$

Appendix D

Integral Constraints

D.1 Useful Identities

For the following identities, we consider a domain $D = [-D_x, D_x] \times [-D_y, D_y]$, where continuous functions $A(x, y, t)$ and $B(x, y, t)$ are periodic at the horizontal boundaries.

Zero area integrals arise when:

1. The integrand is a pure spatial derivative of periodic functions

$$\int_D \frac{\partial}{\partial x}(A(x, y, t)) \;=\; \int_{-D_y}^{D_y} A(D_x, y, t) - A(-D_x, y, t) \;=\; 0 \tag{D.1}$$

2. The integrand is a Jacobian of periodic functions

$$\int_D J(A, B) \;=\; \int_D \frac{\partial}{\partial x}\left(A\frac{\partial B}{\partial y}\right) - \frac{\partial}{\partial y}\left(A\frac{\partial B}{\partial x}\right) \;=\; 0 \tag{D.2}$$

Identity 1

$$AJ(A, B) \;=\; \frac{1}{2}J(A^2, B) \tag{D.3}$$

Identity 2

$$A\left(\nabla^2 - 1\right)A \;=\; -\left[\left(\frac{\partial A}{\partial x}\right)^2 + \left(\frac{\partial A}{\partial y}\right)^2 + A^2\right] + \frac{\partial}{\partial x}\left(A\frac{\partial A}{\partial x}\right) + \frac{\partial}{\partial y}\left(A\frac{\partial A}{\partial y}\right) \tag{D.4}$$

Identity 3

$$B\left(\nabla^2 - 1\right)A \;=\; A\left(\nabla^2 - 1\right)B + \frac{\partial}{\partial x}\left(B\frac{\partial A}{\partial x} - A\frac{\partial B}{\partial x}\right) + \frac{\partial}{\partial y}\left(B\frac{\partial A}{\partial y} - A\frac{\partial B}{\partial y}\right) \tag{D.5}$$

Identity 4

$$\frac{\partial A}{\partial s}(\nabla^2 - 1)A = -\frac{1}{2}\frac{\partial}{\partial s}\left[\left(\frac{\partial A}{\partial x}\right)^2 + \left(\frac{\partial A}{\partial y}\right)^2 + A^2\right] + \frac{\partial}{\partial x}\left(\frac{\partial A}{\partial s}\frac{\partial A}{\partial x}\right) + \frac{\partial}{\partial y}\left(\frac{\partial A}{\partial s}\frac{\partial A}{\partial y}\right) \tag{D.6}$$

D.2 Area Integrals

We now fill in the details of the integral constraint discussion in Sections 3.1.2 and 3.2.4.

Conservation of E_0, where

$$E_0 = \left(\frac{\partial H_0}{\partial x}\right)^2 + \left(\frac{\partial H_0}{\partial y}\right)^2 + H_0^2 \tag{D.7}$$

is determined by considering

$$\int_D \frac{\partial}{\partial t}\left(H_0 q\right) = \int_D H_0 \frac{\partial q}{\partial t} + \int_D \frac{\partial H_0}{\partial t} q \tag{D.8}$$

Substituting (3.56) and (3.63) for the definition and conservation of q,

$$\begin{aligned}\int_D \frac{\partial}{\partial t}\left(H_0(\nabla^2 - 1)H_0\right) = & \int_D H_0\left(-J(H_0, q) + \mathcal{R}\left(-J(H_1, q)\right)\right) \\ & \int_D \mathcal{R} H_0\left(F_1\frac{\partial q}{\partial x} + G_1\frac{\partial q}{\partial y}\right) - H_0\frac{\beta}{\mathcal{R}}\frac{\partial H_0}{\partial x} \\ & \int_D \frac{\partial H_0}{\partial t}(\nabla^2 - 1)H_0,\end{aligned} \tag{D.9}$$

and applying (D.3), (D.4) and (D.6),

$$-\frac{1}{2}\int_D \frac{\partial}{\partial t}E_0 = \mathcal{R}\int_D H_0\left(-J(H_1, q) + F_1\frac{\partial q}{\partial x} + G_1\frac{\partial q}{\partial y}\right). \tag{D.10}$$

Conservation of energy is similar in the leading order equations, (3.40), where the leading order equation $\frac{\partial q}{\partial t}$ (3.29) is used instead.

Conservation of q is determined by integrating (3.63),

$$\int_D \frac{\partial q}{\partial t} = \int_D -J(H_0, q) + \mathcal{R}\left(-J(H_1, q) - F_1\frac{\partial q}{\partial x} - G_1\frac{\partial q}{\partial y}\right) - \frac{\beta}{\mathcal{R}}\frac{\partial H_0}{\partial x} \tag{D.11}$$

$$= \int_D F_1\frac{\partial q}{\partial x} + G_1\frac{\partial q}{\partial y} \tag{D.12}$$

Substituting the definition of q, and applying (D.5),

$$\int_D \frac{\partial q}{\partial t} = \int_D H_0(\nabla^2 - 1)F_1 + H_0(\nabla^2 - 1)G_1 \tag{D.13}$$

Substituting the definitions of F_1,(3.61), and G_1, (3.62),

$$\int_D \frac{\partial q}{\partial t} = \int_D -\frac{\partial H_0}{\partial x} J\left(H_0, \frac{\partial H_0}{\partial x}\right) - \frac{\partial H_0}{\partial y} J\left(H_0, \frac{\partial H_0}{\partial y}\right) \tag{D.14}$$

$$= -\frac{1}{2}\left[J\left(H_0, \left(\frac{\partial H_0}{\partial x}\right)^2\right) + J\left(H_0, \left(\frac{\partial H_0}{\partial y}\right)^2\right)\right] = 0 \tag{D.15}$$

by applying (D.3).

If instead, from

$$\int_D \frac{\partial q}{\partial t} = \int_D F_1 \frac{\partial q}{\partial x} + G_1 \frac{\partial q}{\partial y} \tag{D.16}$$

$$= \int_D \left(\frac{\partial F_1}{\partial x} + \frac{\partial G_1}{\partial y}\right) q \tag{D.17}$$

we substitute the first correction *rSW Height-Divergence Equation*, (3.60) where (3.56) has been substituted for q,

$$\int_D \frac{\partial q}{\partial t} = -\frac{\partial H_0}{\partial t}(\nabla^2 - 1)H_0 = -\frac{1}{2}\int_D \frac{\partial E_0}{\partial t} \tag{D.18}$$

by applying (D.6).

Appendix E

Exact Solution to *rSW QG*^{0}

This appendix provides details for deriving the exact travelling dipole solution to the leading order quasigeostrophic equations, considered first in Sections 3.2.3 and defined as the leading order *rSW QG*^{0} model in Section 3.3.3. From Equation (3.55)[1].

$$\frac{\partial q}{\partial t} + J\left(H_0, q\right) = 0, \tag{E.1}$$

where

$$q = (\nabla^2 - 1)H_0, \tag{E.2}$$

and the Jacobian of two functions, f and g is

$$J(f,g) = \frac{\partial f}{\partial x}\frac{\partial g}{\partial y} - \frac{\partial f}{\partial y}\frac{\partial g}{\partial x}. \tag{E.3}$$

Following the method in [5], consider a travelling dipole solution to q, advecting at constant velocity c in x, by letting $\partial_t = -c\partial_x$, where $\partial_y \not\equiv 0$. Equation (E.1) becomes

$$J\left((H_0 + cy), q\right) = 0, \tag{E.4}$$

with solution $q = -\sigma(\psi + cy) = q$ for $\sigma \geq 0$. For a dipole of radius a, let

$$\sigma = \left\{ \begin{array}{ll} \sigma & r < a \\ 0 & r > a \end{array} \right\}. \tag{E.5}$$

[1]The equivalent equation in Section 3.2.3, equation (3.29), is obtained by letting $h = H_0$ for negligible β.

The solution form is then

$$q = \left\{ \begin{array}{cc} -\sigma\left(H_0 + cy\right) & r < a \\ 0 & r > a \end{array} \right\}$$

For the outer region, $r > a$, $q_{\text{out}} = 0$ is solved for $H_{0\text{out}}$

$$q_{\text{out}} = (\nabla^2 - 1) H_{0\text{out}}^2 = 0 \tag{E.6}$$

with general solution

$$H_{0\text{out}} = \frac{K_n(r)}{K_n(a)} \left(A \sin(n\theta) + B \cos(n\theta)\right) \tag{E.7}$$

for integer n and constants A and B, where $K_n(r)$ is the modified Bessel function of the second kind.

For the inner region, $r < a$, $q_{\text{inn}} = -\sigma(H_{0\text{inn}} + cy)$ is solved for $H_{0\text{inn}}$

$$q_{\text{inn}} = \left(\nabla^2 - 1\right) H_{0\text{inn}} = -\sigma\left(H_{0\text{inn}} + cy\right) \tag{E.8}$$

with general solution, where $y = r \sin\theta$,

$$H_{0\text{inn}} = \frac{J_n(r\sqrt{\sigma - 1})}{J_n(a\sqrt{\sigma - 1})} \left(C \sin(n\theta) + D \cos(n\theta)\right) - \frac{c\sigma}{\sigma - 1} r \sin(\theta) \tag{E.9}$$

for integer n and constants C and D, where $J_n(r)$ is the modified Bessel function of the first kind.

Continuity in $q(r, \theta)$ across the boundary at $r = a$ is imposed by restricting

$$q_{\text{out}}(a, \theta) = q_{\text{inn}}(a, \theta) \tag{E.10}$$

$$0 = -\sigma(H_{0\text{inn}}(a, \theta) + cy) \tag{E.11}$$

where letting $y = a \sin\theta$ on the boundary,

$$H_{0\text{inn}}(a, \theta) = -ca \sin\theta. \tag{E.12}$$

Substituting into the definition of $H_{0\text{inn}}$, (E.9),

$$-ca \sin\theta = \frac{J_n(r\sqrt{\sigma - 1})}{J_n(a\sqrt{\sigma - 1})} \left(C \sin(n\theta) + D \cos(n\theta)\right) - \frac{c\sigma}{\sigma - 1} r \sin(\theta). \tag{E.13}$$

The equation form restricts $n = 1$ and $D = 0$, reducing the above equation to

$$-ca \sin\theta = \left(C - a\frac{c\sigma}{\sigma - 1}\right) \sin(\theta) \tag{E.14}$$

where $C = \frac{ac}{\sigma - 1}$ yields the inner solution

$$H_{0\text{inn}}(r,\theta) = \frac{ac}{\sigma-1}\left(\frac{J_1(r\sqrt{\sigma-1})}{J_1(a\sqrt{\sigma-1})} - \frac{r\sigma}{a}\right)\sin\theta. \tag{E.15}$$

Continuity in $q(r,\theta)$ across the boundary at $r = a$ is imposed by restricting

$$H_{0\text{out}}(a,\theta) = H_{0\text{inn}}(a,\theta) \tag{E.16}$$

$$\frac{K_n(a)}{K_n(a)}\left(A\sin(n\theta) + B\cos(n\theta)\right) = \frac{ac}{\sigma-1}\left(\frac{J_1(a\sqrt{\sigma-1})}{J_1(a\sqrt{\sigma-1})} - \sigma\right)\sin\theta, \tag{E.17}$$

where $n = 1$, $B = 0$ and $A = -ac$ yields the outer solution

$$H_{0\text{out}}(r,\theta) = -ac\frac{K_1(r)}{K_1(a)}\sin\theta. \tag{E.18}$$

Continuity in the geostrophic velocities, $u = -\frac{\partial H_0}{\partial y}$, $v = \frac{\partial H_0}{\partial x}$ ((3.27) and (3.28)), is obtained by imposing continuity in the first spatial derivatives of H_0. Continuity in H_0 implies continuity in $\frac{\partial H_0}{\partial\theta}$, and it is sufficient to impose

$$\frac{\partial H_{0\text{out}}(a,\theta)}{\partial r} = H_{0\text{out}}(r,\theta) \tag{E.19}$$

$$-ac\frac{\frac{\partial}{\partial r}K_1(a)}{K_1(a)}\sin\theta = \frac{ac}{\sigma-1}\left(\sqrt{\sigma-1}\frac{\frac{\partial}{\partial r}J_1(a\sqrt{\sigma-1})}{J_1(a\sqrt{\sigma-1})} - \frac{\sigma}{a}\right)\sin\theta, \tag{E.20}$$

which reduces to

$$(\sigma-1)\frac{K_0(a)}{K_1(a)} + \frac{2\sigma}{a} = \sqrt{\sigma-1}\frac{J_0(a\sqrt{\sigma-1})}{J_1(a\sqrt{\sigma-1})}.$$

By imposing continuity in q, H_0 and $\frac{\partial H_0}{\partial r}$, the spatial derivative of q, $\frac{\partial q}{\partial r}$ is discontinuous at $r = a$. Implications in using this exact solution as a test for numerical convergence are considered in Section 4.5.2.

The complete travelling dipole solution, with radius $r = a$, is of the form

$$q = \left\{\begin{array}{cc} -\sigma\left(H_0 + cy\right) & r < a \\ 0 & r > a \end{array}\right\} \tag{E.21}$$

$$H_0 = \left\{\begin{array}{cc} ac\frac{K_1(r)}{K_1(a)}\sin\theta & r < a \\ \frac{ac}{\sigma-1}\left(\frac{J_1(r\sqrt{\sigma-1})}{J_1(a\sqrt{\sigma-1})} - \frac{r\sigma}{a}\right)\sin\theta & r > a \end{array}\right\} \tag{E.22}$$

$$\tag{E.23}$$

where σ is given by

$$(\sigma-1)\frac{K_0(a)}{K_1(a)} + \frac{2\sigma}{a} = \sqrt{\sigma-1}\frac{J_0(a\sqrt{\sigma-1})}{J_1(a\sqrt{\sigma-1})}.$$

Solving numerically with $a = 1$, the smallest $\sigma \approx 16.3868925833852$.

Appendix F

Exact Solution to *rSW Wave*

This analysis follows that in [8], and provides details in the derivation of the exact travelling wave solution of 3.3.1. Beginning with the *rSW Wave* equations, (3.44), (3.45):

$$\frac{\partial u}{\partial t} + \mathcal{R}\left(u\frac{\partial u}{\partial x} + v\frac{\partial u}{\partial y}\right) - v + \frac{\partial}{\partial x}\left(\frac{\partial v}{\partial x} - \frac{\partial u}{\partial y}\right) = 0, \tag{F.1}$$

$$\frac{\partial v}{\partial t} + \mathcal{R}\left(u\frac{\partial v}{\partial x} + v\frac{\partial v}{\partial y}\right) + u + \frac{\partial}{\partial y}\left(\frac{\partial v}{\partial x} - \frac{\partial u}{\partial y}\right) = 0, \tag{F.2}$$

we seek travelling wave solutions in x with speed c, so that $\frac{\partial}{\partial y} \equiv 0$ and $\frac{\partial}{\partial t} = -c\frac{\partial}{\partial x}$:

$$-(c - \mathcal{R}u)\frac{\partial u}{\partial x} - v + \frac{\partial^2 v}{\partial x^2} = 0, \tag{F.3}$$

$$-(c - \mathcal{R}u)\frac{\partial v}{\partial x} + u = 0. \tag{F.4}$$

To obtain a system of differential equations, first solve (F.4) for $\frac{\partial v}{\partial x}$,

$$\frac{\partial v}{\partial x} = \frac{1}{c - \mathcal{R}u}u, \tag{F.5}$$

then differentiating with respect to x, substitute into (F.3) and solve for $\frac{\partial u}{\partial x}$,

$$\frac{\partial u}{\partial x} = \frac{(c - \mathcal{R}u)^2}{c - (c - \mathcal{R}u)^3}v. \tag{F.6}$$

To obtain the first integral equation, multiply (F.3) by $\frac{\partial v}{\partial x}$, and substitute (F.4)

$$v\frac{\partial v}{\partial x} + u\frac{\partial u}{\partial x} - \frac{\partial v}{\partial x}\frac{\partial^2 v}{\partial x^2} = 0 \tag{F.7}$$

Integrating, and again substituting (F.4) reveals the first integral relation, for constant C:

$$v^2 + u^2\left(1 - \frac{1}{c - \mathcal{R}u}\right) = C. \tag{F.8}$$

Appendix G

Third-Order Runge-Kutta and Adams-Bashforth

This appendix fills in the details in applying the third order Adams Bashforth (AB3) and third order Runge-Kutta (RK3) methods to the integrating factor formulation of $rSW\ QG^{0}$ and $rSW\ QG^{+1}$.

For a general partial differential equation,

$$\frac{\partial \mathcal{Q}}{\partial t} = f(t, \mathcal{Q}) \tag{G.1}$$

AB3 and RK3 are applied to obtain approximate numerical solutions, where n is the number of iterations, and Δt is the uniform time step,

$$\text{AB3}: \quad \mathcal{Q}_{n+1} = \mathcal{Q}_n + \frac{\Delta t}{12}\left(23f(t_n, \mathcal{Q}_n) - 16f(t_{n-1}, \mathcal{Q}_{n-1}) + 5f(t_{n-2}, \mathcal{Q}_{n-2})\right) \tag{G.2}$$

$$\text{RK3}: \quad \mathcal{Q}_{n+1} = \mathcal{Q}_n + \frac{1}{6}(S_1 + 4S_2 + S_3) \tag{G.3}$$

where

$$\begin{aligned} S_1 &= \Delta t f(t_n, \mathcal{Q}_n) \\ S_2 &= \Delta t f\left(t_n + \frac{\Delta t}{2}, \mathcal{Q}_n + \frac{S_1}{2}\right) \\ S_3 &= \Delta t f\left(t_n + \Delta t, \mathcal{Q}_n - \frac{S_1}{2} + 2S_2\right) \end{aligned} \tag{G.4}$$

The integrating factor formulation of $rSW\ QG^{0}$ and $rSW\ QG^{+1}$ is

$$\frac{\partial}{\partial t}\left(e^{\mu|\vec{k}|^8 t}\hat{q}\right) = e^{\mu|\vec{k}|^8 t}\mathcal{N}_{|\vec{k}|}(\hat{q}), \tag{G.5}$$

which assumes the form of (G.1) by letting

$$\mathcal{Q} = e^{\mu|\vec{k}|^8 t}\hat{q}, \tag{G.6}$$

$$f(t,\mathcal{Q}) = e^{\mu|\vec{k}|^8 t}\mathcal{N}_{\vec{k}}\left(e^{-\mu\vec{k}^8 t}\mathcal{Q}\right). \tag{G.7}$$

Evaluated at distinct time intervals,

$$\mathcal{Q}_n = e^{\mu|\vec{k}|^8 t_n}\hat{q}_n, \tag{G.8}$$

$$f(t_n,\mathcal{Q}_n) = e^{\mu|\vec{k}|^8 t_n}\mathcal{N}_{\vec{k}}\left(\hat{q}_n\right). \tag{G.9}$$

This is precisely the form of the AB3 formulation, and so substituting into (G.2).

$$\begin{aligned} e^{\mu|\vec{k}|^8 t_{n+1}}\hat{q}_{n+1} = {} & e^{\mu|\vec{k}|^8 t_n}\hat{q}_n + \frac{\Delta t}{12}\left(23e^{\mu|\vec{k}|^8 t_n}\mathcal{N}_{\vec{k}}\left(\hat{q}_n\right)\right. \\ & \left. -16e^{\mu|\vec{k}|^8 t_{n-1}}\mathcal{N}_{\vec{k}}\left(\hat{q}_{n-1}\right)+5e^{\mu|\vec{k}|^8 t_{n-2}}\mathcal{N}_{\vec{k}}\left(\hat{q}_{n-2}\right)\right) \end{aligned} \tag{G.10}$$

Dividing by $e^{\mu|\vec{k}|^8 t_{n+1}}$, where $t_n = n\Delta t$, gives the time independent integrating factor formulation for AB3:

$$\begin{aligned} \hat{q}_{n+1} = {} & e^{-\mu|\vec{k}|^8\Delta t}\hat{q}_n + \frac{\Delta t}{12}\left(23e^{-\mu|\vec{k}|^8\Delta t}\mathcal{N}_{\vec{k}}\left(\hat{q}_n\right)\right. \\ & \left. -16e^{-2\mu|\vec{k}|^8\Delta t}\mathcal{N}_{\vec{k}}\left(\hat{q}_{n-1}\right)+5e^{-3\mu|\vec{k}|^8\Delta t}\mathcal{N}_{\vec{k}}\left(\hat{q}_{n-2}\right)\right). \end{aligned} \tag{G.11}$$

The RK3 formulation is slightly more complicated, since $f(t,\mathcal{Q})$ is not evaluated at regular intervals. Therefor, we rewrite S_1, S_2 and S_3 by substituting (G.6) and (G.7) into (G.4),

and introduce s_1, s_2 and s_3 as the time independent components

$$\begin{aligned}
S_1 &= \Delta t e^{\mu|\vec{k}|^8 t_n} \mathcal{N}_{\vec{k}}\left(\hat{q}_n\right) \\
&= e^{\mu|\vec{k}|^8 t_n} s_1 \qquad \text{(G.12)} \\
S_2 &= \Delta t e^{\mu|\vec{k}|^8\left(t_n+\frac{\Delta t}{2}\right)} \mathcal{N}_{\vec{k}}\left(e^{-\mu\vec{k}^8\left(t+\frac{\Delta t}{2}\right)}\left(\mathcal{Q}_n+\frac{S_1}{2}\right)\right) \\
&= \Delta t e^{\mu|\vec{k}|^8\left(t_n+\frac{\Delta t}{2}\right)} \mathcal{N}_{\vec{k}}\left(e^{-\frac{1}{2}\mu\vec{k}^8\Delta t}\left(e^{-\mu\vec{k}^8 t_n}\mathcal{Q}_n+e^{-\mu\vec{k}^8 t_n}\frac{S_1}{2}\right)\right) \\
&= \Delta t e^{\mu|\vec{k}|^8\left(t_n+\frac{\Delta t}{2}\right)} \mathcal{N}_{\vec{k}}\left(e^{-\frac{1}{2}\mu\vec{k}^8\Delta t}\left(\hat{q}_n+\frac{S_1}{2}\right)\right) \\
&= e^{\mu|\vec{k}|^8\left(t_n+\frac{\Delta t}{2}\right)} s_2 \qquad \text{(G.13)} \\
S_3 &= \Delta t e^{\mu|\vec{k}|^8(t_n+\Delta t)} \mathcal{N}_{\vec{k}}\left(e^{-\mu\vec{k}^8\left(t+\frac{\Delta t}{2}\right)}\left(\mathcal{Q}_n-\frac{S_1}{2}+2S_2\right)\right) \\
&= \Delta t e^{\mu|\vec{k}|^8(t_n+\Delta t)} \mathcal{N}_{\vec{k}}\left(e^{-\mu\vec{k}^8\Delta t}\left(e^{-\mu\vec{k}^8 t_n}\mathcal{Q}_n\right.\right. \\
&\quad \left.\left.-\frac{1}{2}e^{-\mu\vec{k}^8 t_n}S_1+2e^{-\mu\vec{k}^8 t_n}\right)S_2\right) \\
&= \Delta t e^{\mu|\vec{k}|^8(t_n+\Delta t)} \mathcal{N}_{\vec{k}}\left(e^{-\mu\vec{k}^8\Delta t}\left(\hat{q}_n-\frac{S_1}{2}\right)+2e^{-\frac{1}{2}\mu\vec{k}^8\Delta t}s_2\right) \\
&= e^{\mu|\vec{k}|^8(t_n+\Delta t)} s_3 \qquad \text{(G.14)}
\end{aligned}$$

where

$$\begin{aligned}
s_1 &= \Delta t \mathcal{N}_{\vec{k}}\left(\hat{q}_n\right) \qquad \text{(G.15)} \\
s_2 &= \Delta t \mathcal{N}_{\vec{k}}\left(e^{-\frac{1}{2}\mu\vec{k}^8\Delta t}\left(\hat{q}_n+\frac{S_1}{2}\right)\right) \qquad \text{(G.16)} \\
s_3 &= \Delta t \mathcal{N}_{\vec{k}}\left(e^{-\mu\vec{k}^8\Delta t}\left(\hat{q}_n-\frac{S_1}{2}\right)+2e^{-\frac{1}{2}\mu\vec{k}^8\Delta t}s_2\right) \qquad \text{(G.17)}
\end{aligned}$$

Rewriting the general RK3 method (G.3),

$$e^{\mu|\vec{k}|^8(t_n+\Delta t)}\hat{q}_{n+1} = e^{\mu|\vec{k}|^8 t_n}\hat{q}_n+\frac{1}{6}\left(e^{\mu|\vec{k}|^8 t_n}s_1+4e^{\mu|\vec{k}|^8\left(t_n+\frac{\Delta t}{2}\right)}s_2+e^{\mu|\vec{k}|^8(t_n+\Delta t)}s_3\right)$$

Dividing by $e^{\mu|\vec{k}|^8(t_n+\Delta t)}$ gives the time independent integrating factor formulation for RK3:

$$\hat{q}_{n+1} = e^{-\mu|\vec{k}|^8\Delta t}\hat{q}_n+\frac{1}{6}\left(e^{-\mu|\vec{k}|^8\Delta t}s_1+4e^{-\frac{1}{2}\mu|\vec{k}|^8\Delta t}s_2+s_3\right) \qquad \text{(G.18)}$$

Bibliography

[1] J.G. Charney. On the scale of atmospheric motions. *Geof. Publ.*, 17(2):1–17, 1948.

[2] B. Cushman-Roisin. *Introduction to Geophysical Fluid Dynamics.* Prentice-Hall, 1994.

[3] Description of the ECMWF forecasting system in February 2006, viewed January 2007. http://www.ecmwf.int/products/data/operational_system/description/description_2006.html.

[4] A.E. Gill. *Atmosphere-Ocean Dynamics.* International Geophysics Series. Academic Press, 1982.

[5] S.E. Haupt, J.C. McWilliams, and J.J. Tribbia. Modons in shear flow. *J. Atmos. Sci.*, 50(9):1181 1191, 1993.

[6] R. H. Karsten and G. E. Swaters. A unified asymptotic derivation of two-layer, frontal geostrophic models including planetary sphericity and bottom topography. *Phys. Fluids*, 11(9):2583 2597, 1999.

[7] J.C. McWilliams. Isolated coherent vortices in turbulent flow. *J. Fluid Mech.*, 146:21 43, 1984.

[8] D. Muraki. Notes on rotating shallow water. Rough ideas towards a better understanding of gravity waves and balance, March 2005.

[9] D. Muraki, C Snyder, and R. Rottuno. The next-order corrections to quasi-geostrophic theory. *J. Atmos. Sci.*, 56:1547 1560, 1999.

[10] J. Pedlosky. *Geophysical Fluid Dynamics.* Springer-Verlag, 1987.

[11] G.W. Platzman. The rossby wave. *Q. J. R. Meteorol. Soc.*, 94:225 246, 1968.

[12] L. M. Polvani, J.C. McWilliams, M. Spall, and R. Ford. The coherent structures of shallow water turbulence: deformation radius effects, cyclone/anticyclone asymmetry and gravity wave generation. *Chaos*, 4:177 186, 1994.

[13] R. B. Stull. *Meteorology for Scientists and Engineers.* Brooks/Cole, 2000.

[14] L. N. Trefethen. *Spectral Methods in MATLAB.* SIAM, 2000.

[15] G. K. Vallis. Potential vorticity inversion and balanced equations of motion for rotating stratified fluids. *Q. J. R. Meteorol. Soc.*, 122:291 322, 1996.